Design of next generation optical transmission systems

Hou–Man CHIN

A thesis submitted to the University College London (UCL) for the degree of PhD

Optical Networks Group
Department of Electronic and Electrical Engineering
University College London (UCL)

March 2016

I, Hou-Man Chin, confirm that the work presented in this thesis is my own. Where information has been derived from other sources, I confirm that this has been indicated.

KAPPA

—Twitch Chat

Acknowledgements

FIRSTLY, I gratefully acknowledge the funding of my PhD program, donation of equipment and support from Ciena, in particular from Maurice O'Sullivan, Michel Bélanger, Andrzej Borowiec, Douglas Charlton, Charles Laperle and Doug McGhan. In addition I thank the Next Generation Modem group at Ciena's Ottawa facility for the very warm welcome and their experimental and theoretical expertise during my visit in Ottawa. This work was funded under the auspices of a Ciena university collaborative research grant. I also thank Polatis for the loan of the 16x16 optical switch.

Secondly, I thank my primary supervisor Seb J. Savory for his supervision and support during these four years through which I have never ceased to be amazed by his expertise. I also thank my secondary supervisor Benn C. Thomsen and Manoj P. Thakur for providing me with invaluable experimental help. I am especially grateful to David Ives for beta reading this body of work for me and for the many many hours of discussion we've held, usually over a hot beverage.

Lastly, I thank my family and friends, of which are too numerous to list here.

List of Acronyms

ADC	Analogue to Digital Converter
AWG	Arrayed Waveguide Grating
AWGN	Additive White Gaussian Noise
ASE	Amplified Spontaneous Emission
B2B	Back to Back
BER	Bit Error Rate
BPSK	Binary Phase Shift Keying
BVT	Bandwidth Variable Transmitter
CAPEX	Captital Expenditure
CDF	Cumulative Distribution Function
CR	Cognitive Radio
CON	Cognitive Optical Networks
CW	Continuous Wave
DAC	Digital to Analogue Converter
DBP	Digital Back Propagation
DCT	Design Control Table
DC	Data Centers
DCF	Dispersion Compensating Fibre
DOP	Degree of Polarization
DPSS	Discrete Prolate Slepian Spheroidal Sequences

DSDBR Digital Super-mode Distributed Bragg Reflector

DSF Dispersion Shifted Fibre

DSP Digital Signal Processing

DWDM Dense Wavelength Division Multiplexing

EDFA Erbium Doped Fibre Amplifier

ECL External Cavity Laser

EON Elastic Optical Network

FEC Forward Error Correction

FTTC Fibre To The Cabinet

FTTH Fibre To The Home

FWM Four Wave Mixing

GN Gaussian Noise

HD-FEC Hard Decision Forward Error Correction

IM-DD Intensity Modulated Direct Detection

IP Internet Protocol

IT Information Technology

ITU International Telecommunication Union

LUT Look Up Table

MTM Multi-taper Method

NF Noise Figure

NSR Noise to Signal Ratio

O/E/O Optical-Electrical-Optical

OE Opto-electronic

OF OpenFlow

OOK On-Off Keying

OPEX Operational Expenditure

OSA Optical Spectrum Analyzer

PDA Personal Data Assistant

PDF Probability Distribution Function

PDG Polarization Dependent Gain

PDL Polarization Dependent Loss

PMD Polarization Mode Dispersion

PM-QPSK Polarization Multiplexed Quadrature Phase Shift Keying

PM-16QAM Polarization Multiplexed 16 level Quadrature Amplitude Modulation

PM-64QAM Polarization Multiplexed 64 level Quadrature Amplitude Modulation

PRBS Pseudo Random Bit Sequence

QAM Quadrature Amplitude Modulation

QoE Quality of Experience

QPSK Quadrature Phase Shift Keying

ROADM Reconfigurable Optical Add-Drop Multiplexer

ROSNR Required Optical Signal to Noise Ratio

RxOSNR Received Optical Signal to Noise Ratio

SDN Software Defined Network

SDT Software Defined Transceiver

SMF Single Mode Fibre

SNR Signal to Noise Ratio

SOP State of Polarization

VOA Variable Optical Attenuator

WDM Wavelength Division Multiplexing

WRON Wavelength Routed Optical Network

WSS Wavelength Selective Switch

XPM Cross Phase Modulation

Contents

List of Figures

Abstract

In this thesis investigations were performed into the design of optical channels for coherent optical fibre transmission systems for future optical networks. Firstly, an overview of traditional optical networks design and next generation concepts under research for the next generation of optical networks is given.

The coherent receiver was then investigated experimentally as an investigative tool to provide information for channel provisioning, by fast C-band spectral analysis and estimating neighbouring channel power. An algorithm incorporated these two abilities and successfully provisioned a polarization multiplexed quadrature phase shift keying (PM-QPSK) signal in a populated system.

Probabilistic versus traditional deterministic design methodology was examined to determine its advantages by perturbing intra-link optical power. Experimental results showed that due to the non-linearity of the transmission medium, a more ideal provisioning point could be determined. A three parameter model was proposed to fit the behaviour of optical power and was shown to fit the behaviour of a single channel system. A wavelength division multiplexed (WDM) system was then used to validate the model's prediction ability with high accuracy.

In light of the potential increased polarization dependent loss (PDL) of next generation optical networks, the influence of up to 6 dB distributed link PDL is investigated for a 35 Gbaud coherent WDM system over 120,000 discrete instantiations for PM-QPSK and polarization multiplexed 16-level quadrature amplitude modulation (PM-16QAM) using commercial transceivers. Less than a 1 dB penalty to SNR was observed for a 6 dB range of optical launch powers.

This thesis concludes with a method for estimating the performance margin for a PM-16QAM system using a pre-existing PM-QPSK system with the intended use for adaptive change of modulation format on the fly. The largest error in estimation of this margin is less than 0.4 dB over a range of 4 dB optical launch power.

List of Publications

- **H-M. Chin**, K. Shi, R. Maher, M. Paskov, B. Thomsen and S. Savory, "Fast optical spectrum estimation using a digital coherent receiver," ECOC, 2013.
- **H-M. Chin**, M. P. Thakur, B. C. Thomsen, and S. J. Savory, "Estimating divergently routed nonlinearly interfering channel powers using cross phase modulation," Opt. Express 22, 25506-25515 (2014).
- **H-M. Chin**, B. C. Thomsen and S. J. Savory, "The effect of intra-link power perturbations on channel performance," ECOC, 2015.
- S. J. Savory and **H-M. Chin**, "Probabilistic Design of Nonlinear Optical Transmission Systems," in Optical Fiber Communication Conference, 2016, paper Th3D.4.
- **H-M.Chin**, D. Charlton, A. Borowiec, C. Laperle, M. Reimer, M. O'Sullivan "Experimental Investigation of the Impact of Distributed Link PDL on a Coherent Transmission System," ECOC, 2016.

1 Optical Networks

1.1 Abstract

The currently deployed optical networks have to service an increasing amount of traffic as demand for bandwidth increases [1]. In order to cope with future predicted demand, it is likely that the current optical network architecture may not be sufficient. This chapter provides a brief overview of current optical networks before discussing the proposed concepts under research in order to increase the capacity and capability of next generation systems.

1.2 Current Optical Networks

Optical transport networks can be divided into three different sections, that of the core, metro and access networks. In general the core network tends to compromise the portion of optical transport dedicated to long haul transmission greater than 2,000 km. The metro network incorporates all links below 2,000 km to 100 km. The access network is typically 0 to 100 km, this includes also the 'last mile' connections to the user. The use of fibre-optic transmission technology is the standard in core and metro networks with limited deployment of FTTH in access networks. There is still widespread use of copper, co-axial cables and wireless for the 'last mile' connections to users, incorporating FTTC technology. However there is considerable on-going research into the deployment of

optical networks to the end user [2] [3]. The divisions of distances stated above are a generalization and for smaller geographical networks such as the United Kingdom, will not apply. In the UK for example, there is essentially no differentiation between metro and access.

The previously described demand for capacity has been up to now sated by an increase in the speed of electronics, leading to higher line rates [4] and then by the resurgence of coherent transceivers after initial research in the 1980s [5]. The EDFA provided terahertz of bandwidth which could be amplified which gave rise to the WDM) network. The WDM network was first standardized on the ITU 100 GHz grid and is the predecessor to today's dense WDM (DWDM) network on the ITU 50 GHz grid [6] and the proposed future 12.5 GHz grid [6].

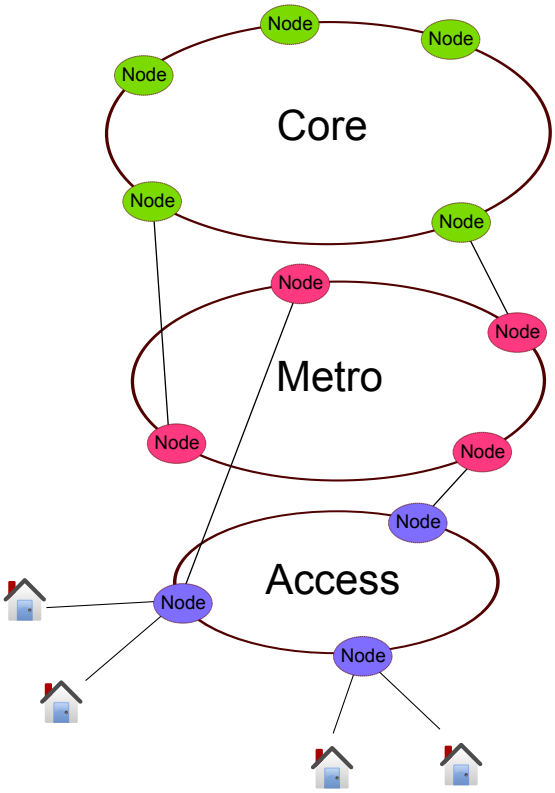

Figure 1.1: Optical Network layout

Though the EDFA provides roughly 5 THz of optical bandwidth conveniently situated around the the point of minimum attenuation in the standard optical fibre [7], it is not infinite therefore there is a hard limit on the scalability of WDM technology. The standard modulation format used was on off keying (OOK) 1.2, which is limited to 1 bit/s/Hz of spectral efficiency and modulates the amplitude of the optical carrier, modulating the phase of the signal generates the BPSK format 1.4. The coherent receiver allows for the detection and recovery of both the amplitude and the phase of the optical signal. Modulating both of these components immediately doubles the spectral efficiency to 2 bits/s/Hz, creating QPSK 1.4. Advances on the transmitter side allows

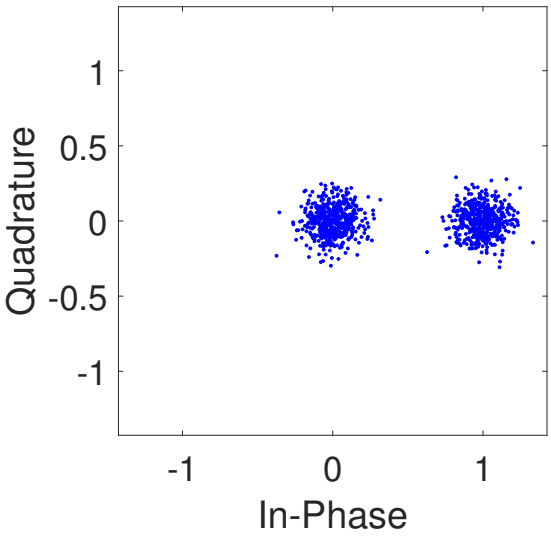

Figure 1.2: OOK constellation diagram

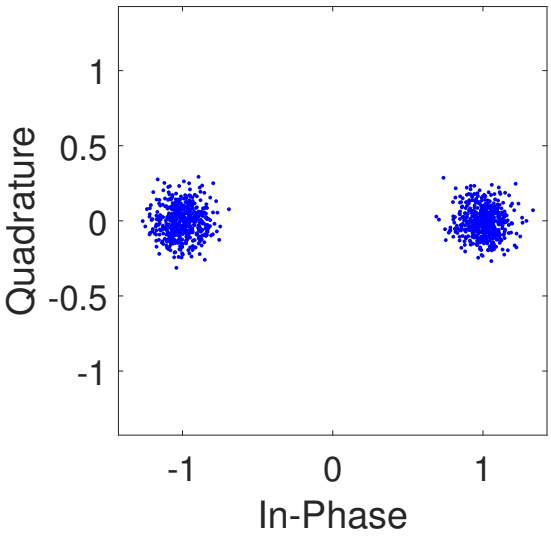

Figure 1.3: BPSK constellation diagram

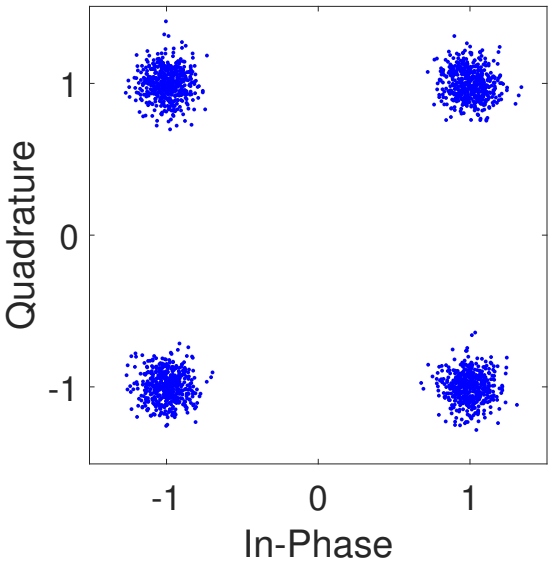

Figure 1.4: QPSK constellation diagram

for multi-level modulation, i.e. the amplitude and phase components is modulated with more than one positive or negative level which further increases the spectral efficiency at the cost of requiring a higher SNR. The coherent receiver is also polarization diverse which allows for polarisation multiplexing (e.g. PM-QPSK), modulation across the two polarisations [8] or time slots for modulation formats in 8 dimensions [9] by modulating across different time-slots.

The ability to recover the full optical field has lead to an increase in the capability of the optical transceiver. It's processing power has been improved to enable it to perform complex DSP such as compensation of chromatic dispersion, polarization mode dispersion and carrier phase recovery [10], in addition to handling increasingly powerful FEC. Recently this has been extended to compensation of non-linear impairments [11] [12] [13]. As transistor technology decreases in size, the power of the DSP incorporated as scaled accordingly.

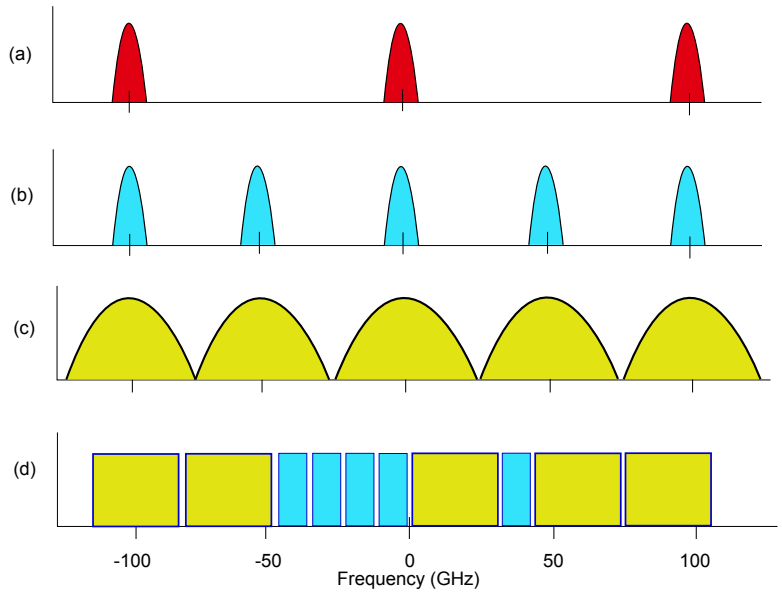

Figure 1.5: Optical Spectrum with 10 Gbit/s OOK (red), 40 Gbit/s PM-QPSK (blue) and 100 Gbit/s PM-QPSK (green) signals on (a) 100 GHz grid, (b) and (c) 50 GHz grid and (d) flex-grid.

The optical networks currently implemented are static entities that once installed remain in operation in the same state until failure or an upgrade cycle is required. This requires them to be exceedingly robust to events that may occur during its service lifetime. In addition it is entirely possible that the customer does not have accurate knowledge of its own installed systems either due to inherited or leased equipment. This requires a greater amount of margin to be provisioned at the network design stage. Margin is defined as the the amount of performance degradation before a system failure event occurs. A reconfiguration or replacement of the component that failed requires an engineer on site to perform the procedure. This is highly undesirable both due to the time required between recognition of the event, sending the appropriate personnel

and then time to fix. The amount of margin available in legacy systems based on a 100 GHz WDM frequency grid and OOK or BPSK modulation formats combined with the static nature of the network has allowed systems designers to account for the expected deterioration of the system over its expected lifetime. An unexpected failure before the end of service time for a component cannot be accounted for except with a protection scheme.

1.3 Next Generation Optical Networks

The ITU optical network standard ITU G.694.1 [6] has evolved by reducing the spacing in between optical channels to take advantage of the finite amount of optical bandwidth available for transmission. It is obvious that having a 10 Gbaud OOK signal residing in a 100 GHz frequency slot is not very efficient (0.1 bits/s/Hz), Fig. 1.5 (a). Coherent 40 Gbit/s PM-QPSK on a tighter 50 GHz grid Fig. 1.5 (b) is a considerable step up in spectral efficiency relative to OOK at 0.8 bits/s/Hz, however in order to meet bandwidth demands [1] this may be considered the previous generation of coherent transceivers as of 2015. The current deployed standard is 100 Gbit/s PM-QPSK on the 50 GHz frequency grid which is 2 bits/s/Hz with a net symbol rate of 25 Gbaud Fig. 1.5 (c). PM-16QAM transceivers have recently become commercially available, this doubles the spectral efficiency for the same symbol rate but places additional demands on the electronics due to the increase in the modulation format cardinality.

From this it is obvious that decreasing the spacing between channels as much as possible is a relatively easy way to increase the capacity of an optical fibre. The standard modulated optical signal typically occupies twice its symbol rate in bandwidth. In order to place channels as close together as possible, root raised cosine pulse shaping is used in conjunction with high speed DACs with sufficient resolution to modulate higher order modulation formats such as PM-16QAM. With ideal root-raised cosine pulse shaping ($\alpha = 0$) it is theoretically possible to put optical channels adjacent to each other without any guard band, turning the entire C-band into a single optical super channel. In practice, factors such as laser frequency drift in addition to the difficulty of maintaining the same calibration between geographically separate frequency dependent components (such as optical filters) over time require a small guard band to be present.

1.3.1 Flexible Frequency Grid

This reduction in guard band and the advent of DACs able to modulate optical signals with an increasingly small roll-off root raise cosine shape ($\alpha = 0.14$ [14] in commercial products) have contributed to the concept of the flexible frequency grid. The name of the concept implies a completely flexible grid (Flex-grid) [15] with arbitrary channel

width and therefore arbitrary frequency grid in an attempt to place channels as close together as possible. This is of course the most efficient use of bandwidth however this places a high demand on the optical equipment used to multiplex and demultiplex these channels, particularly the sharpness of the optical filters, this in turn places a high demand on equipment inventory and/or tunability. The ITU has standardised the flex-grid into a grid of 12.5 GHz [6] with signals occupying multiple slots according to their symbol rate, Fig. 1.5. Therefore the standard 100 Gbit/s PM-QPSK operating at 28 or 35 Gbaud [14] signal fits into 3 slots with bandwidth allowed for the guard band.

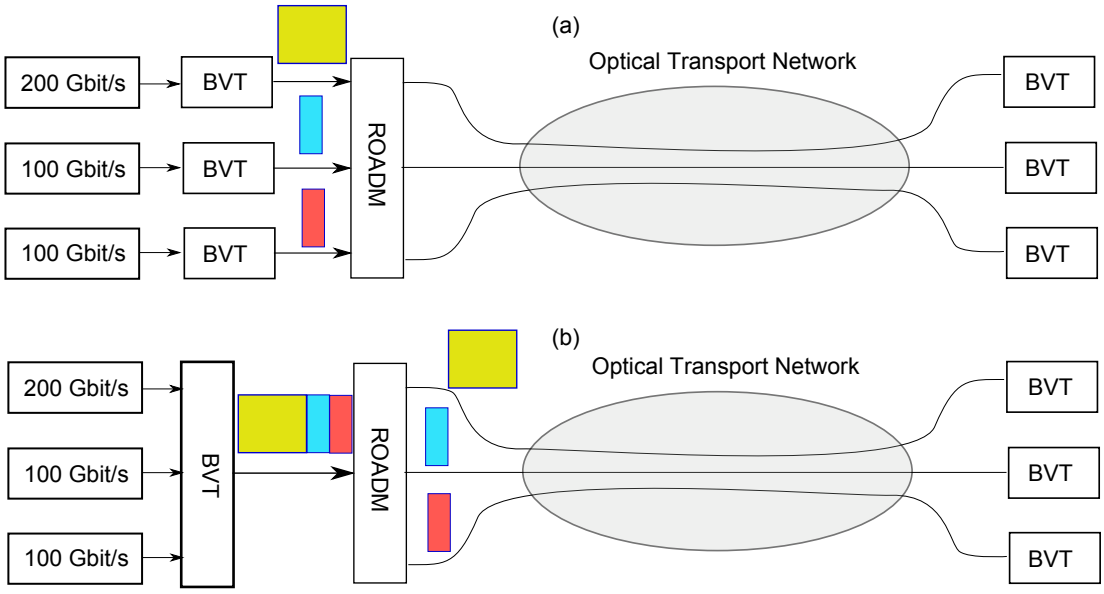

Figure 1.6: 400 Gbit/s capable bandwidth variable transceivers with Nyquist pulse shaping deployed on a flexible frequency grid with (a) separate transceivers and (b) a sliced BVT.

1.3.2 Elastic Optical Networks

The EON is a concept that is a logical out-growth of flex-grid. It makes sense that a network operating on a flexible frequency grid [6] can be adaptively adjusted in order to meet consumer demands and also to increase its efficiency. An important part of this is the BVT [16]. As its name implies, the BVT enables the bandwidth of the optical channel to be adjusted. In literature, this has generally been a coherent optical system which can modulate multiple modulation formats [17] Ṫhe BVT accomplishes this by switching modulation formats in accordance to the link its assigned e.g. PM-QPSK for long haul transmission or PM-64QAM for short haul metro networks. Similarly it is possible for a BVT to vary its baud in order to fit into a flex-grid network. Another capability that may appear is the ability to 'slice' a BVT, that is to subdivide the signal transmitted by a BVT so that one transmitter can serve multiple receivers. Other common functions of a BVT are the ability to change wavelengths and power. This does present a provisioning problem in that the network architecture would have to be

informed if its new baud is higher than its current baud. It can be seen how a BVT operating on its own can easily cause operational problems in a network.

1.3.3 Software Defined Networks

Software defined networks (SDN) can be described in a single sentence - 'It strives to simplify networking by abstracting the data plane functionality away from the control plane' [18]. The typical method requires initialisation of transceivers at the required link's geographical locations and then configuration at the required routing nodes to ensure the link is routed on the correct path, traditionally this is a time intensive process due to the requirement of an engineer to visit each location. The increasing electronic capability of the transmission systems being deployed in optical networks enables remote configuration, greatly decreasing the time required for soft reconfiguration. This may be called the first incarnation of a software defined network where the controlling intelligence sits behind the keyboard. The previously described process provisions an optical link. The envisioned form of a SDN is one that allows the operator to request a link of a certain rate from one point to another, the SDN controller would then provision it autonomously, no other operator input is required. The network devices themselves make the configuration and routing decisions and implementation. This removes the need for operator input, the operator is automatically limited to requesting links that can be provisioned, e.g. the abstraction in Figure. 1.7. Research on SDNs have focused mainly on the network layer with protocols such as OpenFlow [18] [19] and have ignored interaction with the physical layer underneath apart from light path requests [20].

The implication behind the SDN is that the optical network as a whole is more self aware of what data is being carried, it's origin and destination and the capabilities of the links between nodes are transparent to it. This allows operators unprecedented overview of their networks, this in conjunction with the simplified network abstraction allows them to make much faster reconfiguration of their networks remotely. They know what's happening, therefore they can respond as required. This also allows network optimisation with regards to time e.g. heavily loaded links can be split into different paths, or latency, optimisation of routing. A SDN is an example of an autonomous network, defined by high level policies.

The future optical network will therefore be a more agile entity compared to currently deployed systems. This poses a challenge due to the contradiction between the need to provision sufficient margin to guarantee continued operation of provisioned systems in the presence of a dynamic network situation and the demand for capacity which absorbs previously available margin to deploy higher baud systems as well as more advanced modulation formats. The following chapters will attempt to address

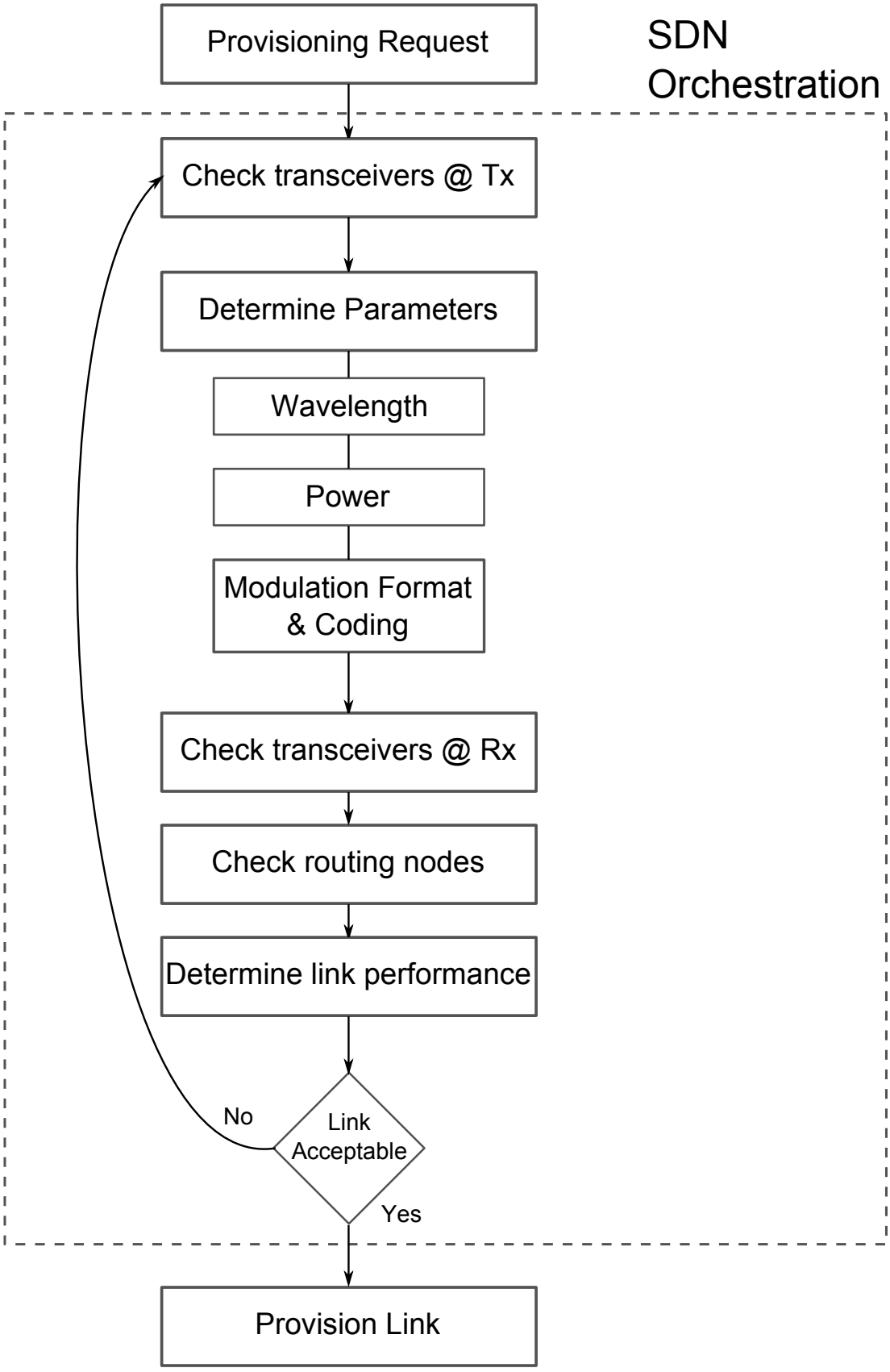

Figure 1.7: Abstraction of a provisioning request using SDN orchestration

some of these questions.

1.4 Generalized Multi-Protocol Label Switching (GMPLS)

GMPLS is an established standard [21] which has similar aims and abilities to the concepts described above in order to develop a dynamic optical network. It focuses mainly on the control plane services that perform connection management for the data plane for packet switched and non-packet switched interfaces. It has four basic functions

- *Routing control* - routing capability, traffic engineering and topology discovery
- *Resource discovery* - capability to track system resource status such as bandwidth, ports and multiplexing ability
- *Connection management* - End to end provisioning capability for heterogeneous services, includes connection creation, modification, status query and deletion
- *Connection restoration* - Administers protection capability using backup paths in case of provisioned path failure

Fundamentally, GMPLS provides dynamic end-to-end provisioning capability to an optical network. However, it does not have an integrated functionality to manipulate the physical layer. Typically a separate Routing and Wavelength Assignment (RWA) algorithm is used to do this. In the context of this thesis, GMPLS sits at a higher level in the network hierarchy (layer 2) compared to this works' layer 0 or 1. Indeed the results presented here could be used in just the RWA. Another service allowed by GMPLS is bandwidth on demand which as its name suggests, allows clients to request connections as required. Taken as whole, it would seem that GMPLS is powerful and flexible.

GMPLS has been used in research to this end [22]. However more recent control architectures such as OpenFlow [23] and Open Daylight [24] while outwardly similar to GMPLS in providing dynamic end to end provisioning in opticla networks, they have many advantages over GMPLS. Primarily, OpenFlow/Open Daylight's reduction in complexity, increased flexibility along with an transition path to introduce them to operator networks [25] make them much more desirable.

2

Software Defined Transceiver

2.1 Abstract

In this chapter, we demonstrate the use of a software defined coherent transceiver as a sensing tool to provide information to provision an optical channel. A fast wideband spectral estimation algorithm is demonstrated using a fast tuning DSDBR laser as the coherent receiver's local oscillator. This technique was then included into an algorithm to sense spectral occupancy of an optical link. The measured BER performance of a test channel transmitting on the desired wavelength was used to infer the optical power of neighbouring co-propagating optical channels which were divergently routed with respect to test channel using a set of LUTs. This method proved successful until there was no measurable impact from the neighbouring channels at which point they could be neglected. A frequency shift of 12 GHz was then applied to the test channel to successfully deduce which neighbour channel was operating at a higher power.

2.2 Introduction

In the previous chapter 1, an overview is provided of the technologies that may emerge in the next generation of optical networks. In particular, the software defined network implies the deployment of software defined transceivers. The latest commercially available coherent transceivers are capable of switching modulation formats, adjusting its transmission power and wavelength. These capabilities exists in the currently deployed generation of commercial transceivers and may be accessed with methods such as a virtual private network, however a comprehensive control plane doesn't yet exist to take advantage of it. It is however envisaged that future optical networks [26] will leverage this capability to implement more efficient systems. A key functionality for a SDN is the ability to sense the environment at a network node. In this chapter the frequency diversity of the digital coherent transceiver is exploited in conjunction with a fast tunable laser to provide the function of wideband spectrum sensing to the transceiver. This enables the transceiver to estimate its environment to best provision the desired optical link.

2.3 Digital Coherent Receiver

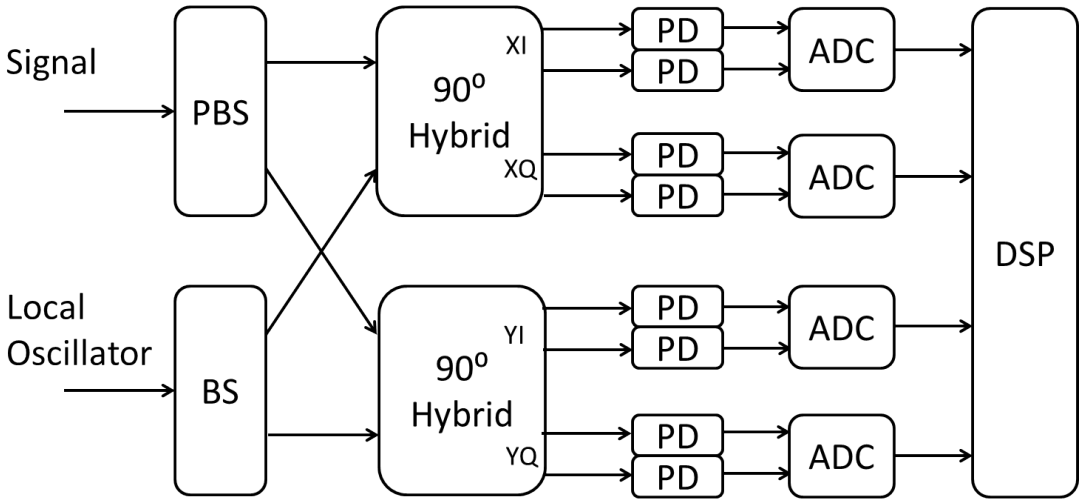

Figure 2.1: Digital coherent receiver

The digital coherent transceiver Fig. 2.1 is a combination of a 90 degree optical hybrid on the front end with a tunable laser used as a local oscillator. The basis of optical heterodyne detection was first explored in 1968 [27] for enclosed optical lightpaths however the coherent optical receiver for optical fibre transmission was not explored until 1979 by Okoshi [28]. English publications then followed in the 1980s [29, 30, 31] but the implementation of coherent transceivers has only recently been popularized

with the addition of digital signal processing [10, 32], due to additional demand for bandwidth. The coherent receivers employed in this work are phase and polarization diverse Fig. 2.1, with three main stages: a polarization de-multiplexing stage; phase diverse coupling and detection. The first stage splits the input optical signal as well as the local oscillator laser into orthogonal polarizations with polarization beam splitters. The received signal is then mixed with the local oscillator. This mixing occurs within a pair of 90 degree optical hybrids, one per polarization. Each hybrid outputs the in-phase and quadrature components for that polarization. Each output has a dedicated OE stage, in either single-ended or balanced configuration. This work employs balanced detection.

The bandwidth that can be detected by the receiver is dictated by the optical bandwidth of the photo-diodes, their electrical bandwidth and the sampling speed of the ADCs after OE conversion. Generally the the sampling speed of the ADCs is twice the baud of the received optical signal, though sampling rates down to 1 sample per symbol have been examined. [33].

2.4 Wideband Spectral Sensing

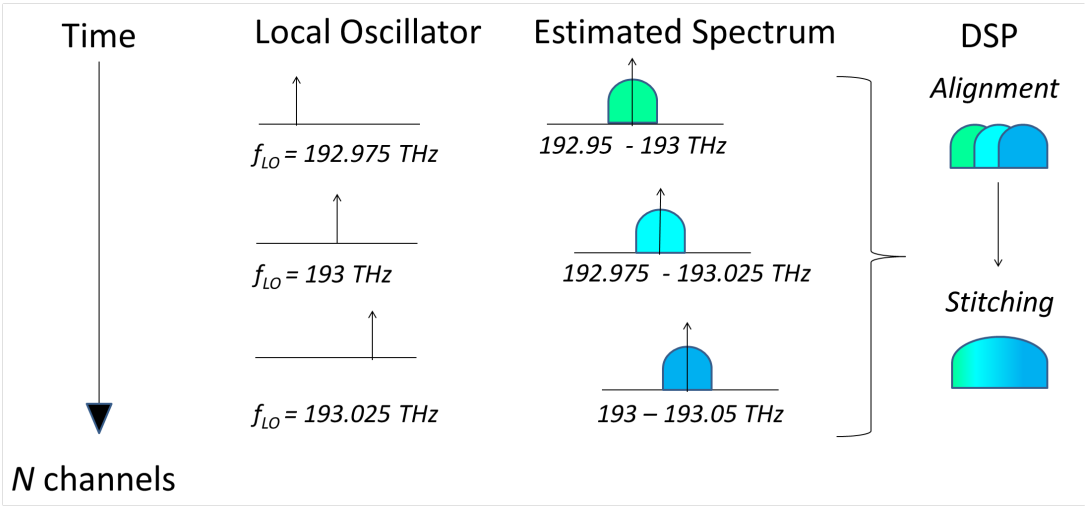

Figure 2.2: Algorithm for wideband spectral sensing

It is possible to use an OSA to performing wideband spectral sensing for the coherent transceiver. There are of course numerous disadvantages mainly in that you require a separate OSA which increases cost. Traditionally the scanning time of an OSA has been on the order of double digit seconds depending on the desired resolution, it is only recently that commercial OSAs are available with a very fast scanning time over the C-band [34]. In place of an OSA, we implement additional digital signal processing at the coherent receiver to recreate its functionality. The coherent receiver's frequency selectivity is key to enable it to perform wideband spectral sensing. The transmission frequency of the samples received by the coherent receiver is dictated by the local oscillator (LO). Therefore transforming the samples from the time domain to the frequency domain will sense a 'slice' of bandwidth equivalent to the sampling speed of the ADCs centred on the LO's frequency. By tuning the local oscillator to a frequency grid at regular intervals and sampling at each of these grid points. It is possible to construct a wideband spectral estimation using a receiver that has a bandwidth much smaller than that of the bandwidth to be estimated. These slices can then be digitally stitched together to form an estimation as wide as the local oscillator can tune.

A digital super-mode DSDBR [35] is used in the coherent receiver to provide a fast scanning ability to capture the spectral slices. Thomson's MTM is used to perform the spectral estimation for each slice [36] which are then combined. As a proof of concept, the DSDBR is configured to switch across 11 channels spaced 25 GHz apart, over a time period of 22 µs. We note that since the local oscillator is a free running laser, the stability of the required laser frequency may drift and our algorithm must account for that. The DSP algorithm consists of the following steps, illustrated in Fig. 2.2.

1. The MTM is used to estimate the spectrum for each spectral slice.
2. The overlapping sections between two adjacent slices are cross correlated to calculate the exact frequency offset from the assumed laser frequency.
3. The slices are realigned according to the calculated frequency offset.
4. The scanned spectrum is digitally stitched together from the realigned slices by averaging the overlapping sections.

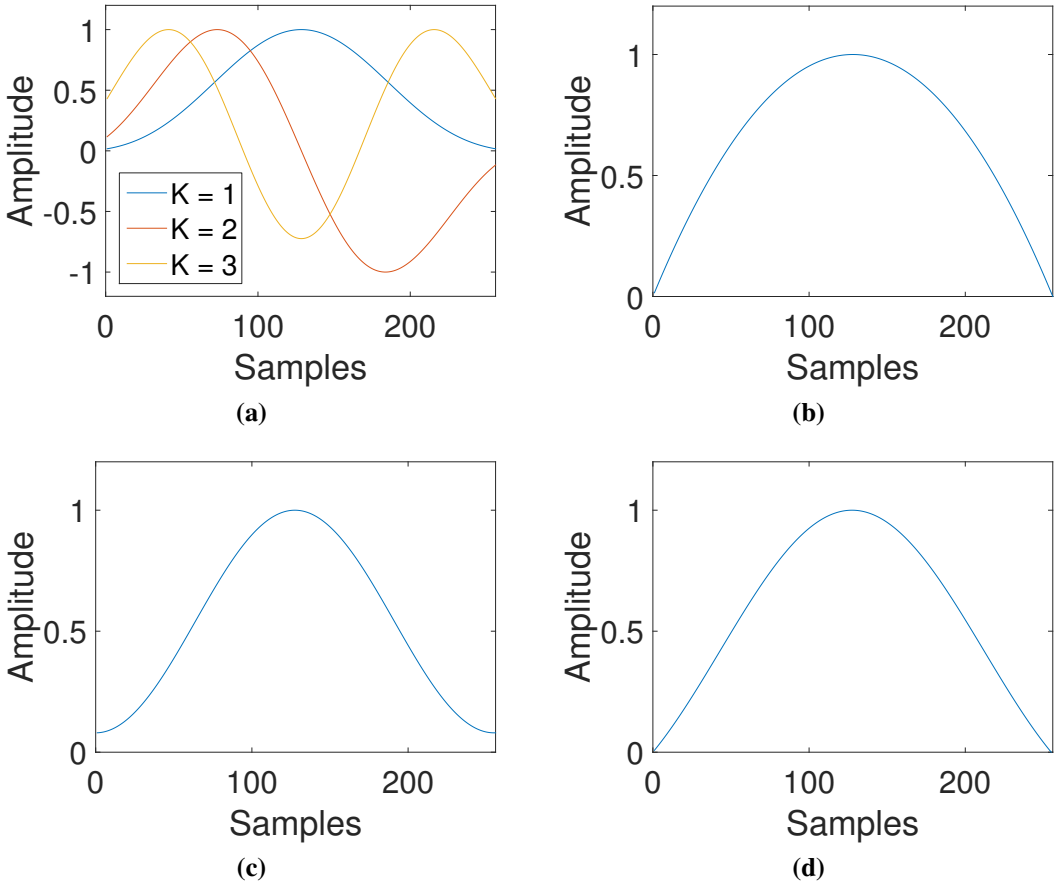

Figure 2.3: (a) K*th* order DPSS windows, (b) Welch window, (c) Hamming window, (d) Sinc window

The MTM is performed in a series of steps, DPSS [37] taper the data samples to create

$$y_k(f) = \sum_{t=0}^{N-1} x(t) \cdot v_t^{(k)}(T,B)\, e^{-i2\pi ft} \tag{2.1}$$

where $y_k(f)$ is the kth tapered set of samples, from which the spectrum is estimated. The Slepian sequences are orthonormal, hence the estimation based on each taper is uncorrelated. The number of tapers K applied is based on the selected time bandwidth product BT where $K = 2BT$, $T = N\delta t$ where N is the number of samples, B is the

resolution bandwidth and $v_t^{(k)}(T,B)$ is the kth Slepian sequence for $k = 0,1,...,K-1$. The multi-taper spectrum estimate becomes

$$\bar{S}(f) = \frac{1}{K}\sum_{K=0}^{K-1} |y_k(f)|^2 \tag{2.2}$$

This is the crudest form of the MTM. The benefit of using the MTM over a standard periodogram is that the variance of the estimate can be decreased by employing multiple tapers, each of which provides an independent estimations of the spectrum using the same samples due to the properties of the DPSS. This therefore reduces the variance without having to resort to detecting larger amounts of samples. This increases the speed of the optical measurement at the expense of increased digital signal processing. The second problem with using a periodogram is the inherent bias due to windowing a continuous time signal with a square window. The bias can be mitigated by other windows such as the sinc or welch windowing functions and DPSS [36]. The variance of $\bar{S}(f)$ also decreases when the number of samples increases for a fixed estimate bandwidth. To perform a fast estimation over a large bandwidth, it is desirable to create an estimation with a minimal amount of samples to decrease the chance of a change in the bandwidth to be estimated while the sweep is being performed. The initial calibration of the frequency offset in step 2 is performed once with a 2^{16} samples for a high frequency resolution, the standard deviation of this calibration was found to be 34 MHz across 10 separate sweeps.

2.4.1 Experimental Setup and Results

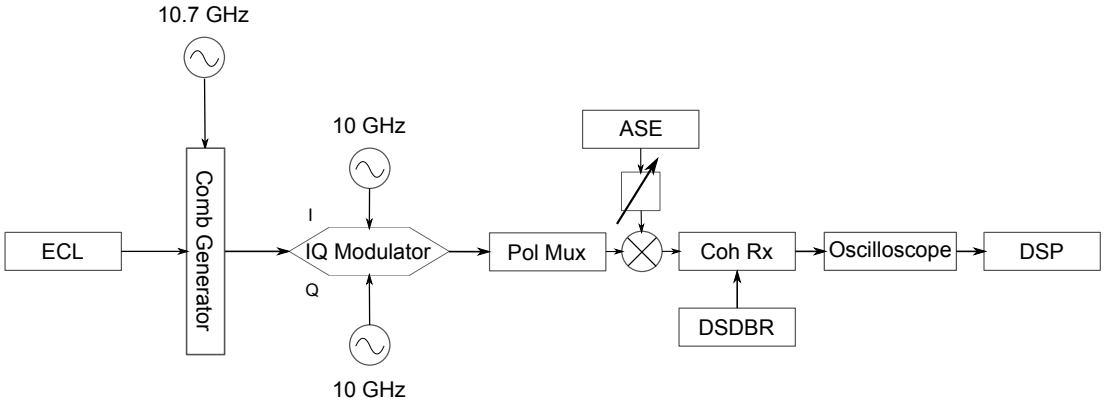

Figure 2.4: Experimental setup for wideband spectral estimation

The experimental setup is laid out as in Fig. 2.4. To calibrate the cross correlation and overlap, we input an unfiltered optical frequency comb [38], (Fig. 2.5(a)), generated by a 15 kHz external cavity laser at 193.29 THz with comb lines spaced at 10.7 GHz. The DSDBR laser is rapidly switched between the optical wavelengths shown in Fig.

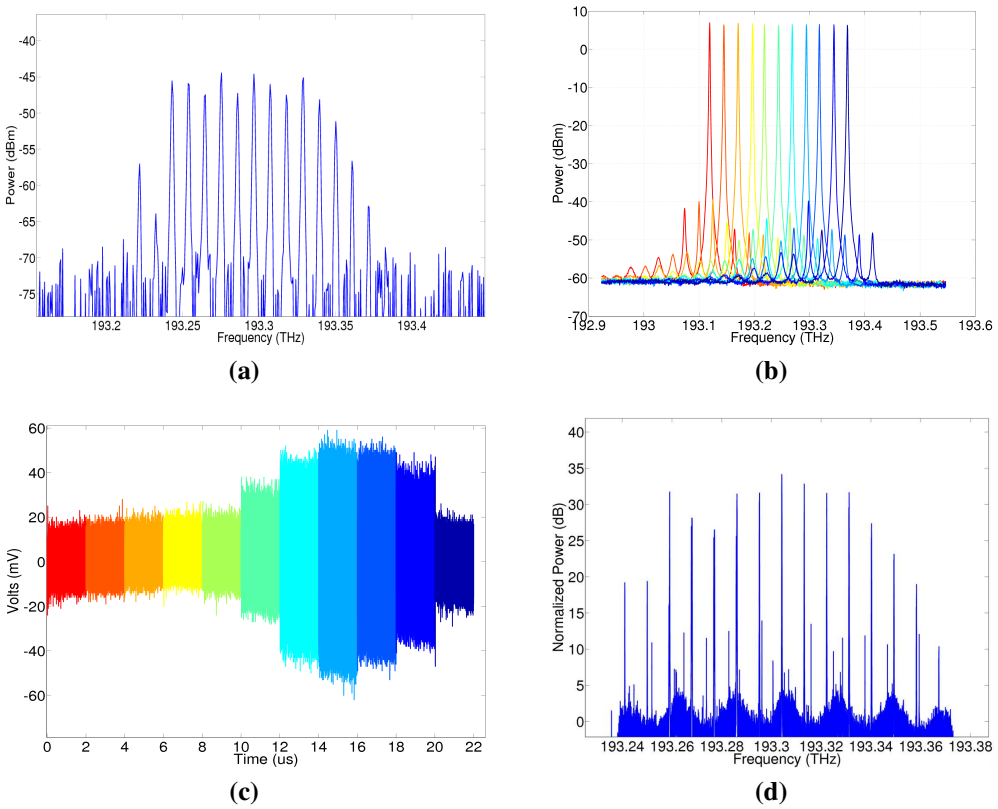

Figure 2.5: (a), OSA trace of input optical comb at 0.01 nm resolution, (b) overlaid OSA traces of DSDBR channels, (c) sampling oscilloscope input with respect to DSDBR switching, (d) 2048 sample MTM estimation

2.5(b) every 2 μs, the effect of this switching on the input signal to the oscilloscope is shown in 2.5(c) and the spectral estimate is shown with 2048 samples per slice in 2.5(d). The output from the coherent receiver is sampled at 50 GSamples/s for 50 GHz detected bandwidth.

After calibration of the cross correlation alignment, less samples are necessary for the estimation if using this method as a frequency diverse energy detector. This allows the laser to switch between channels quicker. We show the estimated spectrum (Fig. 2.7(b)) using 64 samples per spectral slice. The limitation on switching speed is then the settling time of the DSDBR laser which is 50 ns [39]. The minimum number of samples required before the frequency offset estimation became inaccurate is investigated and shown in Fig. 2.6 (a). The cross correlation performance deteriorated after less than 512 samples (temporal resolution of approximately 0.1 ns). This indicates that the sweeping time is primarily limited by the switching time of the DSDBR laser.

The impact of the received SNR on the accuracy of the cross correlation is investigated. The highest SNR comb line used as the measurement reference. The input signal was noise loaded with the maximum possible noise which was then decreased in steps of 2 dB. We see a disparity in the performance of the cross correlation Fig. 2.6 (b). This

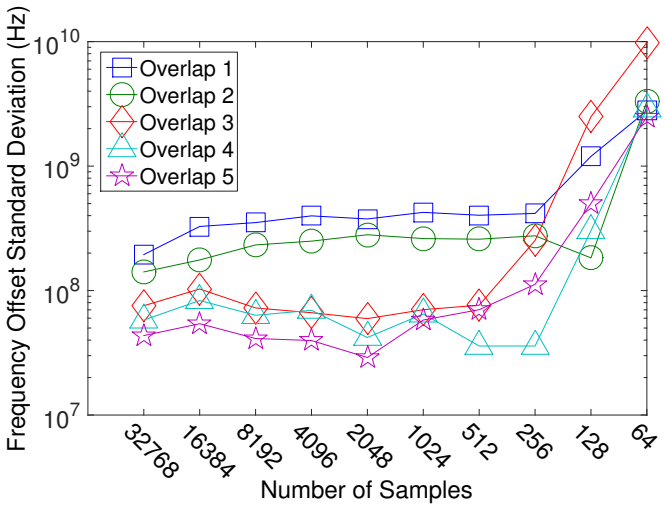

(a)

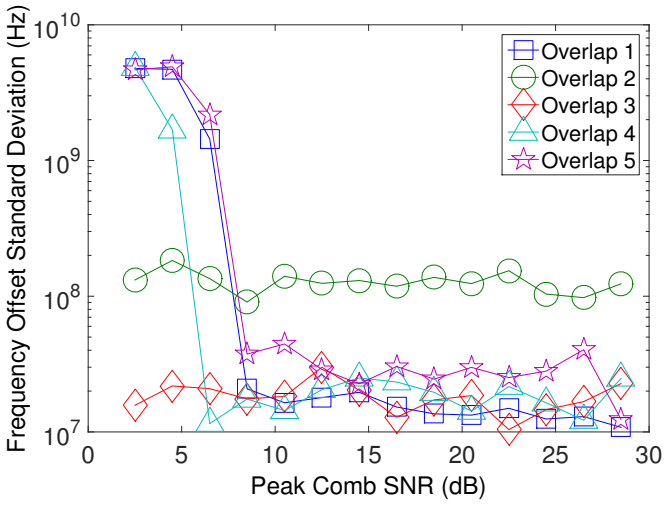

(b)

Figure 2.6: Number of samples (a) and the highest SNR comb line (b) vs frequency standard deviation of the cross correlation. Overlap 1 refers to the overlap between the first and second spectral slices, continuing on for each pair of spectral slices.

is caused by where the comb lines lie on the detected spectrum. While the detected optical bandwidth is 50 GHz, the electrical bandwidth of the oscilloscope, limits this to 32 GHz, beyond which roll off occurs. At lower SNRs, a comb line is deep in the roll off zone of one spectral slice which is then below the noise floor of the overlapping spectral slice. This leads to the cross-correlation being inaccurate. The overlaps which maintain performance are as a result of having the same comb line in both spectral slices that is not deep into the roll off zone in either.

The polarization diverse property of this method for spectrum estimation may be beneficial for operation of cognitive optical transceivers, enabling separate estimation of both x and y polarization spectra as well as the combination of both. After frequency offset calibration, we apply the spectrum estimation algorithm to a modulated signal. We show polarization diverse spectrum estimation of the comb in Fig. 2.8 with 9 channels

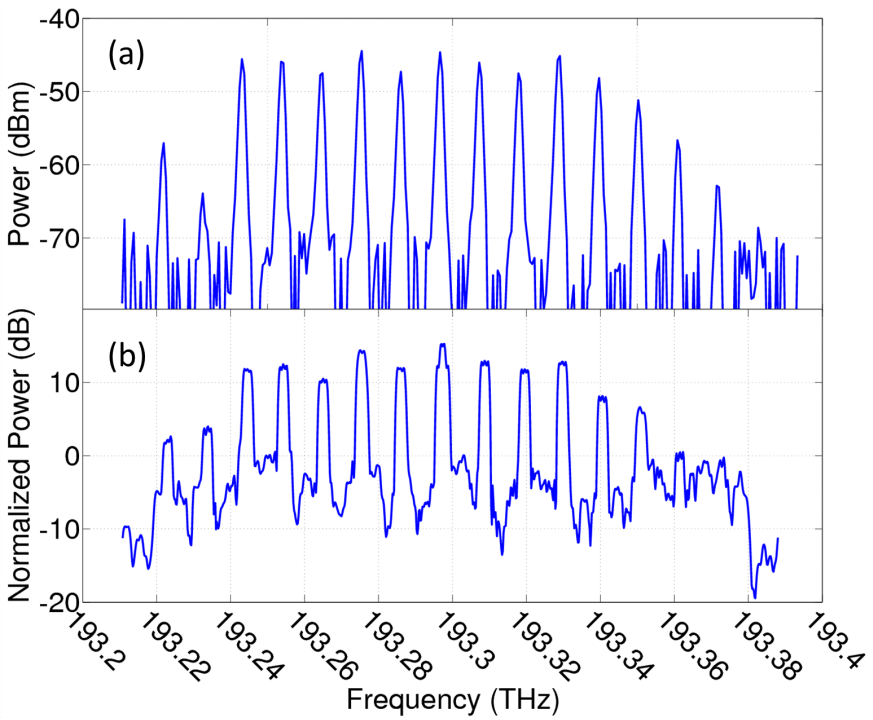

Figure 2.7: (a) OSA trace of the input optical comb, 64 Sample MTM estimate of the optical comb.

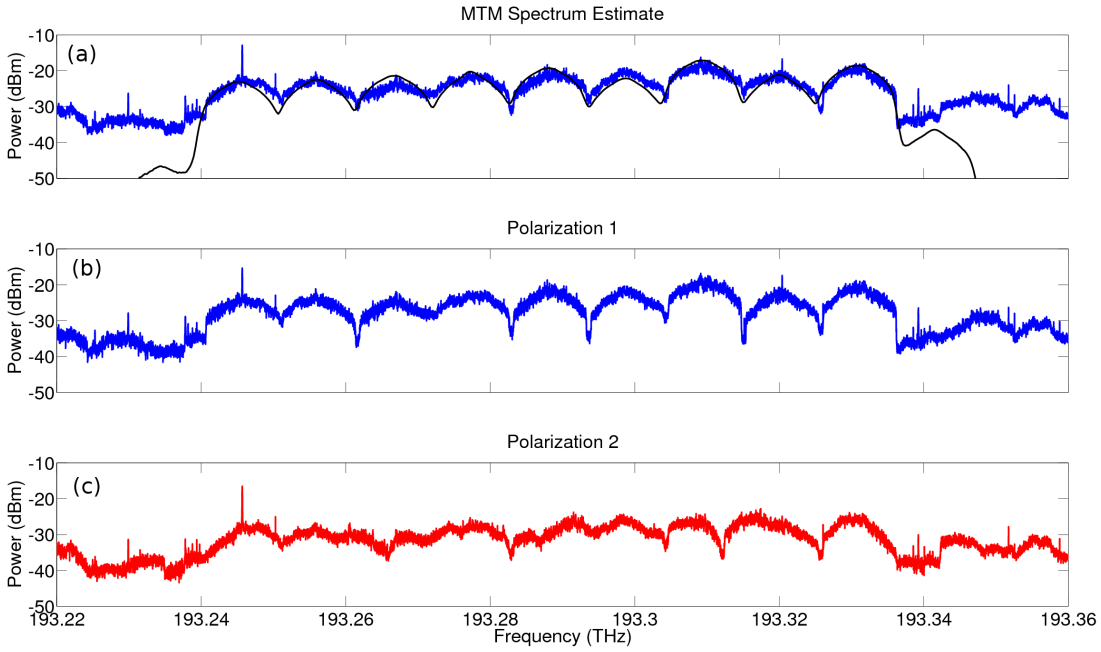

Figure 2.8: (a) Spectrum estimation with OSA trace overlaid in black, (b)(c) Polarization diverse spectrum estimation of 9 channels modulated with 10G PM-QPSK spaced at 10.7 GHz.

modulated with 10 Gbaud Nyquist shaped PM-QPSK using previously calculated frequency offsets and a frequency resolution of ≈ 0.76 MHz. The polarizations were not aligned at the receiver polarization controller to show a difference between the spectrum estimates.

2.4.2 C-band Spectrum Estimation

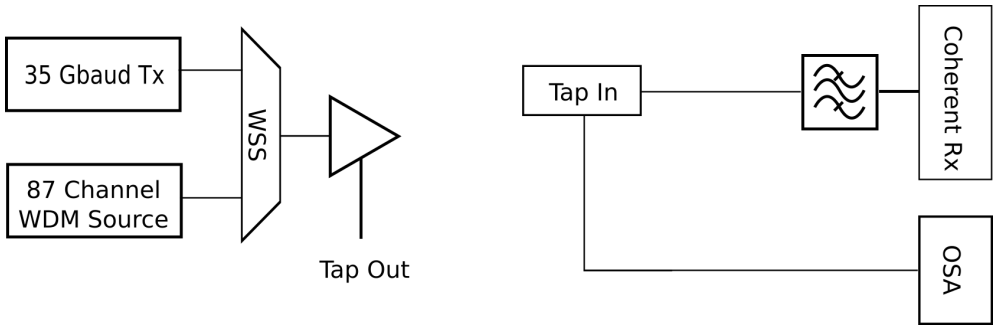

Figure 2.9: Experimental setup for C-band spectrum estimation of 88 channel 35 Gbaud WDM system

The final experiment performs spectrum estimation over the 4.4 THz using the experimental setup detailed in Fig. 2.9. The optical bandwidth is filled with 35 Gbaud PM-QPSK channels in a WDM configuration on the standard ITU 50 GHz frequency grid. Root raised cosine pulse shaping with roll off $\alpha = 0.14$ is applied to all the channels. The system is arranged in a back to back configuration. Commercially available transceivers [14] are used to bulk modulate the channels, each slice of bandwidth that can be estimated is ˜40 GHz in size. 1044 samples are accessible from the card for this experiment, for a frequency resolution of ˜38 MHz, or ˜0.0003 nm. The receiver line card is C-band tunable and is swept along the spectrum in 25 GHz steps. Unlike the previous estimation using a commercial transceiver, there are no gaps in the estimation.

The spectral estimation is generated using the 1044 samples per splice using the MTM method [36] with 39 tapers and then digitally stitched together to form the estimation in Fig. 2.10. The previously used cross correlation for alignment proved to be unnecessary due to the stability of the local oscillator at the line card. It should be noted that if this measurement is used for OSNR estimation that it is inherently limited by the electrical SNR of the transceiver.

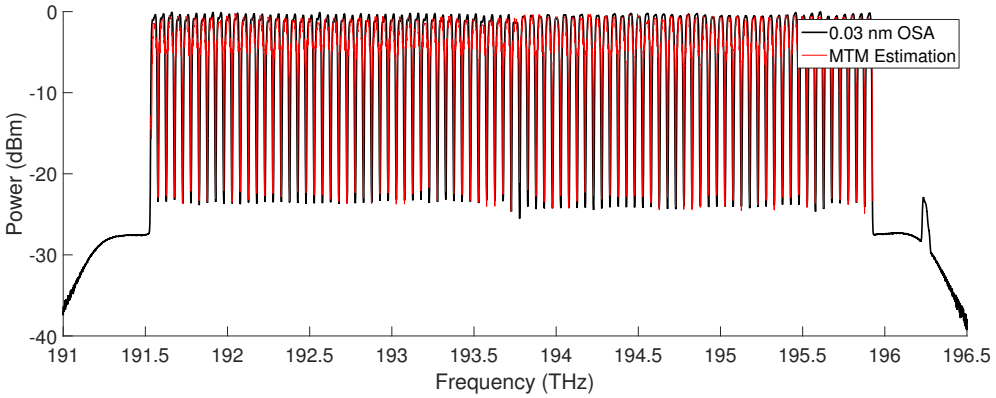

Figure 2.10: Digitally stitched MTM spectral estimation of 88 35 Gbaud PM-QPSK channels over the C-band

2.5 Spectrum Detection and Management

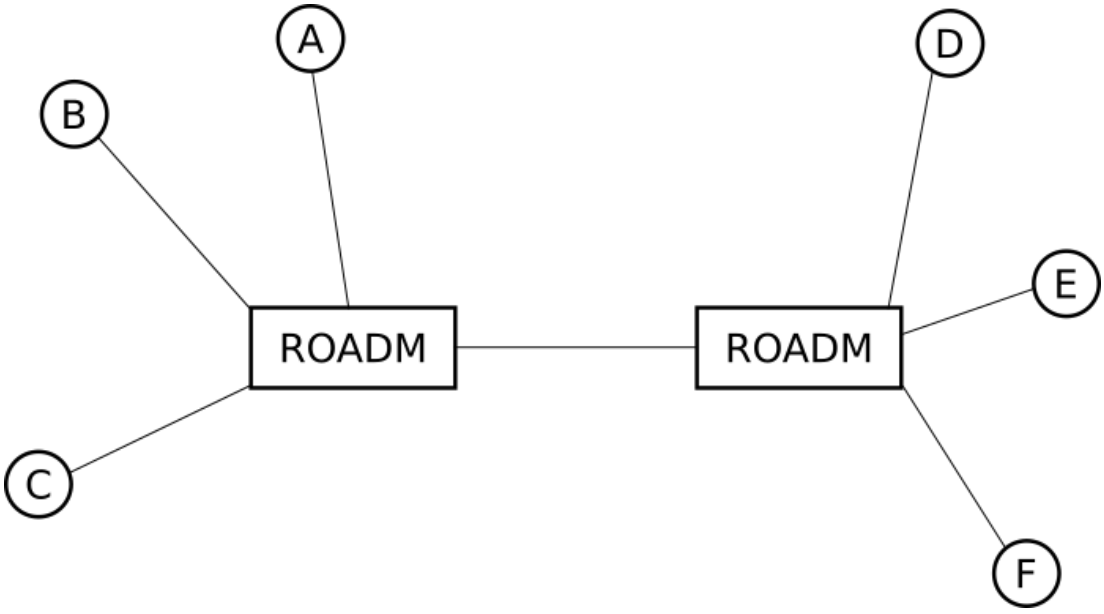

Figure 2.11: Divergently routed 2 ROADM node network topology

In this section, we expand on the previous section's use of a coherent transceiver as a monitoring element, to probe a portion of bandwidth to provision a new channel across a multi node link with in line wavelength add/drop capability. The spectrum estimation method would be easily applicable directly to a wireless network since any interfering channels would be detected if the receiver is sensitive enough. This is analogous to the optical link being a simple point-to-point connection with no intermediate stage add-drop stages. The coherent receiver would be able to quickly sample the optical fields of other signals being transmitted through the fibre and using spectral estimation [40], it would be able to generate a view of the exact spectrum being transmitted as well as further characterize observed channels [41]. However when moving away from a point to point link, this becomes unreliable since there are *unknown actors* on the selected network path, as shown by the example network topology. This is shown in Fig. 2.11 for a simplistic link using 2 ROADMs, if A, B or C wishes to transmit to D, E or F, the transceivers provisioned to setup the link cannot know via spectrum estimation if there is an existing channel setup on its desired wavelength since that lightpath will not reach its transceivers. These *unknown actors* are therefore other network systems that utilize some of the network resources required to establish the desired lightpath that do not terminate at the same physical location as the desired destination.

The spectrum management function of the software defined transceiver contains the process for optical transmission wavelength selection. One of the most crucial functions as the selected channel must not only be vacant but be of sufficient quality to support transmission. It must also be able to decide in a situation where multiple spectral

vacancies are available. This section investigates the BER performance as a metric to infer the channel power of the nearest neighbouring channel, for available spectral slots. By characterizing the BER performance of our probe signal transmitting in one of these slots, we can then deduce sufficient information to initialize the cognitive transceiver. We consider the example network topology shown in Fig. 2.11. The required signal path is transmitted over a length of fibre which passes through two reconfigurable optical add drop multiplexer (ROADM) nodes. Initially we must determine if a wavelength is already occupied. To do this we combine the spectrum estimation algorithm from before with a low power probe. This probe is transmitted over the channels which are deemed vacant by spectrum estimation, which must be investigated. If the probe is not received, the wavelength is in use and was dropped in the middle of the light-path Due to the low power level, the impact on the existing channels is non existent. The deduced vacant wavelength slots are then probed with increasing power to determine its BER performance in the possible presence of unknown interferers. We estimated the power of the nearest neighbours using the BER of the probe channel with respect to its transmission power, and from this characterization determined if operating at this wavelength will give the desired performance. The BER performance will change with respect to the power of the cross phase modulation generated by the interferer channels, impacting the probe channel. We also investigated the impact of the probe on the existing channel BER. A characterization of one spectral slot can therefore allow the cognitive transceiver to deduce the performance of other vacant spectral slots by looking at the power of the deduced neighbouring channels, given no reconfiguration of the network.

2.5.1 Experimental Setup

In this experiment, a commercially available [42] line card is used as the receiver similar to the experiment in section 2.4.2. The line card was also used to transmit a 40 Gbit/s PM-QPSK test signal over 800 km of standard single mode fibre(SMF). Six 10 Gbit/s OOK aggressor channels were added after 200 km SMF at a ROADM. These were generated using 6 separate modulators each independently driven by a 10 Gbaud decorrelated PRBS of length 2^{15}-1, modulating six distributed feedback lasers (DFB) spaced at 50 GHz around the 40 Gbit/s PM-QPSK signal. The combined optical signal is then transmitted over 400 km of SMF to another ROADM. All of the 10 Gbit/s OOK channels were dropped before a single 10 Gbit/s channel was selected to be received. The 40 Gbit/s channel was transmitted over another 200 km SMF and then received by the line card as shown in Fig. 2.12. Dispersion compensating fibre (DCF) was utilized to pre-compensate for 50% of the chromatic dispersion for the 10 Gbit/s channels prior to being combined with the 40 Gbit/s probe, to avoid the non-linearities on the probe

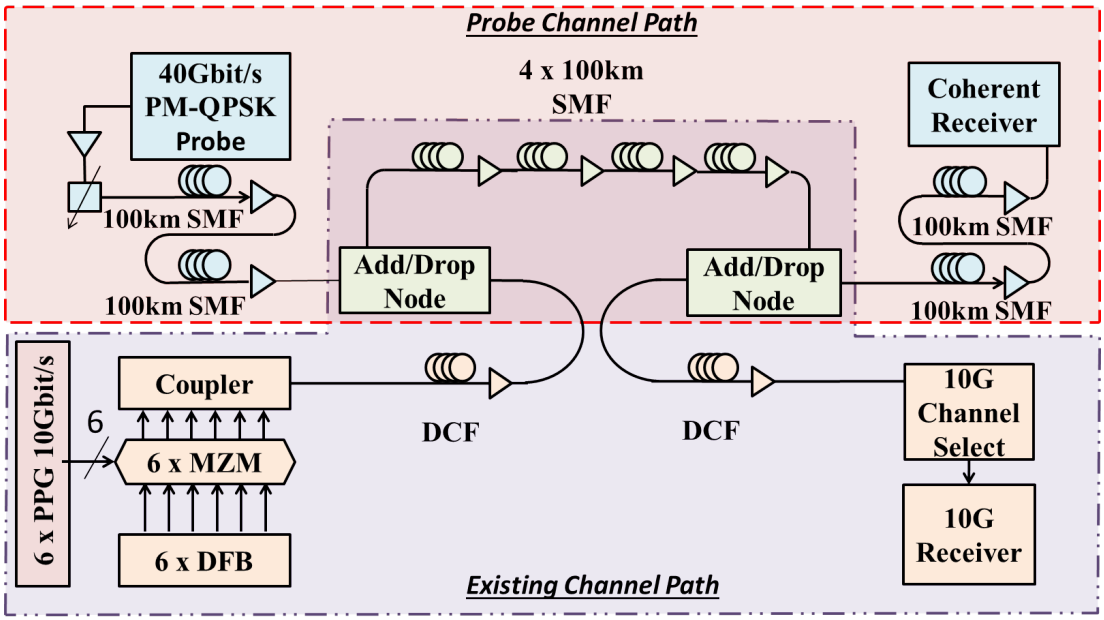

Figure 2.12: Experimental setup incorporating a commercial line card.

channel being increased by in-line dispersion compensation, with the remaining 50% of chromatic dispersion being compensated by the DCF after the 10 Gbit/s channels had been dropped (see Fig. 2.12). The total amount of chromatic dispersion compensated by the DCF is 3,200 ps/nm-km. The line card digitally compensates for the linear impairments (6,400 ps/nm-km of chromatic dispersion), polarization mode dispersion and carrier phase recovery) on the 40 Gbit/s probe channel. We realize the ROADMs of this network setup using Finisar Waveshaper 4000S, couplers and Polatis 16x16 optical switch.

2.5.2 Algorithm

Check for existing data

The algorithm first checks for available information on the network setup before proceeding, e.g. previous characterizations and estimation, knowledge of channels already in service along the proposed transmission path.

Generate spectral slices and Digital stitching

A 50 GSample/s oscilloscope was previously used in addition to a high bandwidth coherent receiver to estimate 50 GHz windows of bandwidth at 25 GHz intervals. This selection allowed for 25 GHz of overlap between two adjacent slices to perform digital stitching. In this proof of concept, a commercially available 40 Gbit/s PM-QPSK line card is used instead. The hardware allows access to sweep the laser frequency of the transmitter/local oscillator up to 12 GHz from the ITU grid in either direction with

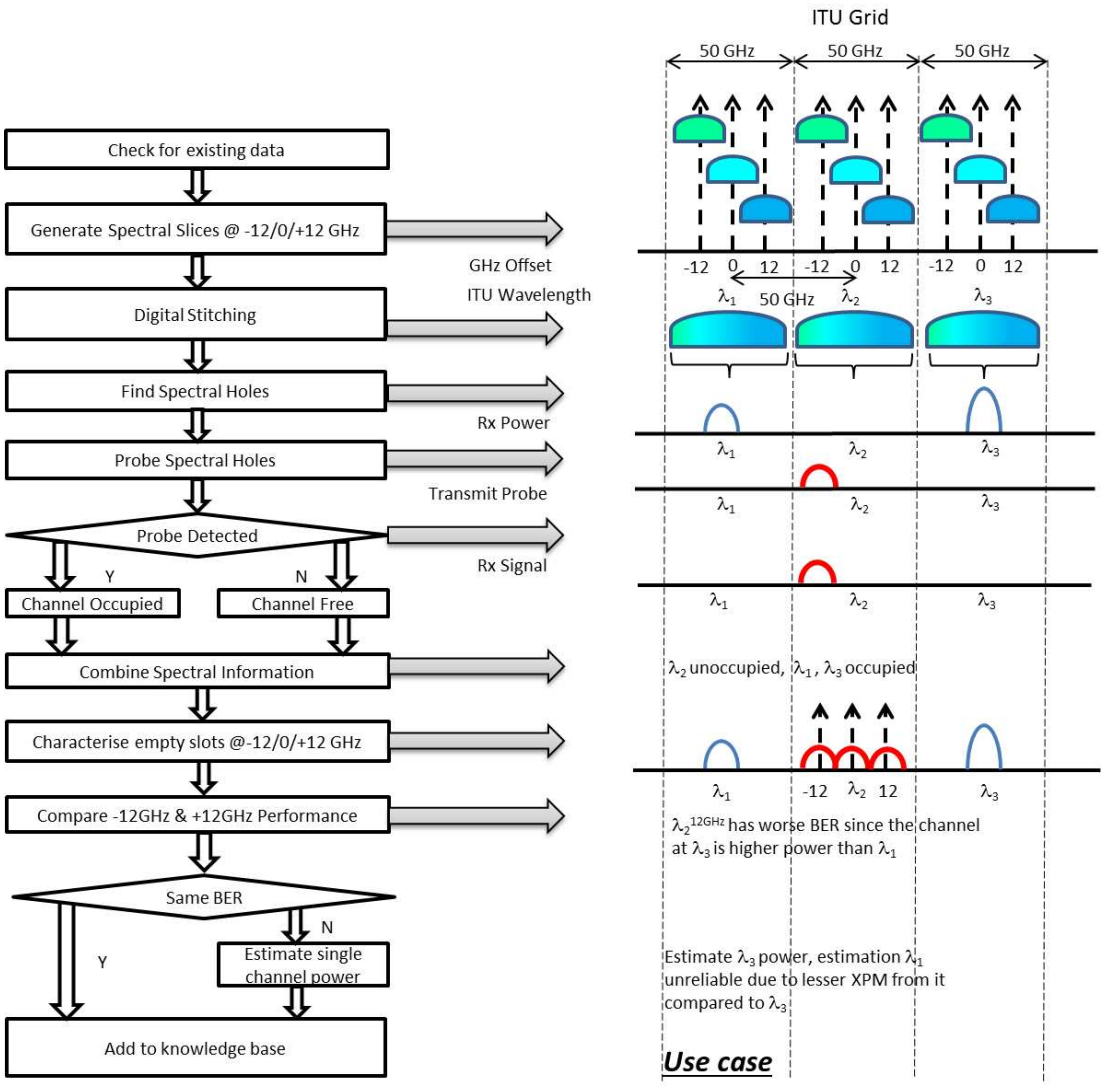

Figure 2.13: Flowchart of the algorithm used to the left, use case to the right.

a sampling speed of 23 GSample/s. To compensate for this, the spectral estimation process is performed with three slices per wavelength instead of two. These slices are taken at the -12, 0 and 12 GHz offset from the ITU 50 GHz grid. As previously, these slices are then digitally stitched for a wider spectral estimation. This digital stitching is performed by cross correlating the overlapping components, aligning the spectral slices and then stitching them together. Overlapping frequency components are averaged. A 3 GHz gap remains between each estimated portion which cannot be estimated, this gap is insignificant given the assumption that 10 Gbaud is the minimum granularity of a transmission channel. The frequency resolution of the estimation is not significant in this work so a relatively coarse estimation of 256 samples is performed at 23 GSample/s compared to the previous [40] 65536 at 50 GSample/s, the technique is employed as a frequency diverse power meter.

Find spectral holes

The spectral estimation is then used to find spectral holes on the 50 GHz grid by integrating across the 50 GHz bandwidth at each point.

Probe spectral holes

A very low power probe is sent along the detected spectral holes, offset 12 GHz from the grid frequency to avoid impacting the performance of existing channels (we assume that the minimum baud granularity is 10 Gbaud as this work is not concerned with access networks which may have baud below 10 Gbaud). The exact power that the probe should be transmitted at should be determined by characterizing a known empty channel, such as one set aside for administration purposes i.e. one beyond channel 1 or 80. A reasonable BER is not required, but it must be detectable and also at a power low enough not to impact channels already in operation. If the probe is received, then the spectral slot is free. If the probe is not detected, then the optical channel at this wavelength has been dropped part way through the link and is therefore in use.

Combine spectral information

The information acquired from the previous steps in the algorithm are then combined to ascertain the occupancy of the spectrum.

Characterize empty slots

The spectral holes which do not have information on their performance within the knowledge base of the cognitive transceiver are then characterized. Characterizing a single spectral hole gives not only the information on its performance but also

information on its neighbouring channels. This comes in the form of XPM, which can be interpreted as a constant noise term if there is no change in the interferer power level. The power of the neighbouring channels can therefore be estimated from the performance of the probe signal. This information is then added to stored knowledge.

This characterization and inference of the neighbouring channel power assumes that both neighbouring channels are being transmitted at the same power level. To account for this, characterization measurements are repeated at -12 and +12 GHz offsets to detect if the adjacent channels are being transmitted at the same powers.

Compare -12 GHz and +12 GHz performance

It is simple to compare the two characterisations if the two neighbouring channels are being transmitted at the same power, the BER at the two offsets should be very close. These specific offsets are the maximum settings accessible with the transmitter used in this experimental setup. Ideally the half way point between allowed optical channel frequencies would be used (25 GHz in this case) since the closer the probe approaches the neighbour, the greater the XPM experienced. This would allow this algorithm to estimate down to lower OOK channel powers. A lower frequency grid granularity would allow for the same effect, however an appropriate look up table would have to be selected. The region of interest is when the BER is at or just below the FEC threshold, and above the point where the non-linear interference from the neighbouring channels is negligible compared to ASE noise. The lower bound of the estimation is the point where the noise floor occurs for the performance of the probe channel. In order to provision the channel, in addition to using the information for future provisioning, it is not necessary to know the exact power in this situation. Similarly, estimation of the power of the aggressor channels when the BER performance is above a FEC threshold is unnecessary since transmission is not possible. This set of characterization measurements is then repeated for all empty wavelength slots that do not already have information about its neighbouring channels. The appropriate slot is chosen and the channel is provisioned.

Add to knowledge base

- Information about the provisioned channel is added to the stored knowledge. Figure 2.13 shows the entire algorithm tree and an example use case.

2.5.3 Experimental Results

A single empty spectral slot with two neighbouring OOK channels on a 50 GHz grid is used to assess the performance of the estimation algorithm. Initially only two aggressor channels are added. The number of aggressor channels is then increased from 2 to 4,

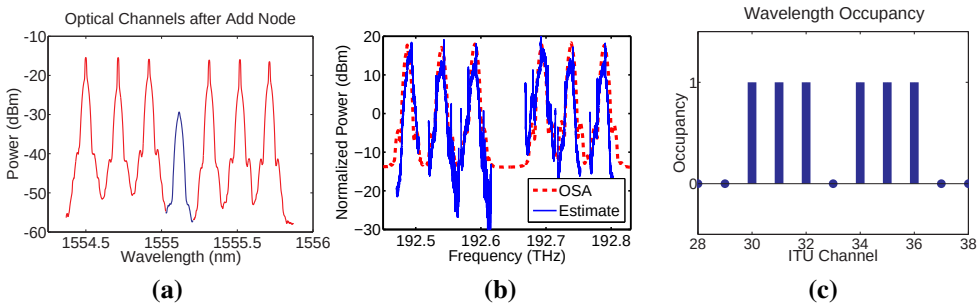

Figure 2.14: (a) OSA trace of the combined co-propagating spectrum, (b) Estimated spectral occupancy of the examined bandwidth, (c) Spectral estimate of 6 10Gbit/s channels.

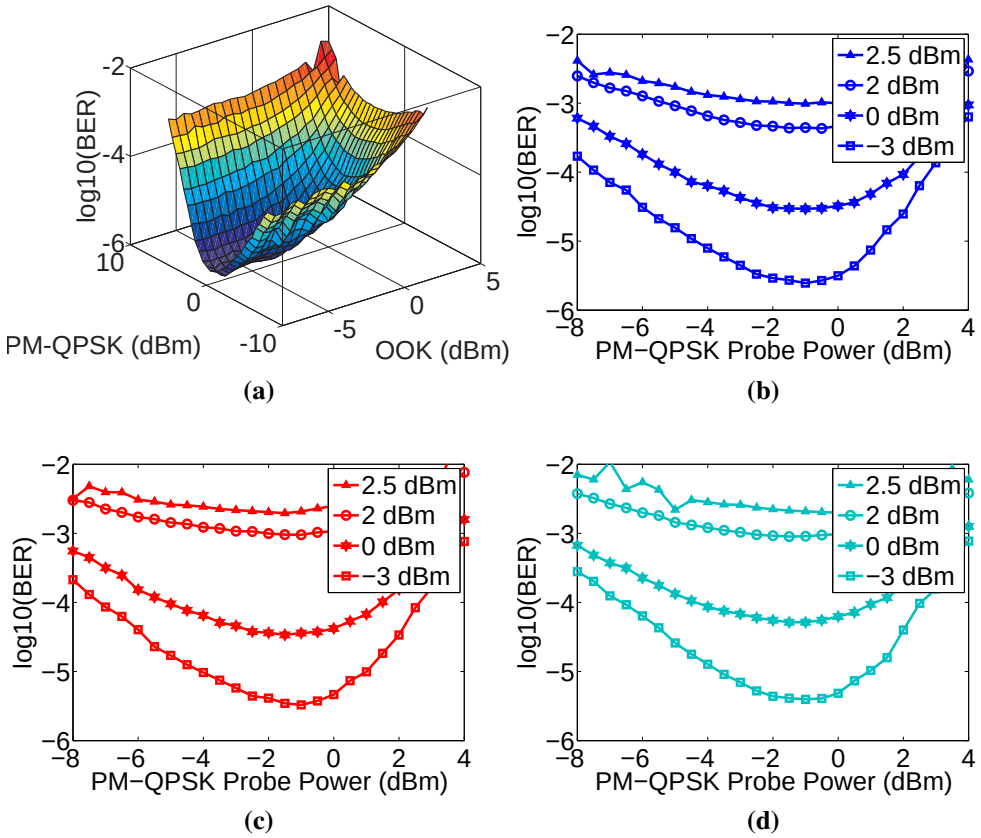

Figure 2.15: BER Performance of probe PM-QPSK channel with 2, 4 and 6 OOK aggressors, (a) surface of power estimation 2 channel look up table, characterizations of prospective transmission channel with (b) 2 , (c) 4 and (d) 6 neighbours at different transmission powers.

and then 6 to examine the impact on the accuracy of the algorithm. Figure 2.14 (a) shows the combined spectrum after the first ROADM node, Fig. 2.14 (b) shows an spectral estimate of 6 10Gbit/s channels and Fig. 2.14 (c) shows the spectral occupancy as detected by the initial part of the algorithm.

The initial configuration with only two aggressor channels is used to create the power reference look up table with the PM-QPSK probe located at 0 GHz offset. The two 10 Gbit/s aggressor channels from -8 dBm to 2 dBm in steps of 0.5 dBm. Higher

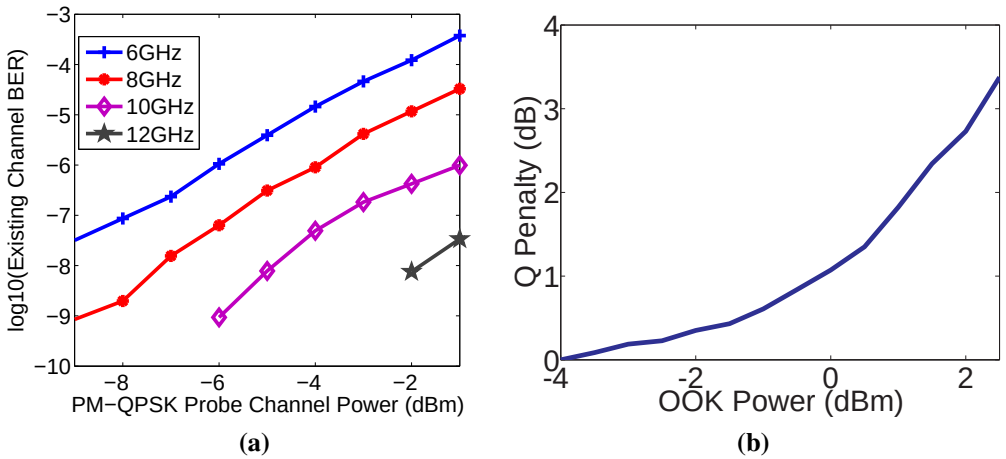

(a) **(b)**

Figure 2.16: (a) Performance of the OOK channel when the probe PM-QPSK signal is moved closer at increasing transmission power. (b) Q penalty incurred by the probe channel at 0 GHz offset, when aggressor OOK power increases.

powers were not investigated since measurement of the BER became unstable. For each power step the launch power of the 40 Gbit/s probe channel is swept from -8 dBm to 4 dBm in steps of 0.5 dBm. This creates the surface plot of BERs as in Fig. 2.15(a). The 40 Gbit/s probe is measured 10 times at intervals of 3 seconds. The averaged BER performance is shown in the BER_{40G} curves for a given OOK launch power. This averaged BER measurement is then compared to the reference *look up table* generated by previous measurements of a system with 2 neighbouring channels. The power of the OOK channels are estimated by taking the lowest BER of the PM-QPSK channel for the test measurement and minimizing the Euclidean distance between the lowest BER of the test measurements and the reference BER. Figures 2.15(b)– 2.15(d) show the measured BER performance of the 40 Gbit/s channel for different OOK channel launch powers, it must be noted that the oscillation in the measured BER in the case of a 6 aggressor channels is caused by a combination of high aggressor power channel in addition to low probe channel optical signal to noise ratio. The effect of moving the probe channel closer to the existing channel is shown in Fig. 2.16(a). It can be seen that the impact of the probe at 12 GHz offset from the existing channel is negligible. Figure 2.16(b) shows the Q factor penalty when increasing the power of the OOK aggressor channels. The estimated OOK power is then plotted against the actual launch power Fig. 2.17(a)– 2.17(c). The estimation algorithm becomes less accurate when the effect of XPM on the probe channel decreases at -2 dBm. Prior to that the estimated power level corresponds to the transmitted power level.

The impact of different numbers of neighbouring channels is measured. It is shown that the BER performance of the 40 Gbit/s channel becomes slightly worse when increasing from 2 channels to 4, however the increase from 4 to 6 neighbours is minimal. The power estimation algorithm remains accurate at high OOK channel powers down to

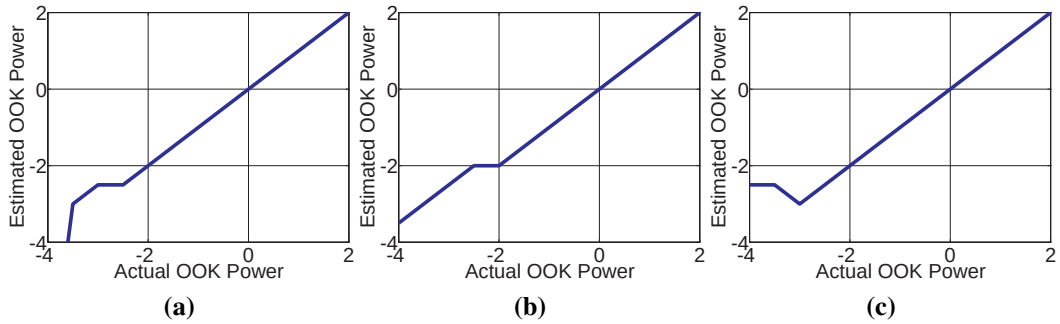

Figure 2.17: Estimation of neighbouring power with (a) 2 channels, (b) 4 channels and (c) 6 channels.

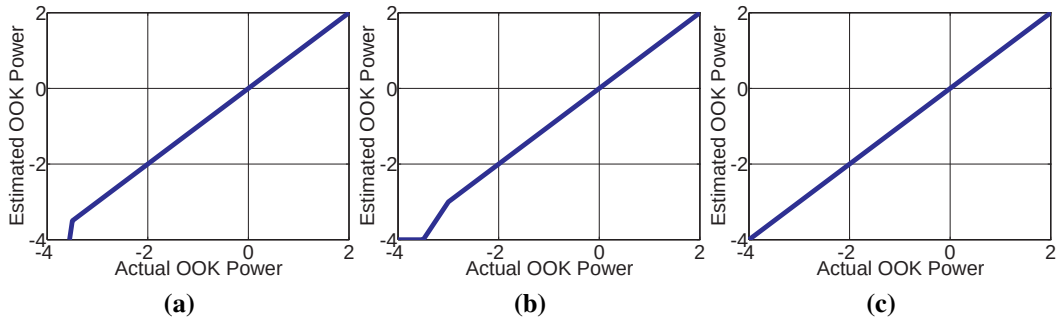

Figure 2.18: Estimation of the higher power neighbour channel using a 6 channel look up table of -/+12 GHz BER performance with one attenuated neighbour, (a) 1, (b) 2 and (c) 3 dBm difference between the two nearest neighbours

-2 dBm (the optimum launch power in this network configuration is 3 dBm), when using the previously generated two channel look up table Fig. 2.15(a). If only 1 neighbouring channel is present, it would be detected by the spectral occupancy test earlier in the algorithm and a more appropriate look up table can then be selected.

The scenario in which the two nearest neighbours are at different powers is investigated. The BER of the probe channel is measured at -12 and +12 GHz from the grid, if they are equivalent then the two neighbours are at the same power. In the previous set of estimation, the performance of the algorithm was limited by the amount of XPM experienced by the probe channel. The probe channel is moved 12 GHz towards the higher channel, which is determined by comparing the BER measured at -12 GHz and +12 GHz. The worse performing offset is then the offset towards the higher channel power. This measurement is then used in the algorithm, using a different look up table to take into account the 12 GHz offset. It can be seen from Fig. 2.18 that the estimation performs accurately down to -3.5 dBm OOK power, an improvement from the previous limit of -2 dBm. The side that the higher power channel exists on is determined by the inequality in BER performance at the two offsets, however estimating the lower power aggressor is unreliable using this approach. We note that it is possible that the neighbouring channels are changing in power, leading to a fluctuation in the measured BER.

The measurements used in this work are averaged over a subset of 10 measurements taken over a period of 30 seconds. By averaging multiple measurements or taking the BER over a longer time-scale, the effects of this fluctuation in BER can be minimized and the composite BER is then used for estimation. However, it is possible that the peak BER is higher than the FEC limit, which would render the channel unsuitable for provisioning.

2.5.4 Summary

In this chapter, the software defined coherent optical transceiver was investigated as a stand alone instrument to investigate its network environment. Initially this was accomplished by exploiting the frequency selective properties of the coherent transceivers to create an estimation of the detected optical spectrum. Due to the bandwidth detectable by the coherent receiver being much smaller than the potential 4.4 THz bandwidth of the optical C-band within which the desired channel can be provisioned, the coherent receiver is used to generate 'slices' of optical spectrum with a size equivalent to the sampling speed of its ADCs. These slices are then digitally recombined to generate the whole estimation of the spectrum. To demonstrate this method, initially a fast frequency tuning DSDBR was used in conjunction with a 50 GHz real time sampling oscilloscope to estimate the spectrum of an unmodulated optical comb and then the comb modulated with PM-QPSK. This spectrum estimation is also useful for remote diagnostic purposes when a coherent transceiver is available.

This spectral estimation and stitching forms the initial part of an algorithm to detect spectral occupancy by using a very low power test optical signal as a probe. The experimental setup was modified to use a commercially available 11.5 Gbaud PM-QPSK line card [42] instead of the standard laboratory setup. The principle of the spectral occupancy detection method is that due to the ROADMs, the test optical channel will never arrive at the receiver if that wavelength is in use, therefore it cannot be used. The very low power of the probe signal ensures that the performance impact on existing channels is negligible as this technique is designed to be used in legacy optical systems utilising 10 Gbit/s OOK signals in which operators are deploying 40 Gbit/s PM-QPSK coherent technology in order to upgrade system capacity.

This work assumes that the software defined transceiver is responsible for self provisioning and has no information on the network level. Extensive pre-calibration is also required to generate the set reference look up tables on a system the same or very similar to the transmission system. A set of measurements matching the current network conditions is required to for accurate algorithm performance and also to ensure that the network cannot go outside these bounds and therefore outside the algorithm's performance regime. Since this work was performed, it is increasingly likely that further integration will happen from the network layer to the physical layer with a SDN controller existing to abstract the physical provisioning for application use. Accordingly later chapters of this thesis shift to examining how to most efficiently provision optical systems.

3
Probabilistic Design

3.1 Abstract

In this chapter, an overview of the deterministic design methodology utilised in optical systems is described. An alternative design process is investigated for use in optical systems called probabilistic design. The benefits of probabilistic design are demonstrated in an experimental WDM system transmitting PM-QPSK and PM-16QAM by introducing uncertainty into the intra-link power profile. Initial experiments were conducted using single channel transmission at 11.5 Gbaud modulating PM-QPSK over 4 and then 10 spans of 100km SMF. This was later increased to 11 channel WDM transmitting PM-QPSK and PM-16QAM at 35 Gbaud over 10 spans of 80 km SMF. In all cases, probabilistic design was shown to decrease the outage probability with respect to a deterministically designed system at the cost of the average link performance. A three parameter model was proposed to fit the performance of a link with such optical power uncertainties. The initial results obtained using single channel PM-QPSK were fit to the model and were consistent over the worst case scenarios over a several different uncertainty magnitudes. The model was further validated by prediction of the WDM PM-QPSK and PM-16QAM performance using parameters acquired from fitting to an ideal reference performance.

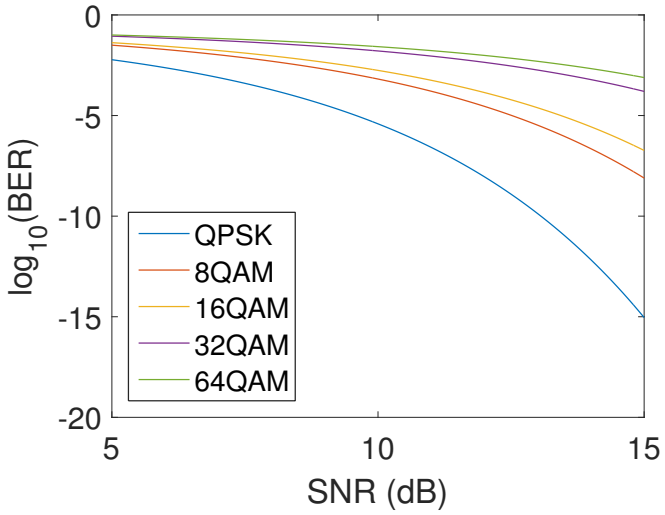

Figure 3.1: Theoretical performance of QPSK, 16QAM, 32QAM and 64QAM modulation formats

3.2 Introduction

The design and implementation of an optical network has traditionally been quite straight forward. A generalization of the design process is if the light path specified provides sufficient performance to enable the desired capacity for the duration of its service life. At first glance the light path performance can be determined from [43].

$$OSNR_{dB} = 58 + P_{tx} - Loss_{span} - NF - 10 \times log_{10}(Number\,of\,Spans) \tag{3.1}$$

Equation 3.2 provides an estimation of the OSNR over 0.1 nm of bandwidth at the end of the specified optical fibre link, P_{tx} is the signal's launch power in dBm, $Loss_{span}$ is the attenuation experienced by the signal per span, NF is the noise figure of the optical amplifier per span, assuming lumped amplification. The 58 is based off of $h\upsilon f$ where h is Planck's constant, υ is the photon frequency and f is the OSNR reference bandwidth.

The criteria for the required link performance for a certain transmission system configuration that will enable the required capacity has traditionally been labelled as the ROSNR. The difference between the OSNR after transmission through the link and the ROSNR is the performance margin inherent to the optical system and that specific optical signal. The ROSNR itself is dependent on the type of modulation being carried by the optical signal being transmitted, vendor specific implementation of the hardware components as well as digital signal processing at the transmitter and the receiver. The theoretical relationship between OSNR and BER can be found in [44].

Figure 3.1 shows the theoretical BER performance of a selection of modulation formats with respect to SNR. The margin calculated using the theoretical performance would therefore be the maximum possible margin available. In practice there exists an implementation penalty for each modulation format which decreases the available

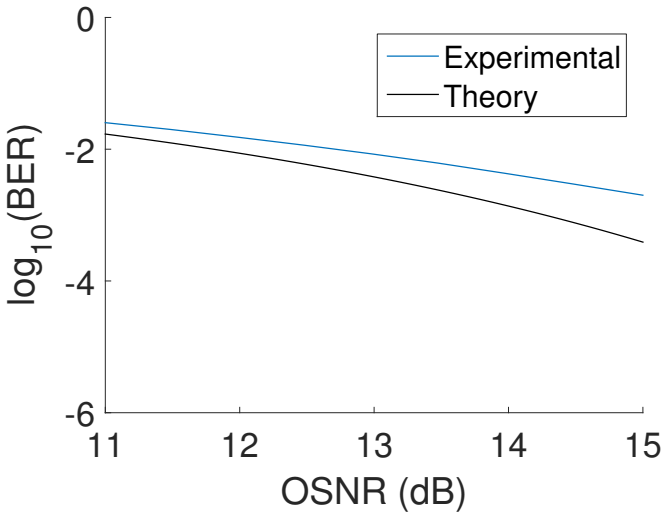

Figure 3.2: Experimental 35 Gbaud PM-QPSK back to back performance

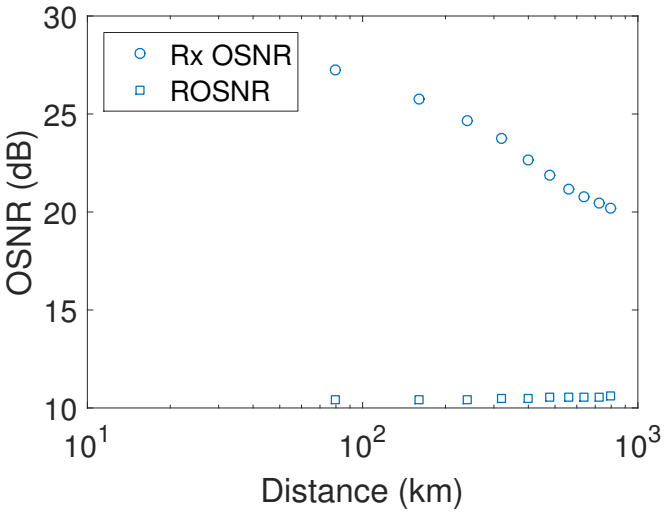

Figure 3.3: Evolution of ROSNR (for 3.4% bit error rate) and received OSNR (Rx OSNR) with distance in a system with 80 km spans of SMF for a 35 Gbaud PM-QPSK WDM system launched at 1.5 dBm

margin.

This can be seen in Fig. 3.2 where a 35 Gbaud PM-QPSK signal is examined by connecting the transmitter directly to the receiver while coupling in optical noise of variable power in order to determine its performance in different OSNR regimes. It is clear that the practical implementation does not perfectly align with the theory due to the aforementioned implementation penalty, in addition the penalty in general increases as the required BER threshold decreases.

The change in the received OSNR is shown in Fig. 3.3 for the PM-QPSK signal, transmitting over 80 km spans of SMF. As expected the received OSNR decreases with distance due to the addition of extra EDFAs to compensate for the fibre span loss. It should be noted that there is a slight increase in the ROSNR with respect to distance due to the fibre non-linearity which has cubic relationship to the power of the optical

signal and its effect can be described in SNR as

$$SNR_{eff} = \frac{P_{sig}}{P_{ase} + P_{nl}} \tag{3.2}$$

where $P_{sig}, P_{ase} and P_{nl}$ are the power of the optical signal, ASE noise and non-linear noise in watts and SNR_{eff} is linear. Increasing the launch power also increases the OSNR as per Eqn. 3.2, therefore system designers will increase the optical power to maximize the OSNR margin. In practice, this is limited by the non-linearity of the optical fibre [45] [46], creating an optimum launch power. At the optimum, the margin is then used to account for various factors that might impair the performance of the optical system, such as the effect of ageing. An optical system is a significant investment that is expected to operate on the order of a decade, however it is realistic to expect that components will experience wear and tear due to operation, therefore deteriorating the performance. This is the most obvious factor to account for. There are other numerous factors such as factory calibration tolerances, wavelength dependent gain profile of the optical amplifiers, maintenance work on the fibre being used incurring extra loss (re-splicing broken fibres), time dependent polarization effects. At least some of these have to be accounted for when designing the optical system. A guideline on link parameter tolerances has been established by the ITU [47].

After all these factors are included, then what is left of the margin is used to account for unforeseen events or upgrade possibilities, such as the migration from WDM to DWDM which moved to a 50 GHz frequency grid, putting channels closer together, therefore increasing the non-linear XPM experienced by the channels. The DWDM grid therefore traded margin for system capacity.

This approach of designing at the optimum and then provisioning margin is deterministic design methodology. If all link parameters were constant and precisely known to the design engineer then system performance could be predicted quite easily, allowing for the minimal required margin. In practice, the amount of margin added to account for the aforementioned link impairments and component design and performance that are within a specified tolerance is based on measurement of previous systems, and the engineer's judgement. The amount of margin specified for a system is inversely proportional to the likelihood of failure. It is not known exactly how safe an applied margin is.

3.3 Probabilistic Design

Deterministic design methodology relies on what is believed to be good enough based on previous similar systems and projected performance of the system under design. An example of this is in the early 1930s, where a 1.5 factor of safety became a formal requirement of the United States Air Corps. This factor evolved alongside other design requirements in an effort to rationalise aerospace structural design criteria. This factor hasn't changed despite problems and structural failures, instead changes were made to design specifications, load prediction and manufacturing techniques. The 1.5 factor is based on what was considered to be representative ratios of design to operating manoeuvre load experienced by aircraft in the 1920s and 1930s. The adverse tolerances necessitating this 1.5 factor are however unknown.

The deterministic design methodology has long been in use in optical telecommunications when optical systems operated on a very widely spaced frequency grid using low baud OOK transceivers. These systems had a large amount of margin available, especially with the introduction of the EDFA [48]. To the present day, the introduction of coherent transceivers increased the sensitivity of receivers as well as allowed for higher bit rates while maintaining the same baud (40 Gbit/s PM-QPSK replacing 10 Gbit/s OOK), while still having a large amount of margin. It is easy to overlook just how far optical telecommunications has come over the past three decades. The conservativeness of deterministic design made it attractive since there was a limited amount of information on system performance, due to the relative immaturity of the currently deployed technology because of the introduction of the EDFA and coherent transmission. A deterministic worst case was used to ensure sufficient link margins against uncertainties. This is also quite a practical approach from both the engineering and management viewpoints as shown by its dominance in industry. There is however no information on the likelihood of failure and therefore is impossible to perform risk assessment or cost trade-off analysis. The requirement for higher capacity has necessitated the introduction of higher order modulation formats which require a higher OSNR to maintain the same BER. This in return reduces the available margin which can be allocated to deterministic design therefore a more sophisticated approach to network design is required.

The alternative design methodology is probabilistic design, it is not an unknown philosophy but one that has been applied to many other fields such as aerospace [49, 50], earthquake hazard assessment [51], nuclear reactors [52] and deep space telecommunication systems engineering [53, 54]. The driving factor behind the switch to probabilistic design as opposed to deterministic design has largely been consistent across a number of fields, albeit with some differences in application. Primarily in telecommunications, this has been a dissatisfaction with the amount of margin required

[54, 55], and an attempt to engineer the system for a desired amount of reliability. In other fields it has been the other side of the coin to attempt to assess the risk of a particular design. This is understandably a greater driving factor in fields such as nuclear power generation.

The philosophy of probabilistic design is to treat all design parameters of the system as variables and from that obtain a probability of failure. Therefore the crux of this methodology is to have a deep understanding of the design parameters, they must be statistically defined either by experimental measurement, numerical or analytical research. This knowledge allows for in depth analysis of the designed system such as :

1. Probability of failure
2. Design variability
3. Optimum inspection intervals
4. Cost reduction scenarios

Probabilistic design therefore also knows the contribution of each parameter to the overall likelihood of failure, this enables design and manufacturing to focus efforts on the greatest contributors to optimize the system. Once the probabilistic model is created for the system, the parameters can then be varied to yield acceptable solutions. The model can be used for sensitivity analysis and/or optimization.

The process of probabilistic design can be laid out into the following steps as in [53], similarly for optical telecommunications:

Step 1 Optical telecommunications systems are designed to be ideal, therefore they only have the design specifications and an adverse tolerance. These two numbers are assigned to most link parameters in a DCT. The measure of how well an optical system performs is generally related in BER, therefore the impact of the adverse tolerance upon BER is what is critical. Some like Kerr generated non-linear noise can be modelled as AWGN) which as in Eqn. 3.2 is a straight penalty to the performance. Effects on the optical signal such as amplifier gain [56], chromatic dispersion [7] and similar effects are wavelength dependent and also the amount of cross phase modulation experienced by an optical signal depends on the other optical signals being co-propagated with it. This leads to a very complex DCT.

Step 2 The link parameters specified in the DCT should be arranged into independent groups.

Step 3 These independent groups should have a joint probability density function of the group of link parameter adverse tolerances on the signal.

Step 4 The mean and variance of each group can then be computed.

Step 5 These means and variances can then be applied to the model ideal system to estimate the performance of the equivalent deployed system.

Probabilistic design of an optical telecommunications system is complex due to the non-linearity of the transmission medium. The power of the non-linear noise has a cubic relationship with optical power, which implies that even if an input parameter is normally distributed, the effect on performance may not be equivalently shaped. Other effects such as polarization dependent loss [57] are also impacted by this. The coherent receiver is however a very powerful tool to mitigate some of these adverse tolerances which as shown later can simplify the design process. This does not change the fact that the optical system is an inherently non-linear transmission system at which the optimum design balances on the edge between a pseudo-linear system and non-linear. Other transmission systems such as those used in deep space telecommunications [54] may assume a normally distributed design parameter to have a normally distributed effect on systems performance. In an optical system this not be the case and in this chapter the non-linear link design parameter is investigated.

In principle there is no need for margin when using probabilistic design. In practice, there will likely be a need for some margin since it is unrealistic to have perfect information on the exact probability distributions of the link parameters. However, the amount of margin required will be greatly reduced.

3.3.1 Probabilistic Design - Link Power Investigation

One aspect of link design that is seldom heard about in research is the manufacturing tolerance of components. An example of this is the optical amplifier, the factory is supplied a specification for the allowable tolerance. The smaller the allowed tolerance, the more costly it is. In this section, we examine the effects of this uncertainty in the channel power and how probabilistic design can provide more optimal provisioning options for optical communications in an experimental laboratory setting. Another situation that may cause this difference in loss budget is fibre splices required for repair [58].

The system under investigation is a link with multiple fibre spans. The uncertainty in the optical power input to each span is simulated using a fixed value perturbation with an equal likelihood of positive or negative summation relative to the 'ideal' optical power which is the power input to the previous span (i.e. the loss of the previous fibre span is perfectly compensated). Given a sufficiently large number of spans, this approximation should hold via the central limit theorem. This approximation also allows for the sum of adverse tolerances i.e. worst case scenario to occur without doing

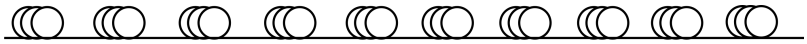

Binary Word	0	0	1	0	1	1	1	1	0	0
$P_{SPAN\ INPUT}$(dBm)	-1	-2	-1	-2	-1	0	1	2	1	0

Figure 3.4: Binary code word for a 10 span system

an extensive experiment of normally distributed perturbations. For a system with N number of spans, there are 2^N different combinations. Therefore each combination can be represented by it's own N bit binary word with a '0' representing a negative perturbation and a '1' representing a positive perturbation, as in Fig. 3.4

4 Span System - Experimental Setup

Initial investigations were performed using the experimental setup detailed in Figure 3.5. using a commercially available 46 Gbit/s line card, modulating PM-QPSK at 11.5 Gbaud over 4 spans of 100 km standard SMF. Each span is followed by a gain flattened EDFA with a nominal noise factor (NF = 4.5 dB). Six 10 Gbit/s BPSK channels are used as 'load' channels and co-propagated through the link to load the EDFAs, these channels are transmitted at constant power and affected by the intra-link perturbations. These channels are distributed through the optical C-band and the closest BPSK channel is 5 nm away from the test PM-QPSK channel which is located at 1550.52 nm. Each span and transceiver is connected through an optical switch which provides integrated power monitor and variable optical attenuation (VOA) capabilities. This functionality is used to perturb the input power to each span, relative to the previous span. In the case of the first span, it is relative to the transmitter launch power. The 4 span system has $2^4 = 16$ different possible configurations. The applied optical perturbations are 0.5, 1, 2 and 3 dB, the PM-QPSK optical power is incremented from -8 to 8 dBm in 0.5 dB steps. The test signal is then band-pass filtered using a 50 GHz filter before being received by the line card's receiver. Standard commercial coherent digital signal processing is performed in real-time as it is a product on the market. The system is allowed to rest before BER measurement is performed to allow the line card to re-lock its DSP if needed and for the EDFAs to reach a stable state. The BER measurement is taken over 1 second.

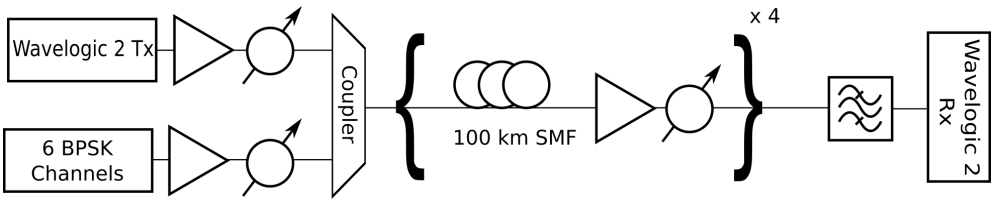

Figure 3.5: Experimental setup for 4 100 km SMF span system propagating a 46 Gbit/s PM-QPSK test channel

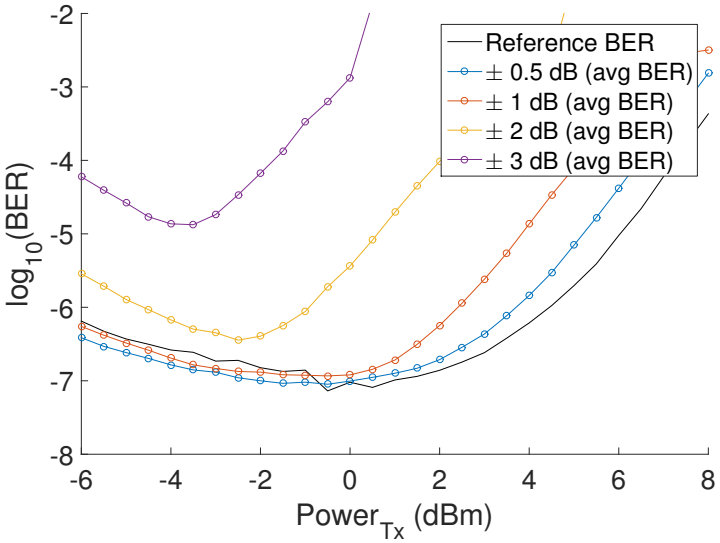

(a) Average BER performance over 16 different code words per test channel power

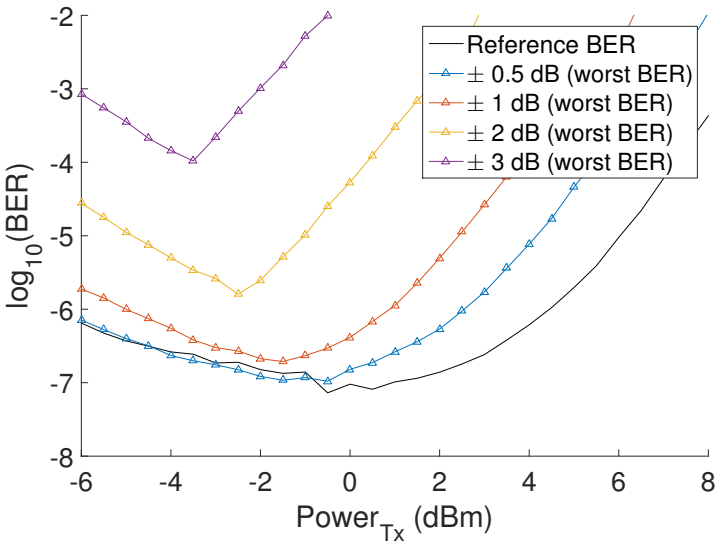

(b) Worst BER performance over 16 different code words per test channel power

Figure 3.6

4 Span System - Results

Figure 3.6a shows the averaged BER performance over the 16 different cases per the 33 different launch powers for each perturbation, the worst case performance is shown in Fig. 3.6b. Typically, the binary word causing the worst case BER switches from a monotonically decreasing power profile, the '0000' code word in the linear regime and the '1111' code word where the test signal system monotonically increases in power. The linear regime being described as the launch powers lesser than the optimum launch power of the ideal system. The non-linear regime are the launch powers greater than the optimum. In the linear regime, the '0000' code word decreases the signal power, thereby decreasing the SNR of the signal which translates into an increase in the BER. In the

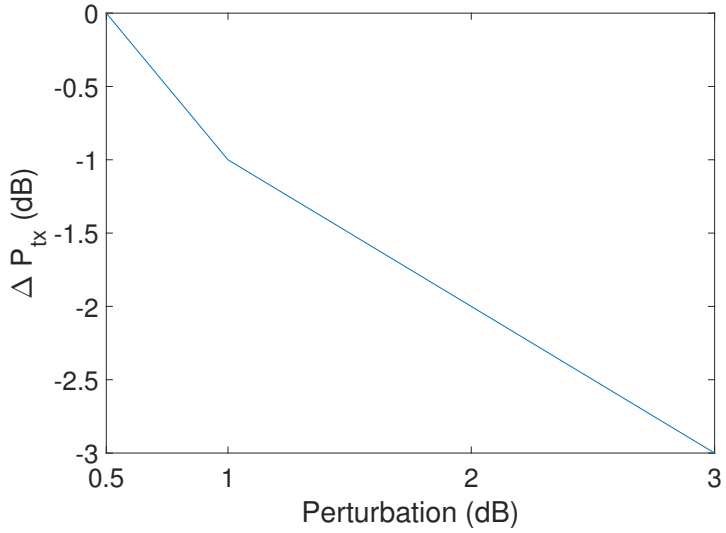

(a) Change in optimum launch power with respect to perturbation

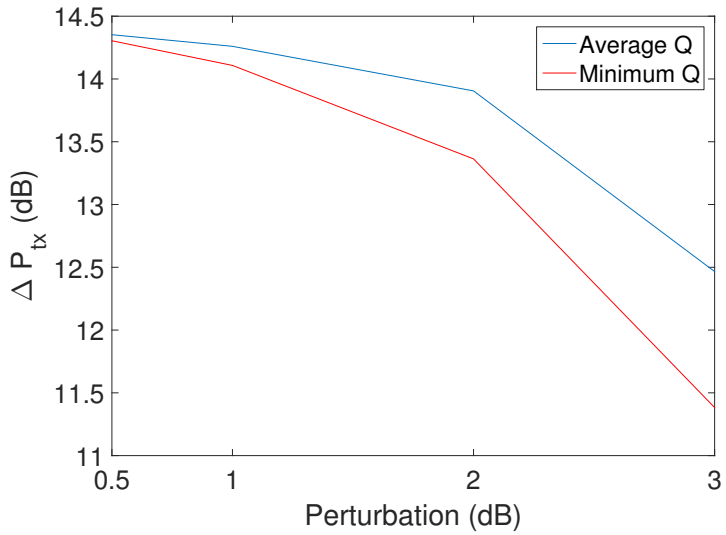

(b) Change in Q for the average and worst case with respect to perturbation

Figure 3.7

non-linear regime, the increase in optical power of one deviation per span increases the non-linearity experienced by the optical signal which then decreases the effective SNR of the signal. The best case is therefore the opposite of the worst case in their respective regimes. Around the optimum launch power, this swaps to one of the intermediate states. The average BER performance across the 16 different states is highly influenced by the worst case's performance due to the dominance of the worst case BER. The impact of the perturbation on the optimum launch power is shown in Fig. 3.7a. Due to the cubic dependence of the non-linear Kerr effect on the optical power, the optimum launch power is reduced with an increase in the magnitude of the applied perturbation. Figure 3.7a shows the change in the signal Q at their respective optimum launch powers as the perturbation magnitude increases. It should be noted that at the extreme value

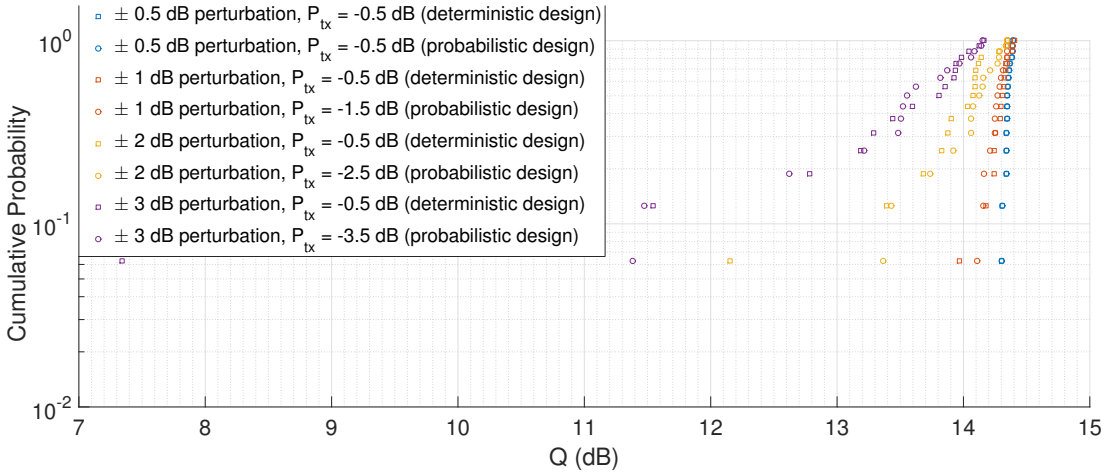

Figure 3.8: Cumulative probability for the performance of the 4 span system for deterministic and probabilistically designed systems

of a 3 dB perturbation, a system launching at the optimum launch power of an ideal system at 0.5 dBm, the BER would be greater than a HD-FEC threshold for correcting transmission errors, while if the system was launched taking into account the sum of adverse tolerances, i.e. probabilistically designed, the system would remain operational. The trade-off is essentially the difference between the performance of the ideal system at its optimum launch power and the compared to the same system's performance at the probabilistically designed optimum launch power, this is an increase from 10^{-7} BER to 3×10^{-7} for a system designed for a 3 dB perturbation, shown by the reference BER at 0.5 dBm power compared to -3.5 dBm power in Fig. 3.6b. This is not a concern since it remains below the BER threshold for the HD-FEC. Figure 3.7b shows the effect of perturbation on a system implemented with probabilistic design. The cumulative probability of the system performance is shown in Fig. 3.8. The deterministically designed point at a 3 dB perturbation which has a $Q \approx 7$ dB is below the equivalent Q threshold of ≈ 8.5 ($BER = 3.8 \times 10^{-3}$) and therefore does not work, compared to the probabilistically designed system has a $Q \approx 11.4$ dB in the worst case scenario, an increase of nearly 4.5 dB which does not have to be accounted in system margin.

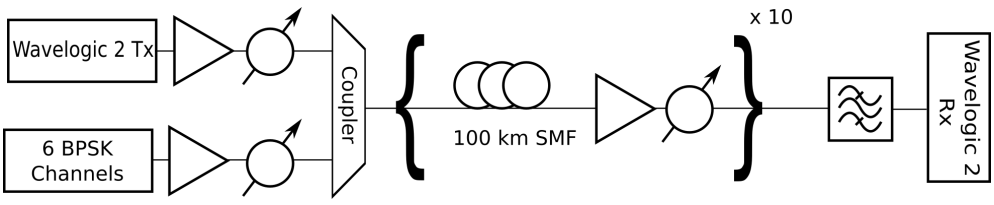

Figure 3.9: Experimental setup for investigation of perturbation in a 10 x 100 km SMF span system

10 Span Single Channel System - Experimental setup

The experimental setup from Fig. 3.5 is extended by another 6 spans of optical fibre to create a system with 10 x 100 km span of SMF. The same configuration of transceivers with a single test 46 Gbit/s PM-QPSK signal is co-propagated with six 10 Gbit/s BPSK signals. The main difference this has on the experiment is that the number of link configurations that will be examined increases from $2^4 = 16$ to $2^{10} = 1024$. The perturbations applied are 0.1, 0.3, 0.5, 0.7 and 1 dB in magnitude. These are smaller in value since using the same values as the 4 span system would require the EDFA output power to exceed their capabilities by the end of the link. The power from the transceiver is swept from -4 to 4 dBm in steps of 0.5 dB. As before, the perturbations are a fixed magnitude with equal likelihood of positive or negative application. Each measurement takes about 8 seconds for the system to settle in addition to BER measurement. The set of measurements comprises 87,040 measurements and is at the limit of what can be accomplished in a reasonable amount of time.

10 Span Single Channel System - Results

Figure 3.10a shows the averaged BER over the 1024 different possibilities for all launch powers per each of the 5 different power perturbations per span, Fig. 3.10b shows the worst case BER. The binary word causing the worst case remains similar to the 4 span system, i.e. '0000000000' and '1111111111' for a monotonically decreasing and increasing power profile in the linear and non-linear regimes respectively. We see again that the average BER performance is heavily influenced by the worst case due its higher BER even though the number of link configurations is increased to 1024, Fig. 3.11a shows the change in optimum launch power with the increase in perturbation magnitude. There is again an almost linear behaviour with respect to perturbation, similar to the 4 span system. However, this should be taken with some caution as it may not hold for other systems. The effect of the applied perturbations are shown in Fig. 3.11b in Q (dB) for the average and worst case performance, there is a deterioration of up to 3.7 dB in the worst case performance when the perturbation magnitude is increased to 1 dB per span, representing a Q of 9.7 dB. This leaves a margin of 1.2 dB in system performance relative to a HD-FEC threshold of Q = 8.5 dB. For a deterministically designed system is reached however it can be seen from Fig. 3.10b that the BER at its optimum launch power is significantly above 3.8×10^{-3} making this system inoperable for transmission. Figure 3.12 shows the cumulative probability across all 1024 cases for the optimum launch power in both the deterministically and probabilistically designed systems. At 0.1 dB perturbation there is effectively no difference between the two methodologies, there is a 0.1 dB difference in the worst case at 0.3 dB perturbation, extending to 0.6, 1.4 and 3.7 dB difference at 0.5, 0.7 and 1 dB magnitude perturbation. The worst case

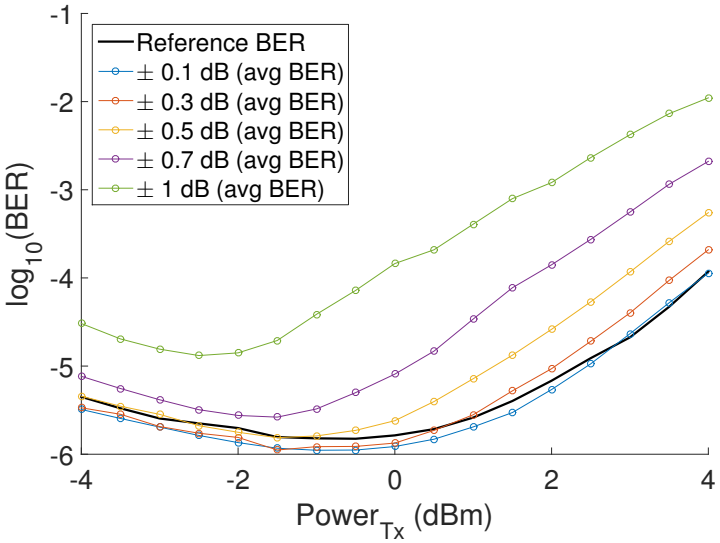

(a) Average BER performance over 1024 different code words per test channel power

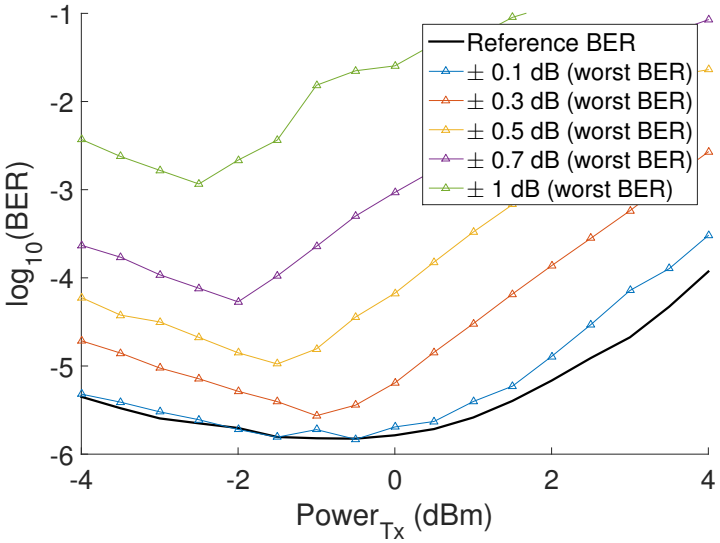

(b) Worst BER performance over 1024 different code words per test channel power

Figure 3.10

for 1 dB perturbation represents an outage probability of 0.2% for a deterministically designed system.

Theoretical Model

It is clear from the above results that applying a probabilistic design philosophy to designing an optical network can remove a significant proportion of the currently specified margin. To most accurately model this, it is required to model the probabilistic distribution functions of the system parameters, along with their respective impact on system performance. The experiment detailed previously involved non-linear fibre propagation over 87,040 measurements, using real-time transceivers enabled a measure-

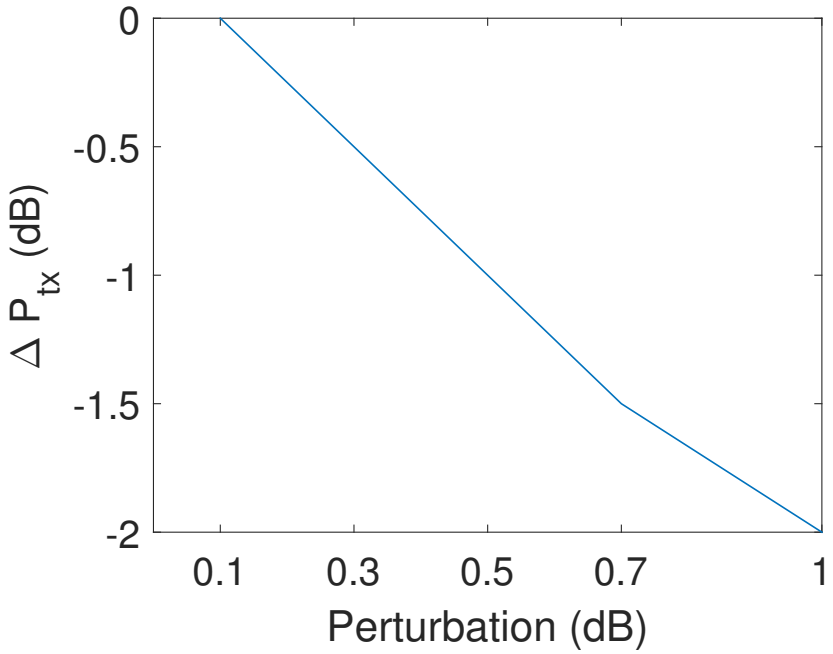

(a) Change in optimum launch power with respect to perturbation

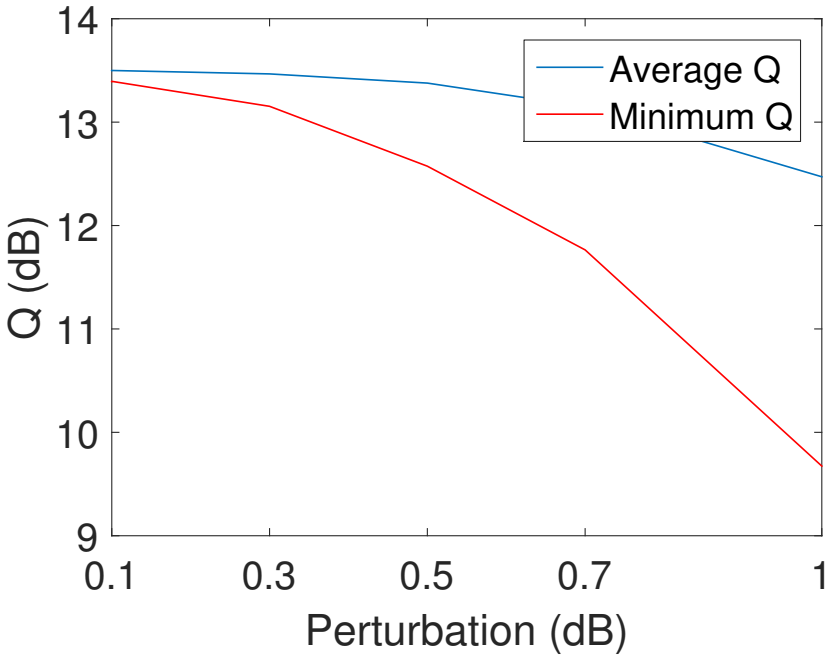

(b) Change in Q for the average and worst case with respect to perturbation

Figure 3.11

ment time of 8 seconds per scenario. To do a Monte Carlo style investigation would involve a much greater number of measurements. Therefore it is desirable to have a method of examining a multitude of scenarios while still obtaining within a reasonable time frame results with sufficient accuracy. In this respect, it should be noted that simulation investigation of the perturbed cases was not conducted due to the computational cost required for split step fourier non-linear propagation. One possibility is to use an analytical model such as the GN model [59]. These models calculate the non-linear

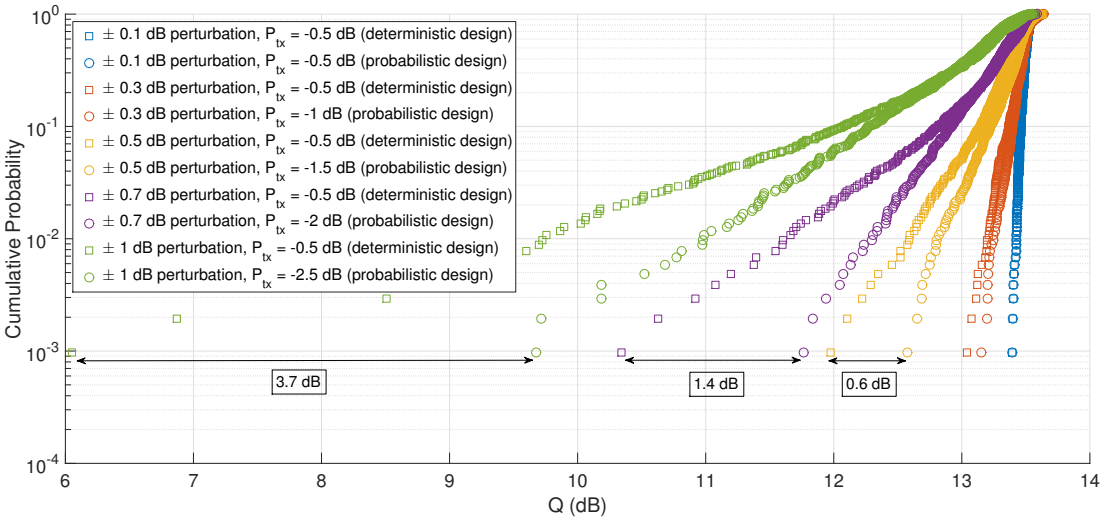

Figure 3.12: Cumulative probability for the performance of the 10 span system for deterministic and probabilistically designed systems

noise power which is then used in Eqn. 3.2 to calculate the BER. We propose a three parameter model on the basis that the non-linear noise power accumulates incoherently across the fibre spans, hence they can simply be added. The model is as follows:

$$NSR_{span} = \frac{b + cP_{span}^3}{P_{span}} \tag{3.3}$$

$$NSR_0 = a \tag{3.4}$$

$$NSR_{total} = \sum_0^n NSR_{span} \tag{3.5}$$

Where a is the B2B transceiver noise, b is the amplifier ASE noise and c is a non-linear coefficient scaling the non-linear noise power, NSR is the noise to signal ratio, used here for ease of presentation.

To examine the validity of the model, we fit it to the worst cases for perturbations greater than 0.3 dB. The worst cases are used since the extreme values are of most interest for outage probability. Figure 3.13 shows this fit with parameters $a = 0.0284$, $b = 8.4509 \times 10^{-7}$ and $c = 791W^{-3}$. Most importantly, the model fits across the 4 sets of perturbation values using the same parameters. This indicates that it may be a good method of describing an optical system.

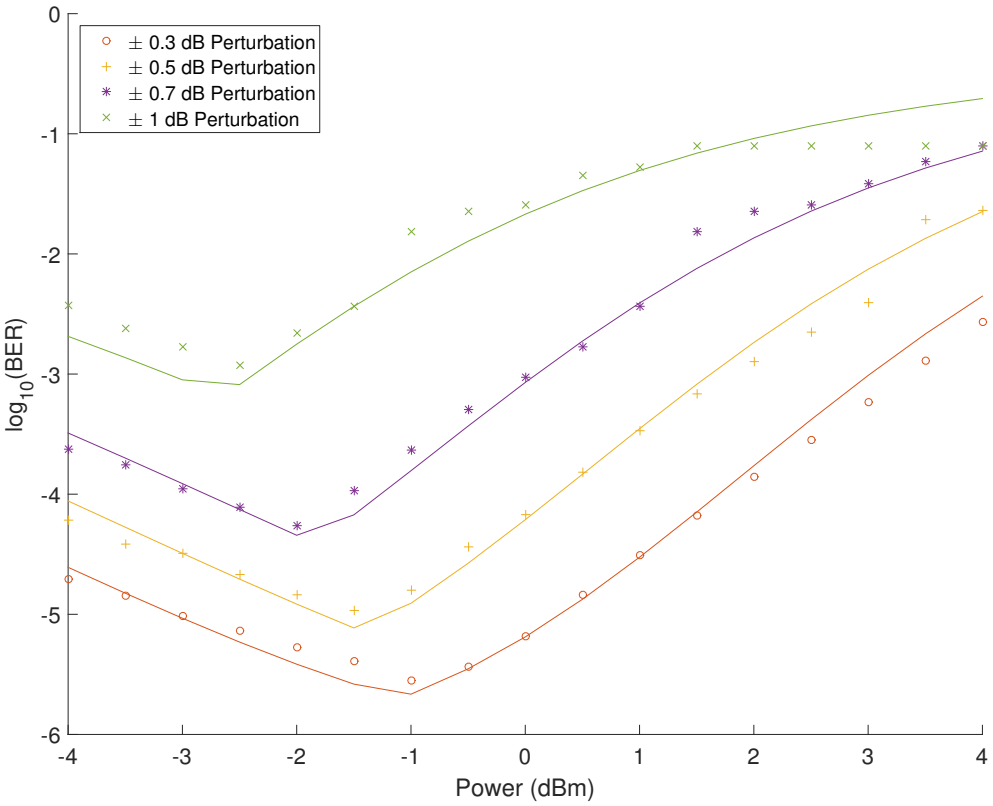

Figure 3.13: Fit of the BER performance for the worst case performance

10 span WDM system - Experimental Setup

The previous experimental investigations were performed using a single channel system. This is unlikely to be the case in a deployed system, WDM channels on a 50 GHz frequency grid are more likely to be provisioned. Therefore the experiment is expanded to a WDM system. The experimental setup is shown in Fig. 3.14, a commercially available 35 Gbaud transceiver [14] capable of modulating PM-QPSK or PM-16QAM is used to generate the test signal at 1547.316 nm. 10 external cavity lasers with nominal line width 20 kHz are bulk modulated using a modified version of the test signal modem with the same modulation format as the test signal at 35 Gbaud , these channels are then independently optically de-correlated before being recombined using an AWG. The de-correlated WDM channels are then combined with the test channel on a 50 GHz frequency grid using a WSS which also equalizes the channel power. Nyquist

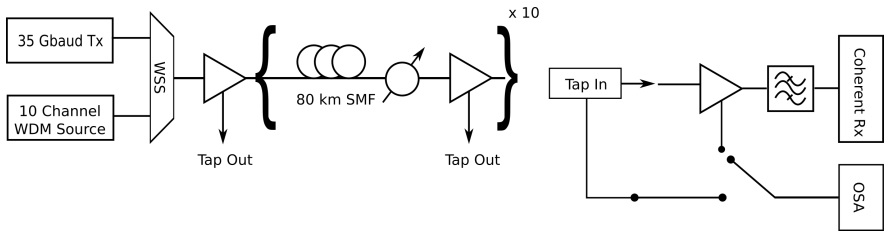

Figure 3.14: Experimental setup for WDM investigation of probabilistic design

pulse shaping with $\alpha = 0.14$ roll-off is applied to all channels at the transmitters. The first EDFA's gain is adjusted to provide the desired optical signal power per channel while the remaining amplifiers are set to constant gain mode. The VOAs adjust the loss per span to apply the optical perturbation. The link consists of 10 x 80 km spans of standard SMF. The EDFA after each span has a monitoring port which is used to tap out the optical signal which is then band-pass filtered before being received by another real-time modem. Digital signal processing is then performed before the BER is measured over a period of 1 second. Only 10 channels are used instead of the entire C-band due to the limitation of the maximum output power from the last EDFA after applying a '1111111111' perturbation to the system, similar to previous experiments.

10 span WDM system - Results

This experimental setup is used to both validate the 3 parameter model as well as to investigate the behaviour of a WDM transmission system in the presence of power perturbations. Equation 3.5 does not differentiate between a single channel and a WDM system, therefore it should still be applicable though it is expected that the non-linear coefficient c will be higher in value. The most ideal use of the 3 parameter model would be to first describe the ideal system using it's parameters and from there calculate the NSR contributions per span per perturbation case. Figure 3.15 shows the reference BER points along with its fitted curve, the power points from -1 to 3 dB in steps of 0.5 dB are fitted for symmetry around its optimum launch power, the parameters are $a = 0.06, b = 5.66 \times 10^{-6}, c = 1591W^{-3}$. It should be noted that Eqn. 3.5 incorporates the XPM from neighbouring channels into parameter c.

The average and worst BER performance are shown in Fig. 3.16a and Fig. 3.16b

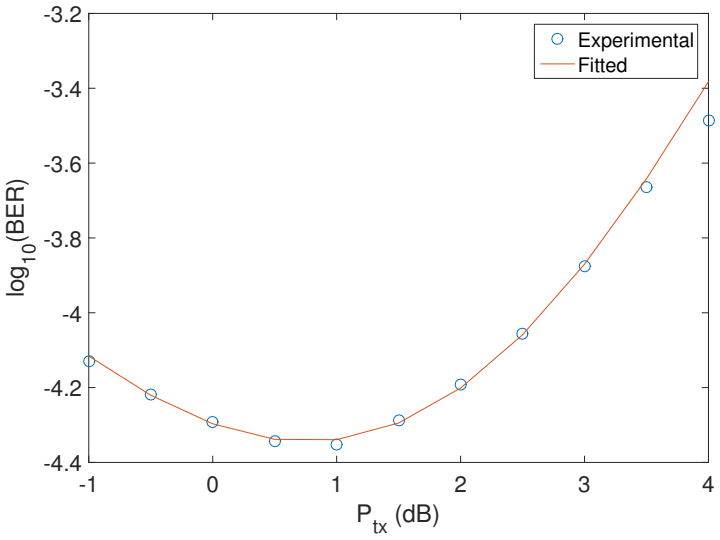

Figure 3.15: Reference BER performance for 10×80 km SMF, 10 channel 35 Gbaud PM-QPSK WDM system with ideal power profile

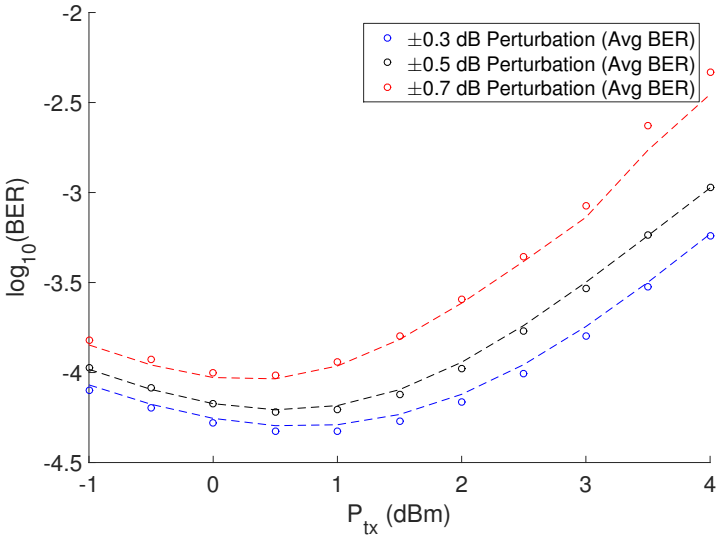

(a) Average BER performance over 1024 different code words per channel launch power - experimental (markers), fitted model (dashed line)

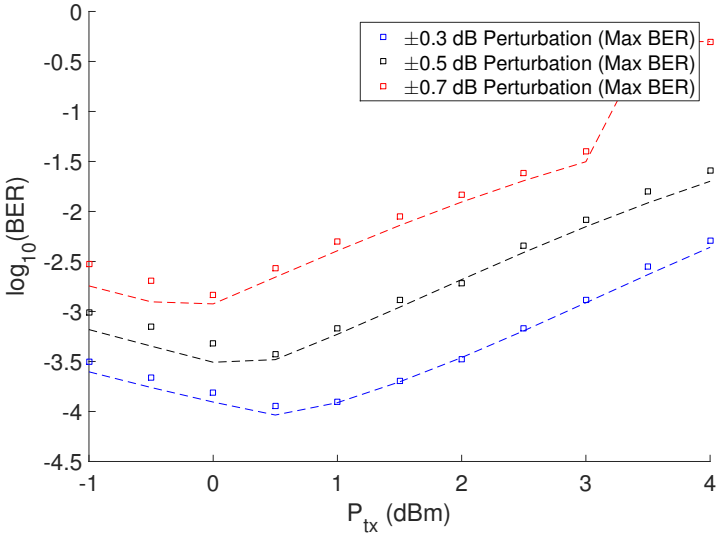

(b) Worst BER performance over 1024 different code words per channel launch power - experimental (markers), fitted model (dashed line)

Figure 3.16

respectively along with the predicted performance using the 3 parameter model fitted using the reference BER curve. Predicted BER values above the 3.4% BER threshold are converted to 0.5, representing a failure in the link. Both predicted curves show a very good agreement with the experimental results. As in previous experiments, the optimum launch power in a deterministically designed ideal system reduces as the applied perturbation increases from the deterministic 1 dBm optimum launch power to 0.5 dBm at a 0.3 dB perturbation, 0.5 dBm for a 0.5 dB perturbation and 0 dBm for a 0.7 dBm perturbation. For this system though, the deterministic methodology would still result in a working system since the BER performance at all perturbations would remain below 3.4%. If probabilistic design was used, for 0.3, 0.5 and 0.7 dB

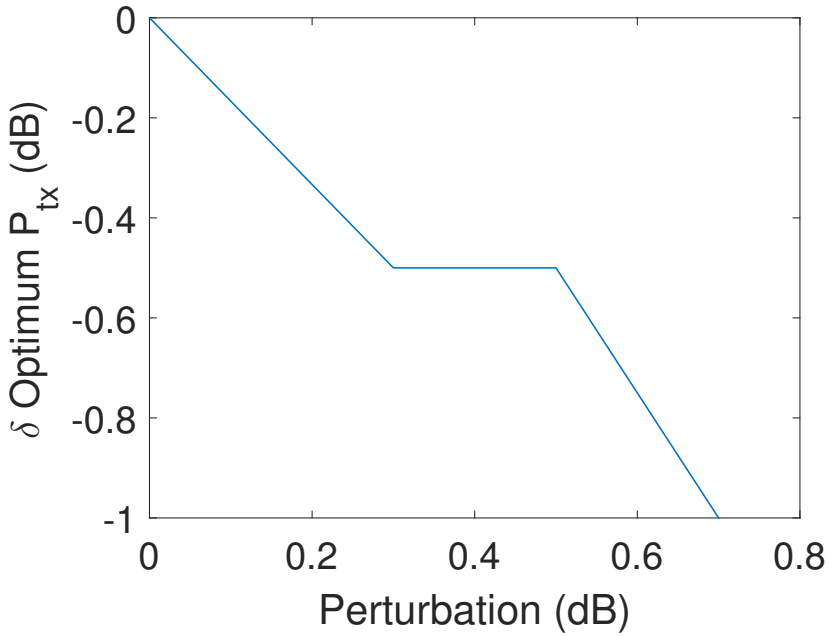

(a) Change in optimum launch power with respect to perturbation

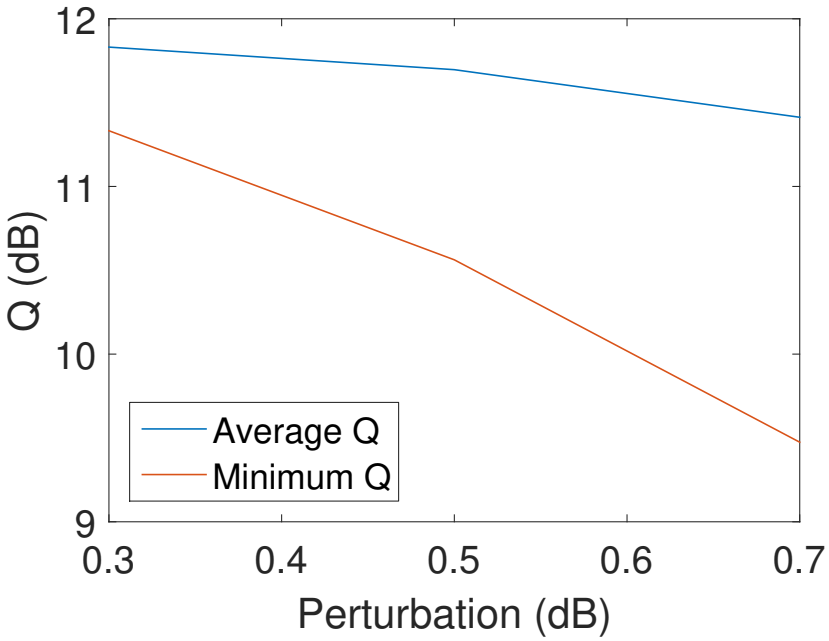

(b) Change in Q for the average and worst case with respect to perturbation

Figure 3.17

perturbation respectively, there would be 0.5, 1.2 and 2.3 dB performance gain in Q in the worst case scenario.

Figures 3.17a shows the change in the optimum launch power with respect to perturbation magnitude. The optimum launch power decreases somewhat linearly with respect to perturbation, similar to previous results. Figure 3.17b shows the change in the average and worst case Q (dB) as the perturbation increases.

Figures 3.18a, 3.18b and 3.18c show the cumulative probability distributions

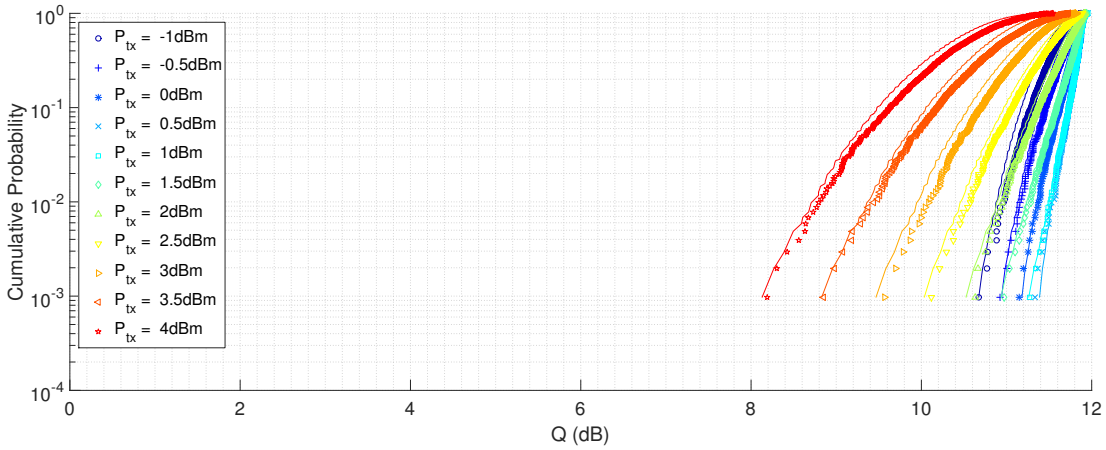

(a) Cumulative probability for 0.3 dB perturbation (symbols), with fitted 3 parameter model (line)

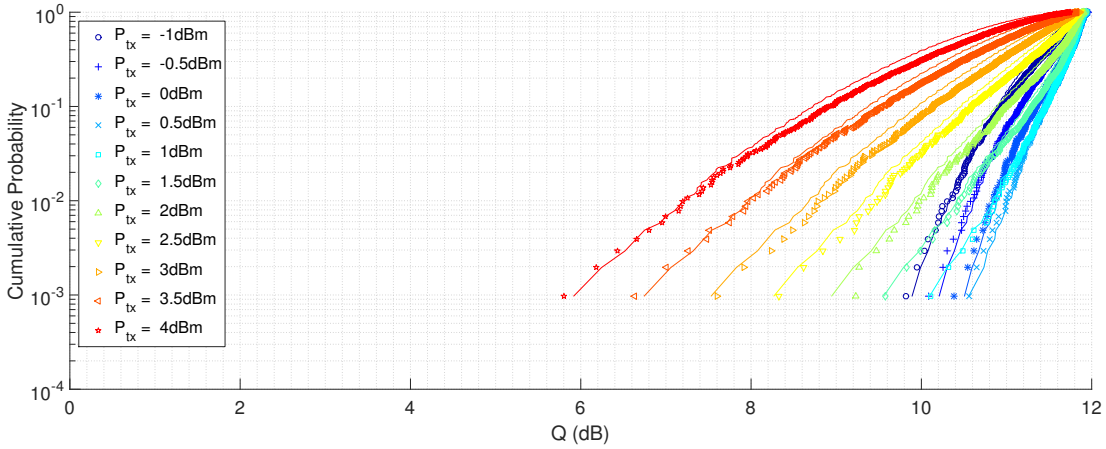

(b) Cumulative probability for 0.5 dB perturbation (symbols), with fitted 3 parameter model (line)

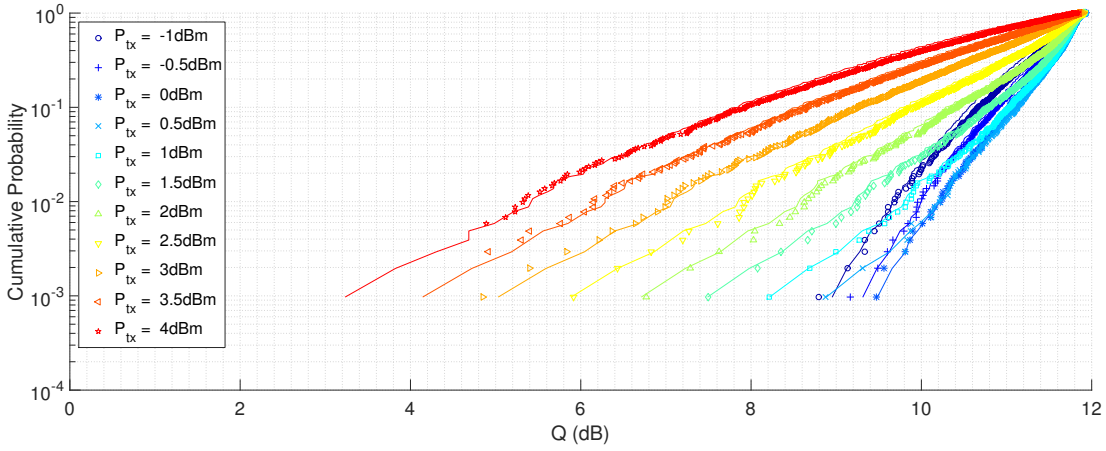

(c) Cumulative probability for 0.7 dB perturbation (symbols), with fitted 3 parameter model (line)

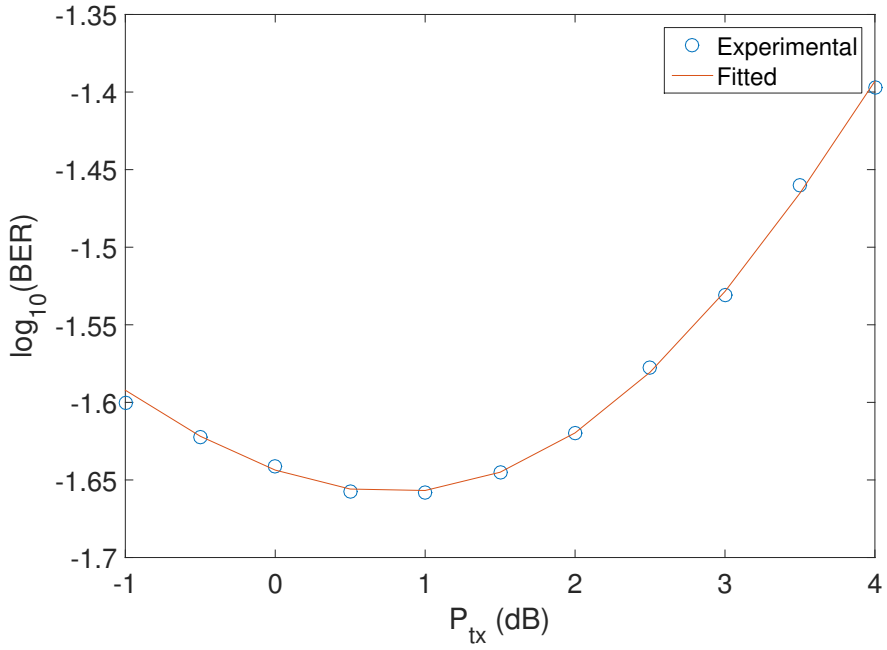

Figure 3.18: Reference BER performance for 10×80 km SMF, 10 channel 35 Gbaud PM-16QAM DWDM system with ideal power profile

for 0.3, 0.5 and 0.7 dB power perturbations respectively. The 3 parameter model predicted cumulative probability distribution for each perturbation and launch power is shown on the same graphs and shows similarly good agreement with the previous BER performance graphs and model fits.

The test and WDM channels are then switched to PM-16QAM, again the reference BER performance is shown in Fig. 3.18 fitted with the 3 parameter model with parameters $a = 0.1138, b = 8.795 \times 10^{-6}, c = 2547W^{-3}$.

The average and worst BER performance for the PM-16QAM system are shown in Fig. 3.19a and Fig. 3.19b respectively along with the predicted performance using the 3 parameter model fitted using the reference BER curve. Predicted BER values above the 3.4% BER threshold are converted to 0.5, representing a failure in the link. Both predicted curves show a very good agreement with the experimental results albeit not as good as the PM-QPSK, the digital signal processing performs differently as the BER performance approaches the FEC threshold. As in previous experiments, the optimum launch power in a deterministically designed ideal system reduces as the applied perturbation increases, Fig. 3.20a. The optimum launch power decreases somewhat linearly with respect to perturbation, similar to previous results. Figure 3.20b shows the change in the average and worst case Q (dB) as the perturbation increases.

Figures 3.21a, 3.21b and 3.21c show the cumulative probability distributions for 0.3, 0.5 and 0.7 dB power perturbations respectively. The 3 parameter model predicted cumulative probability distribution for each perturbation and launch power is shown on the same graphs and shows similarly good agreement with the previous BER

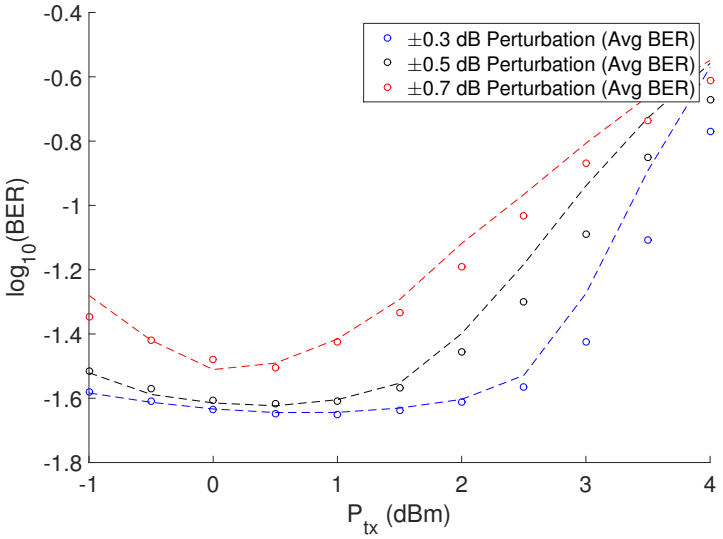

(a) Average BER performance over 1024 different code words per channel launch power for PM-16QAM - experimental (markers), fitted model (dashed line)

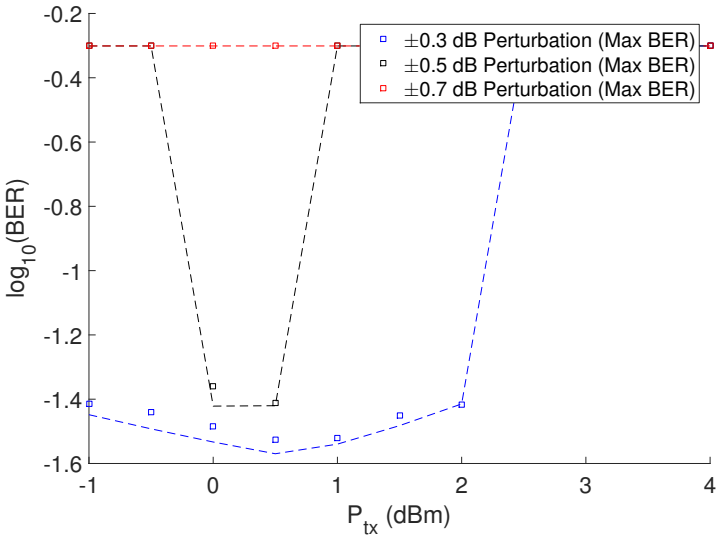

(b) Worst BER performance over 1024 different code words per channel launch power for PM-16QAM - experimental (markers), fitted model (dashed line)

Figure 3.19

performance graphs and model fits. The benefit of probabilistic design is clearly evident, given that for a 0.5 and a 0.7 dB perturbation, a deterministically designed equivalent system would not be operable. So as to support the higher cardinality modulation format, probabilistic design allows for a system without any outage probability given a perturbation magnitude of 0.3 or 0.5 dB. For a 0.7 dB case, transmission at -1 dBm is possible with an 8% outage probability.

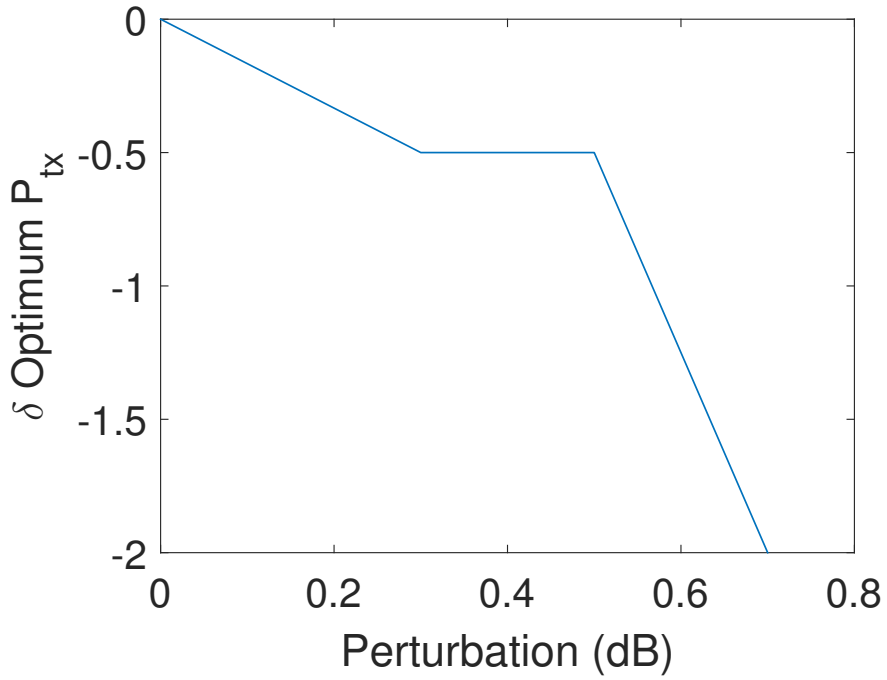

(a) Change in optimum launch power with respect to perturbation

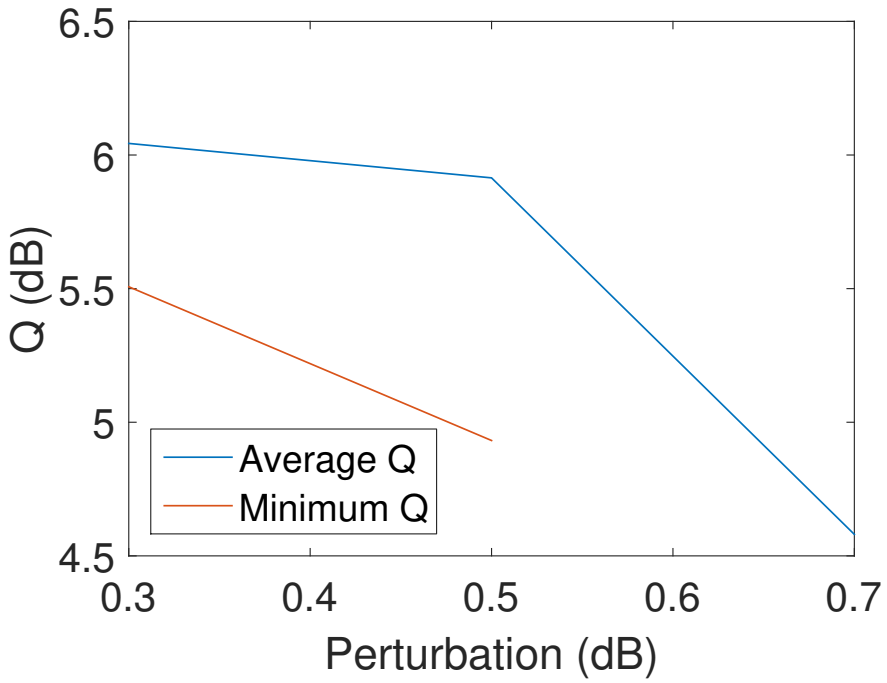

(b) Change in Q for the average and worst case with respect to perturbation

Figure 3.20

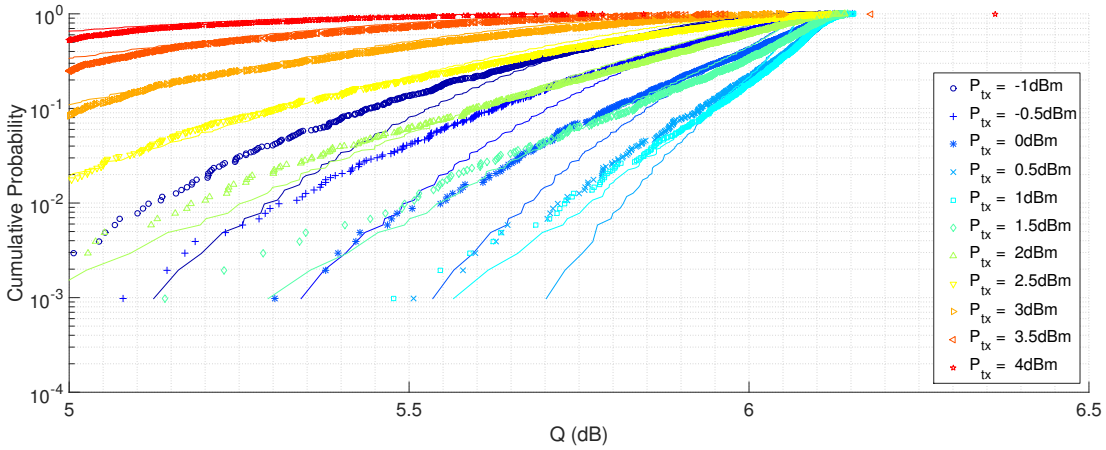

(a) PM-16QAM cumulative probability for 0.3 dB perturbation (symbols), with fitted 3 parameter model (line)

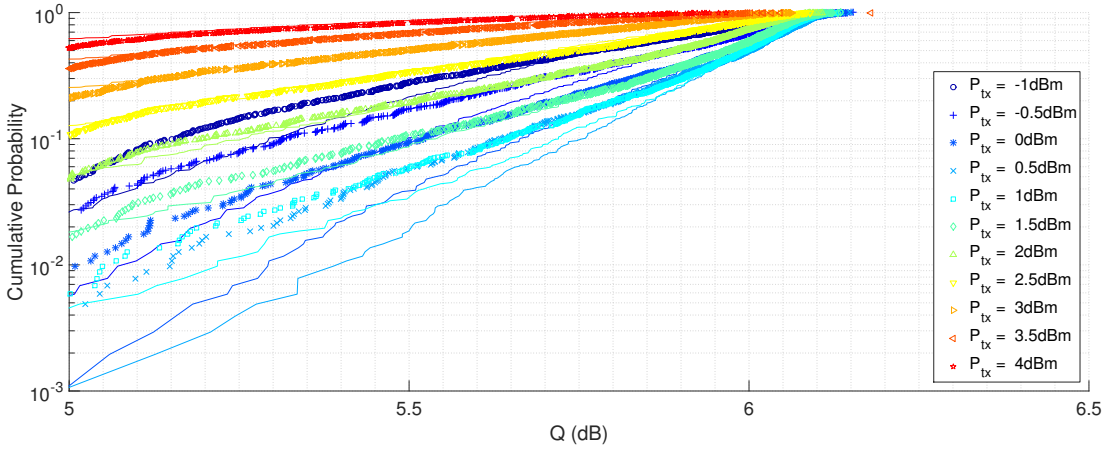

(b) PM-16QAM cumulative probability for 0.5 dB perturbation (symbols), with fitted 3 parameter model (line)

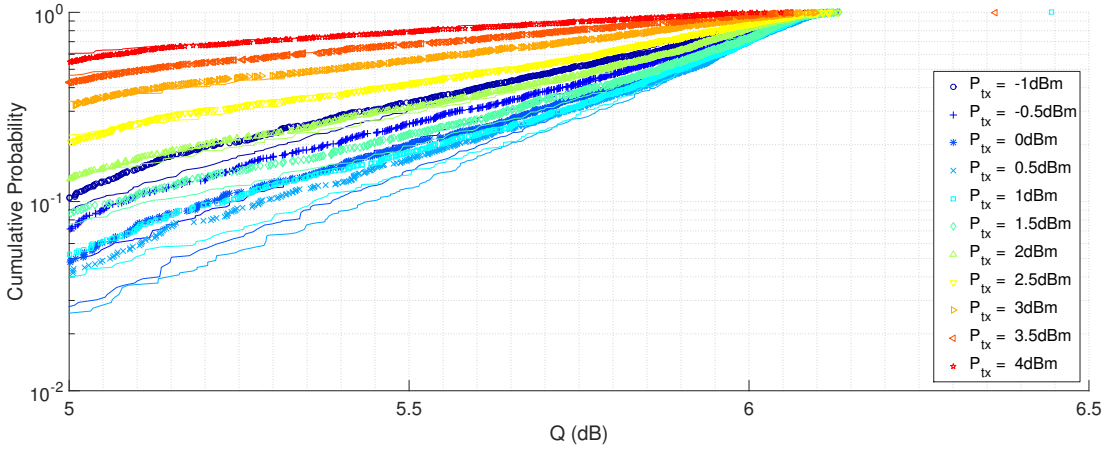

(c) PM-16QAM cumulative probability for 0.7 dB perturbation (symbols), with fitted 3 parameter model (line)

Figure 3.21

3.3.2 Summary

In this chapter, an overview of the probabilistic design philosophy was provided and compared to the traditional deterministic design philosophy prevalently used in past and currently deployed optical transmission systems. While probabilistic design has been implemented in other areas of engineering such as aerospace [49, 50], earthquake hazard assessment [51], nuclear reactors [52] and deep space telecommunication systems [53, 54] where reliability is paramount, optical systems are unique in that the transmission medium is non-linear. The effect of this non-linearity is proportional to the cube of the optical power.

The optimum from a systems design viewpoint if all parameters are precisely known and time invariant is at the balance point the linear regime where the increase in SNR provided by increasing the optical power is counter-acted by the effective SNR penalty generated by the same action. Therefore, even if system parameters are normally distributed, the effect on the system performance is not. This renders the optimum design point null since in the presence of link imperfections, the optimum provisioning for the system changes. Therefore it is possible to design a more reliable system if this effect is accounted for.

The application of probabilistic design is first shown for a single channel 11.5 Gbaud PM-QPSK system transmitting over 4 spans of 100 km SMF. To minimize the set of measurements to be taken, a fixed magnitude perturbation with equal likelihood positive or negative was applied to the optical power input to each span relative to the previous, for the first span, this is relative to the transmitter launch power. For a perturbation of 3 dB, a gain of nearly 4.5 dB in Q factor was achieved compared to the equivalent deterministic system, which had an 6.25% outage probability over the measurements. The optimum provisioning point with respect to optical launch power shifted to be 3 dB less due to the non-linear effect of the fibre.

Investigation of more realistic perturbation values was achieved by implementing the same type of measurements over a 10 span system, again utilising a 11.5 Gbaud PM-QPSK test channel. Similar behaviour was observed with the optimum launch power decreasing by 2 dB at the maximum applied perturbation magnitude of 1 dB. The benefit of using probabilistic design is clear since it allows for reliability analysis, showing that the deterministic design provisioning point would have an outage probability of 0.2% at a 1 dB perturbation. The probabilistically designed system does not have this probability.

It should be noted that 87,400 measurements were taken which was only practical through the use of real-time transmission systems. In practice, performing these measurements requires a significant investment in time and equipment and simulation would require a extreme amount of computation time. Therefore a simple model was

introduced which was validated on the results from the 10 span single channel system. This model was then used on a similar 10 span system incorporating 80 km spans and 35 Gbaud transceivers modulating PM-QPSK and PM-16QAM and a total of 11 WDM channels. The model predicted the perturbed system performance using the reference system performance of an ideal system with a high degree of accuracy for both modulation formats.

Probabilistic design is an extremely powerful tool for the design of optical systems, in particular due to the inherent non-linearity. In this chapter we used probabilistic design as an analytic tool to leverage the non-linearity of the system for a better systems design from the perspective of reliability. Probabilistic design will allow engineers to design a system for a required degree of reliability instead of providing a safety margin, which if under-engineered is undesirable for system performance. Over-engineering squanders the potential of the optical system. Next generation optical networks as described in chapter 1 will be much more dynamic in nature, using deterministic design would require a sufficient margin to account for the increase in network dynamics. Therefore it would be desirable to perform probabilistic design on these networks. It is however more likely that in practice a combination of the two will be used due to the many degrees of freedom in the optical network.

4

Polarization Dependent Loss Induced Penalty in Coherent Systems

4.1 Abstract

This chapter provides a brief overview of polarization dependent loss and its effect on dual polarization optical coherent systems. It is likely that future optical systems will have higher innate PDL due to inclusion of more optical components to support future functionality. The impact of PDL on coherent systems has been investigated in the academic laboratory environment and in simulation, albeit mostly using single large PDL element. The experiments performed in this chapter utilize commercially available transceivers in order to obtain results on the likely performance of future optical systems with respect to an optical link with multiple discrete PDL elements. A DWDM system is used with a total of 63 channels as the test system. Eight discrete PDL elements are used with polarization controllers to create a total of 120,000 independent instantiations of link PDL. The performance impact was found to be less than 1 dB at 6 dB of link PDL for PM-QPSK and PM-16QAM. Using a simple lumped PDL model and advanced DSP, this impact was discovered to be roughly as expected.

4.2 Introduction

Traditionally, the focus of polarization related effects on optical transmission systems has been on PMD due to the deployment of OOK optical transceivers as the primary technology for the delivery of optical telecommunications. In an ideal optical fibre, the optical signal has two orthogonal polarizations that propagate at the same speed, the signal has a random polarization orientation but orthogonality would be maintained. In practice, there are random imperfections that occur which break the circular symmetry of the optical fibre and the presence of residual mechanical stress or strain, causing the two polarizations to travel at different speeds, hence dispersing the two polarizations. The effect has been been extensively studied in literature [60][61].

Due to the introduction of coherent optical systems and digital signal processing, it is possible to compensate for the effect of PMD at the coherent receiver which is polarization and phase diverse [10]. This chapter focuses on the impact of multiple PDL elements distributed throughout an optical light-path on the performance of the current generation of commercially available coherent transceivers operating at 100 Gbit/s and 200 Gbit/s. At the moment of writing, there exists no work that experimentally investigates the effect of distributed PDL in DWDM coherent transmission systems. Such work is is required in probabilistically designed systems to create the DCT.

4.3 Polarization Dependent Loss

Polarization dependent loss has become an increasing concern to the design of optical communication systems, PDL is typically found in components such as fibre amplifiers, optical couplers, isolators, AWGs and more pertinent to the deployment of next generation optical systems, ROADMs at network nodes. In practical networks, these components are distributed throughout. The impact of PDL is of increasing importance due to the number of components used to construct a ROADM [62], the potential PDL of a ROADM may well exceed 1 dB [63]. It is clear that the amount of PDL in a network will increase with the deployment of ROADMs, therefore the impact of PDL on system performance must be carefully considered.

PDL may be described as the following Jones matrix [64],

$$T_{PDL} = \begin{bmatrix} 1 & 0 \\ 0 & 10^{-PDL_{dB}} \end{bmatrix} \tag{4.1}$$

where the PDL_{dB} is the value of the PDL element. The light incident axis to the polarization element is represented by the rotation matrix R

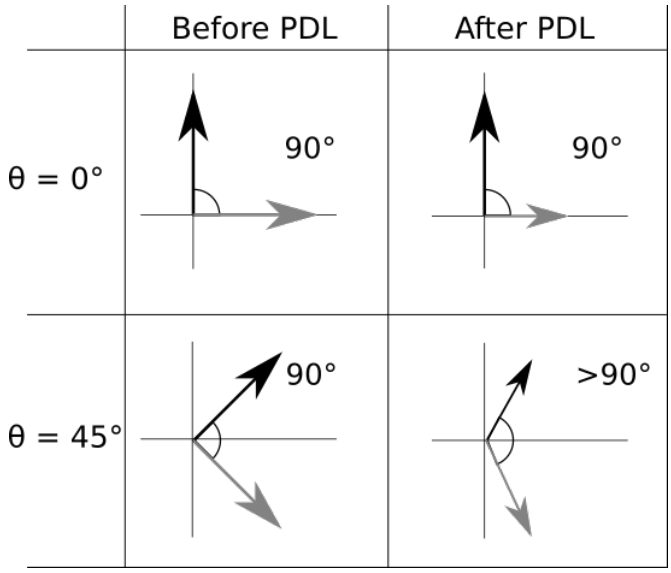

Figure 4.1: Impact of PDL on the optical signal when incident light is at $\theta = 0^\circ$ and $\theta = 45^\circ$

$$R = \begin{bmatrix} \cos\theta & \sin\theta \\ -\sin\theta & \cos\theta \end{bmatrix} \tag{4.2}$$

where θ is the angle of the light incident to the PDL element relative to the PDL axis. The impact of the system PDL on coherent optical systems has been investigated previously in literature [65][66] [67], indicating that coherent systems implementing standard digital signal processing [10] may be very vulnerable to systems with a significant amount of PDL. In a linear system, the impact of the link PDL is determined by the angle θ [65][66] [67], bounded by

$$H_{worst} = T_{PDL}R(\theta = 0^\circ) \tag{4.3}$$

$$H_{best} = T_{PDL}R(\theta = 45^\circ) \tag{4.4}$$

In the scenario that $\theta = 0^\circ$, there is degradation of SNR on one axis relative to the other. If $\theta = 45^\circ$, then both polarizations would have the same SNR, however there is a loss of orthogonality between the polarization vectors Fig. 4.1.

This chapter aims to look at the performance of current generation coherent optical systems in the presence of distributed PDL elements to determine the potential system impact on performance.

4.4 Experimental Setup

The experimental setup is as shown in Fig. 4.2. The same WDM transceiver setup is utilized as in chapter 3 with a commercially available coherent transceiver [14] modulating

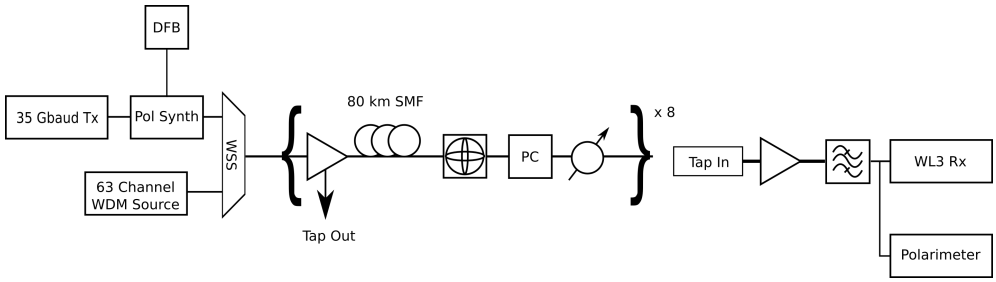

Figure 4.2: Experimental setup investigating the impact of distributed PDL in a coherent optical systems transmitting at 35 Gbaud and modulating PM-QPSK or PM-16QAM

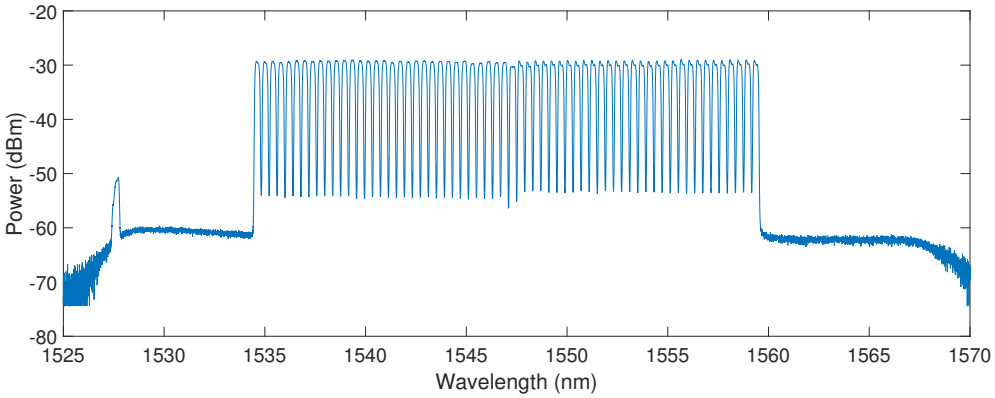

Figure 4.3: Spectrum of the flattened 63 channels

either PM-QPSK or PM-16QAM at 35 Gbaud as the test optical signal at 1547.319 nm. 62 external cavity lasers with nominal line width 20 kHz are bulk modulated using a modified version of the test signal transceiver with the same modulation format as the test signal at 35 Gbaud, these channels are then independently optically de-correlated before being recombined using an arrayed waveguide grating (AWG). The de-correlated WDM channels are then combined with the test channel on a 50GHz frequency grid using a wavelength selective switch (WSS) which also equalizes the channel power, the WDM system is equalized for maximum flatness across all 8 spans with Fig. 4.3 being the spectrum input to span 5. Nyquist pulse shaping with $\alpha = 0.14$ roll-off is applied to all channels at the transmitters. In order to establish a relative polarization state for the test channel, a polarization synthesizer is used. The dual polarization signal from the transmitter is nominally unpolarized and therefore the synthesizer would not be able to stabilize the polarization vector. To provide an optical reference, the test channel is coupled with a 10 dBm higher power single polarization laser source. The test channel and laser source are then jointly stabilized using the polarization vector of the laser source. This allows the polarization synthesizer to establish a relative polarization state for the test signal. The single polarization laser is de-multiplexed by the WSS before launching into the fibre link. The link consists of 8 x 80 km spans of SMF, after each span there is a PDL element and then a polarization scrambler. The EDFA after each span has a monitoring port which is used to tap out the optical signal which is then

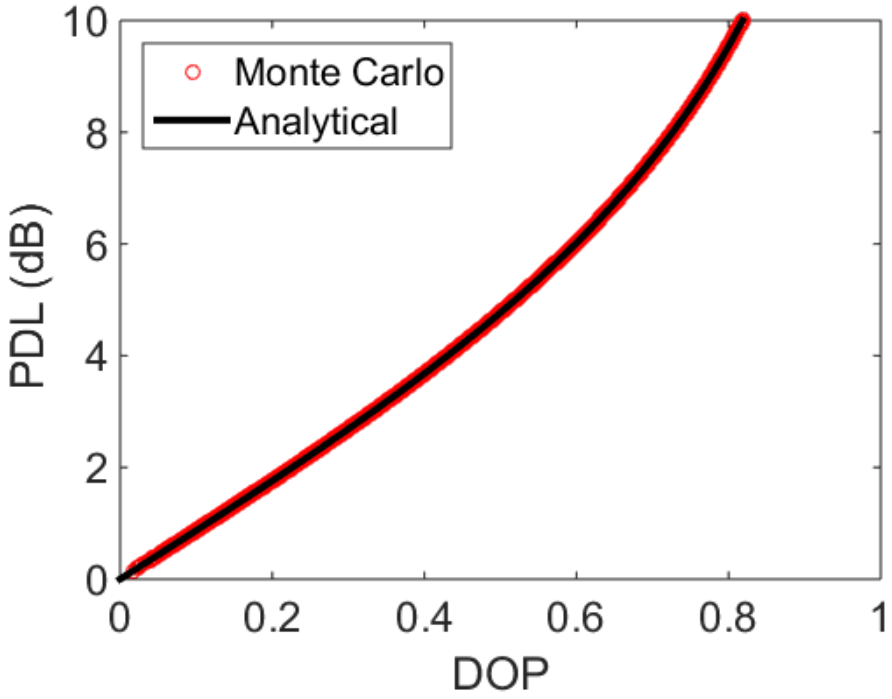

Figure 4.4: Degree of polarization versus polarization dependent loss for analytical expression and 1000 runs of Monte Carlo simulation

band-pass filtered before being received by another real-time modem.

Digital signal processing is then performed before the BER is measured over a period of 1 second. The stokes vector of the test signal after propagation are measured by a polarimeter. From this the DOP is calculated using [68]

$$DOP = \mathbb{R}\left(\sqrt{\frac{S_1^2 + S_2^2 + S_3^2}{S_0^2}}\right) \tag{4.5}$$

where S_0, S_1, S_2 and S_3 are the measured stokes parameters . The PDL of the link can be extracted from this since a polarization multiplexed signal is essentially de-polarized. Propagation through an optical element with PDL colours the signal according to the magnitude of it's PDL [68].

This relationship is shown in Fig. 4.4 for 1000 runs of a Monte Carlo simulation and the analytical relationship is described by

$$PDL_{dB} = \tanh^{-1}(DOP) \times 20/\ln 10 \tag{4.6}$$

where PDL_{dB} is the PDL in logarithmic units and $\tanh^{-1}$ is the inverse hyperbolic tangent. See Appendix for derivation of this equation.

4.5 Results

4.5.1 Investigation of dependence on initial state of polarization

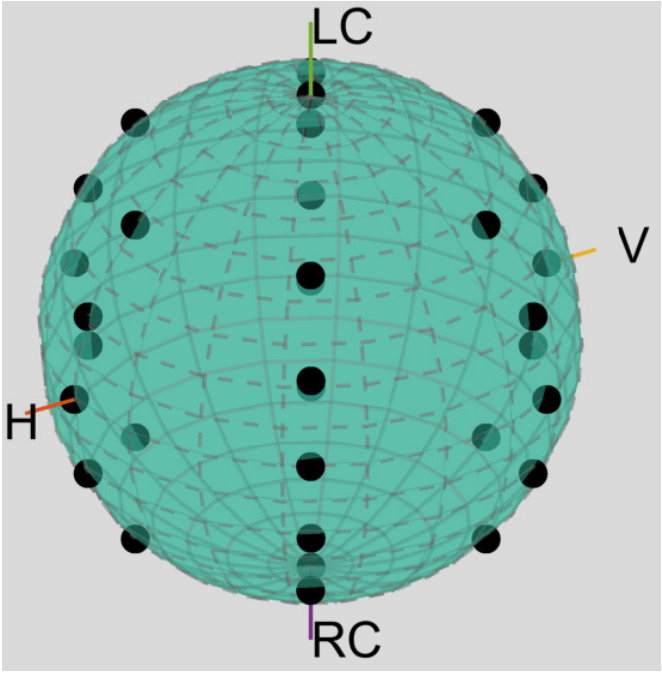

Figure 4.5: Distributed SOP states

Initially the dependence of system performance on the transmitter state of polarization was investigated to examine its effect. 40 different states of test channel polarization were implemented using the polarization synthesizer, distributed roughly equally over the Poincaré's sphere, Fig. 4.5. 60 instances of link PDL were generated by randomly

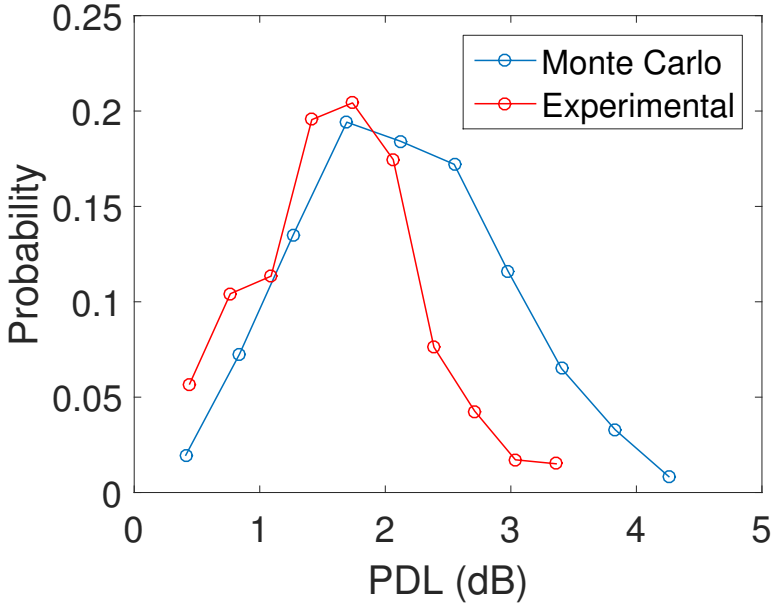

Figure 4.6: Probability distribution of 60 link PDL instances

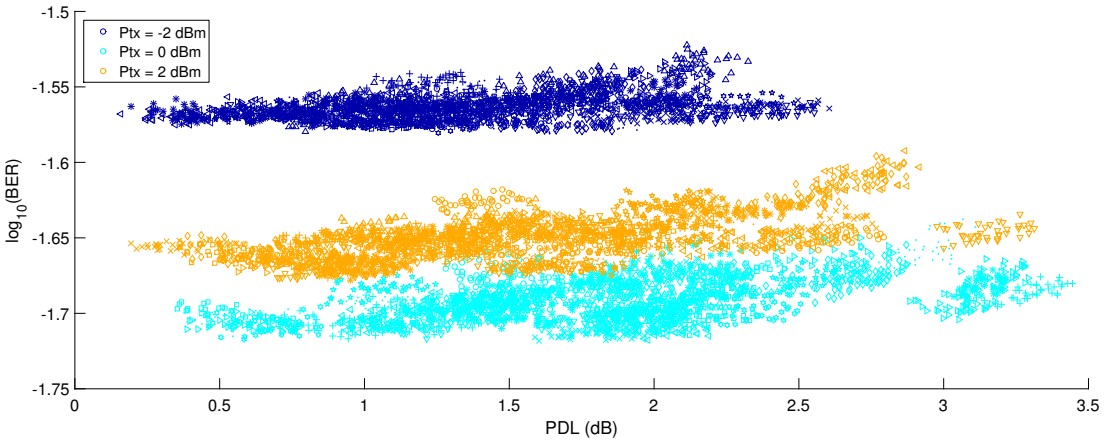

Figure 4.7: BER performance for 60 instances of link PDL with 40 transmitter launch polarizations, each group of 40 SOPs are denoted by the same symbol

scrambling the polarization controllers, this is repeated for each transmitted launch power for a total of 660 link PDL instances. The test and WDM channels are modulated with 35 Gbaud PM-16QAM and their launch powers are swept from -2 to 3 dBm in steps of 0.5 dB.

For each instance of link PDL, the transmitter polarization is scanned across the Poincaré's sphere and a measurement taken for each initial SOP. The PDL elements utilised were nominally 1 dB and 0.5 dB elements interleaved with the 1 dB element after fibre spans 1, 3, 5 and 7, the other spans have the 0.5 dB elements. The probability distribution function of the link PDL has a mean PDL of 1.44 dB and as is Maxwellian

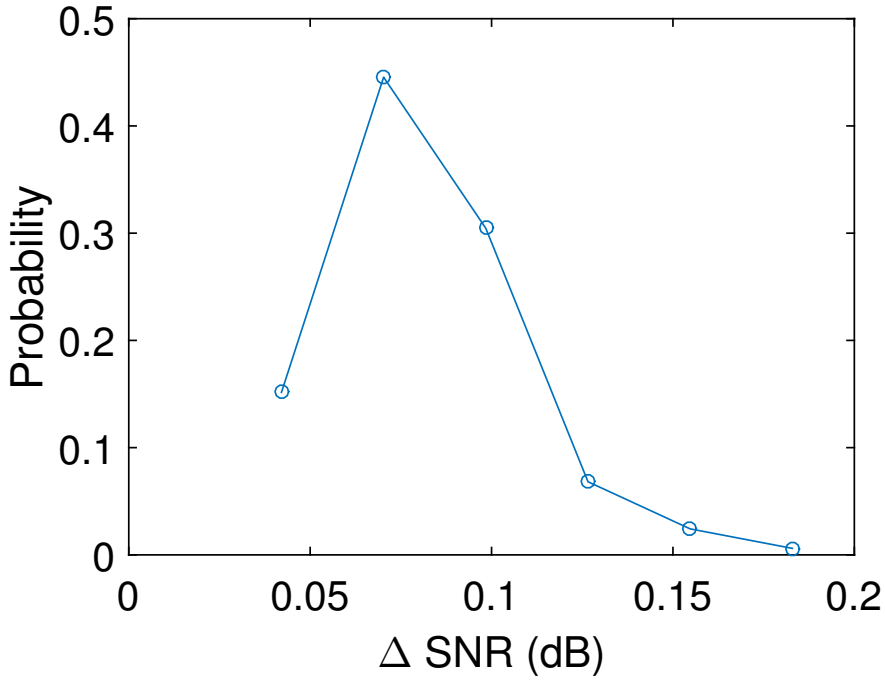

Figure 4.8: The probability distribution of the performance difference in SNR between the best and worst transmit polarization states over 40 states

[64][69], Fig. 4.6. The expected mean link PDL is roughly 2 dB from [69], 2400 runs of a corresponding Monte Carlo simulation obtained a mean PDL of 2.1 dB. The differential is believed to be from polarization dependent gain from the optical amplifiers partially compensating for the presence of of the PDL element therefore decreasing the overall link PDL value. The measured link PDL value from the polarimeter was independently verified by an on card measurement.

The BER performance of the test signal under the effect of link distributed PDL and transmit SOP state is shown in Fig. 4.7. It can be seen that though there is some effect on the BER performance with respect to both link PDL value and the transmit SOP state, it is quite small. This is quantified by the probability distribution of the difference between the best and worst performance is denoted by the difference in the effective signal SNR in Fig. 4.8. The mean difference in SNR impact is 0.078 dB which is difficult to capture. This allows the initial transmit SOP to be disregarded as a factor.

4.5.2 Investigation of impact of link PDL on performance

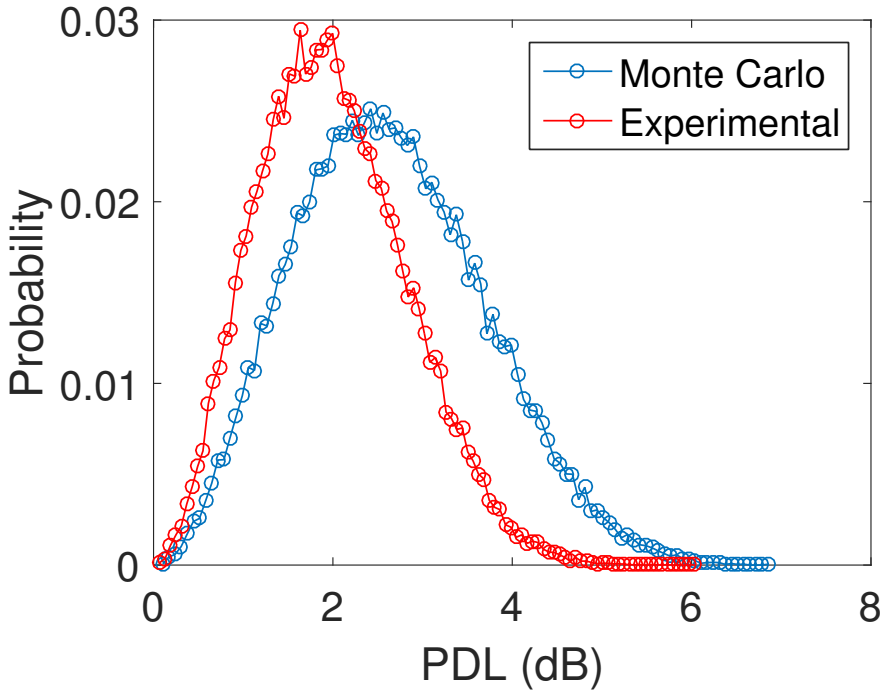

Figure 4.9: Probability distribution function of the link PDL over 60000 randomly generated instances for experimental and simulated setups

From the prior experiment, the initial SOP is discarded as a significant factor in the experiment. Accordingly, the transmitter SOP is stabilised by the polarization synthesizer at a single SOP with the help of the coupled single polarization laser. For each transmitter launch power, 10,000 instances of link PDL are generated using the polarization controllers as previous. In an effort to reach higher values of link PDL,

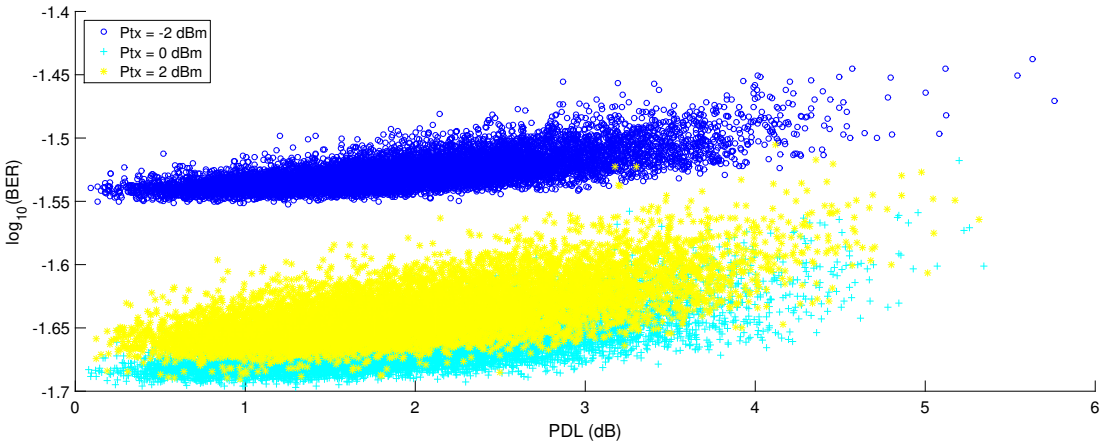

Figure 4.10: PM-16QAM BER performance for -2, 0, 2 dBm launch power

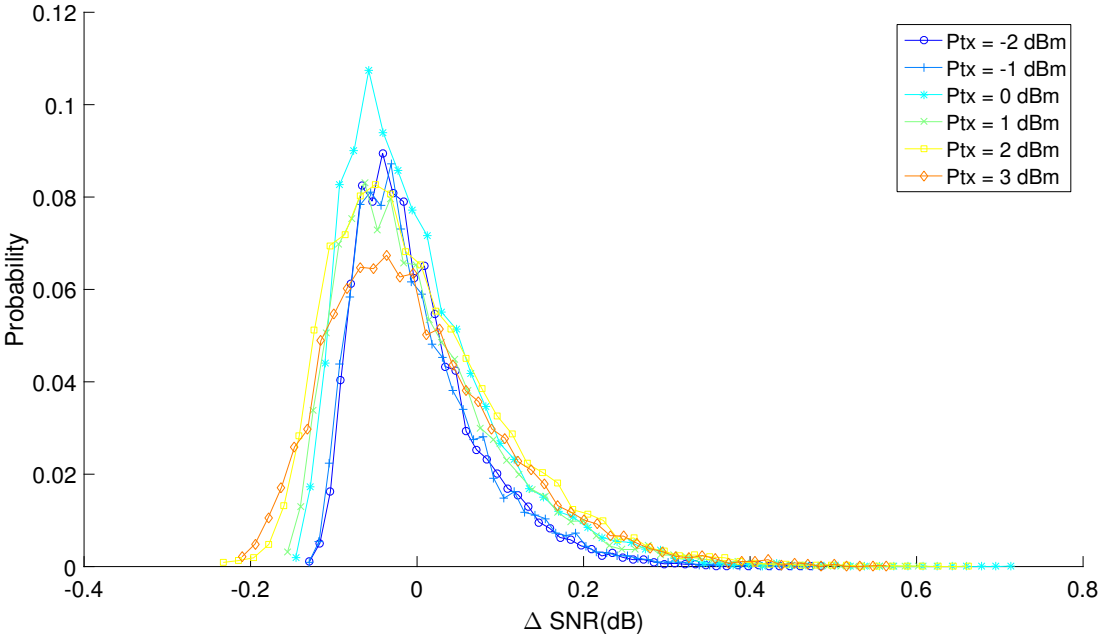

Figure 4.11: Probability distribution of the PM-16QAM SNR spread for each launch power with respect to the mean SNR

the 0.5 dB PDL elements are replaced with 1 dB value elements for a total of eight 1 dB elements. The probability distribution function is shown in Fig. 4.9 in addition to the simulated PDF of link PDL. The mean experimental link PDL is 1.8 dB while the theoretically calculated mean is 2.5 dB, and 60,000 runs of Monte Carlo simulation obtained a mean link PDL of 2.4 dB. There is again some disparity between the simulation and the experimental results, believed to be due to the inherent polarization dependent gain of the EDFAs, equating to approximately a 0.3 dB reduction in the value of the PDL element. The transmitter power is incremented from -2 to 3 dBm in steps of 1 dB. The increase in step size is to facilitate more instances of link PDL to be examined.

The BER performance is shown in Fig. 4.10 for a transmitter launch power of

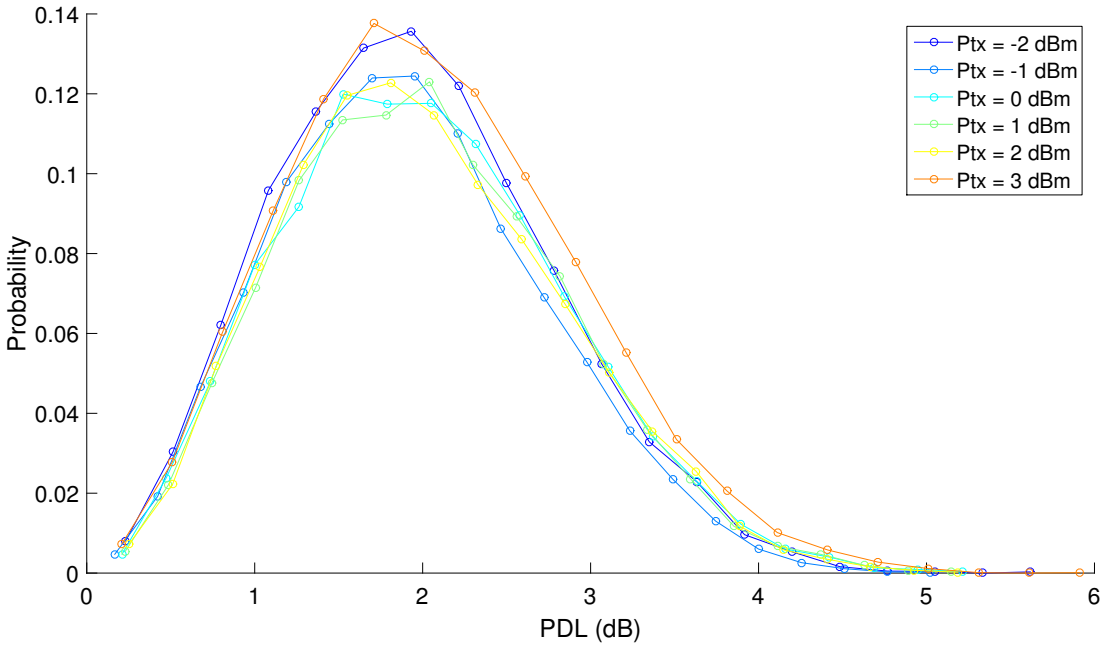

Figure 4.12: Probability distribution of the link PDL instances per launch power for PM-16QAM measurements

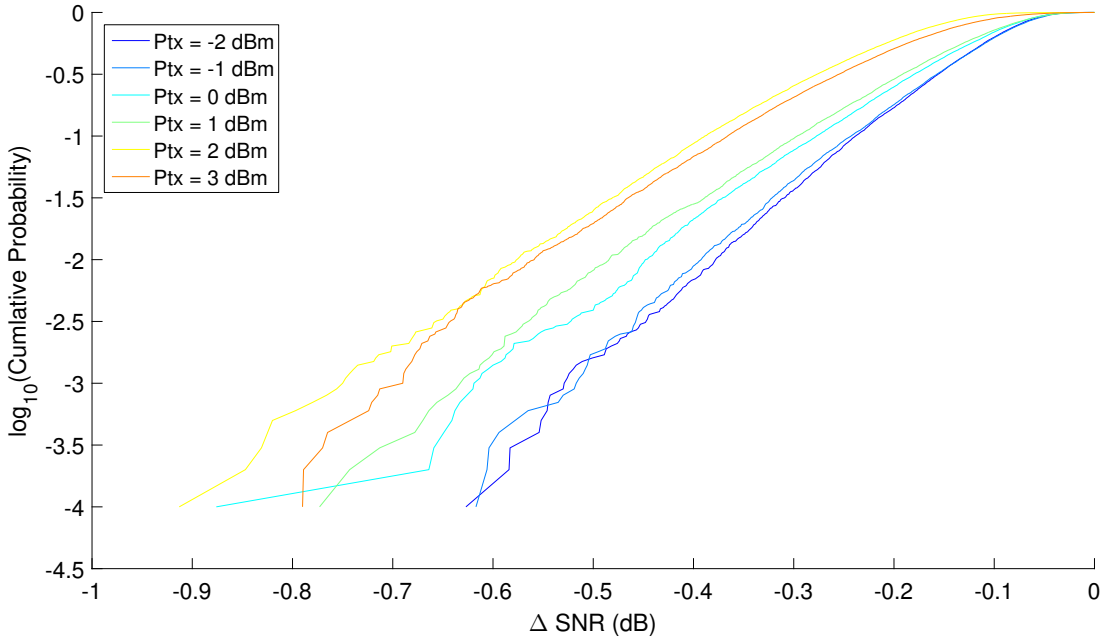

Figure 4.13: Cumulative probability for a SNR change with respect to no link PDL for each PM-16QAM launch power

-2, 0 and 2 dBm. Note that the performance spread is again very similar despite the difference in launch powers. The impact of the increase in launch power is more easily discerned in Fig. 4.11 in which we can see that the there is a general trend that an increase in launch power increases the SNR spread over the 10000 link PDL instances. The increase is however extremely small, at 0.01 probability there is only an extra 0.1 dB of SNR penalty. Since the 10000 instances of link PDL that are tested for each

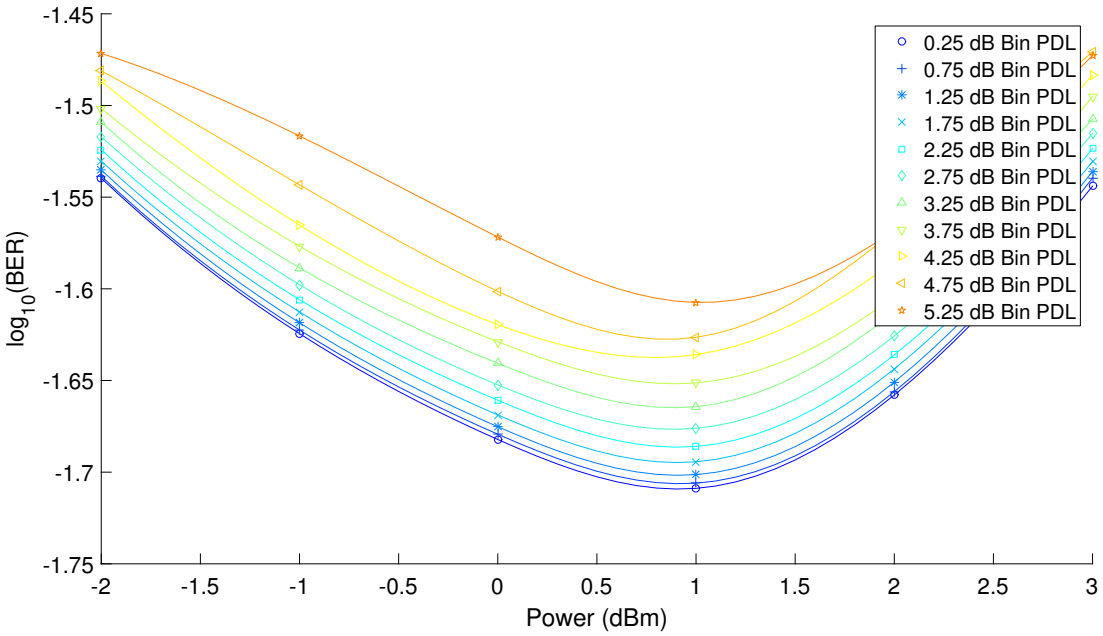

Figure 4.14: Averaged BER performance per 0.5 dB bin of PDL

launch power are not the same, the accompanying distributions of each set of 10000 are shown in Fig. 4.12. In terms of probability of SNR penalty, this is shown in Fig. 4.13 which verifies that there is a slight dependence of the impact of PDL with respect to optical launch power due to the the interaction of PDL with non-linearity. Fig. 4.13 is normalized with respect to the mean SNR at that launch power, hence the 3 dBm launch power performance is better than the 2 dBm due to experimental error at one measurement. However it suffices to illustrate the PDL-NL interaction.

To examine the effect of PDL on provisioning the 35 Gbaud PM-16QAM channel, the PDL values are sorted into bins centred around 0.25 dB to 5.25 dB of PDL with a 0.5 dB spread. The BER performance of the respective BER measurements are then averaged to achieve Fig. 4.14 and fit with a cubic interpolation. It can be seen that as expected from the results in Fig. 4.14, there is essentially no difference in the optimum launch power, with a 0.25 dB decrease from 1 dBm to 0.75 dBm.

The experiment is then repeated for a PM-QPSK WDM system utilising the same experimental setup shown in Fig. 4.2 and 4.3. 10000 random instances of link PDL are explored for the optical launch powers sweeping from -2 to 3 dBm in 1 dB steps.

Figure 4.15 shows the BER performance for each set of 10000 link PDL instances for -2, 0 and 2 dBm optical launch power per channel, it can be seen that there is again remarkably little difference in performance as the amount of link PDL increases. There is 1 dB maximum spread in the SNR between best and worst cases for all optical launch powers.

In comparison to the PM-16QAM measurements, Fig. 4.16 shows that the effect of increasing the optical launch power is decreased with a negligible decrease in the

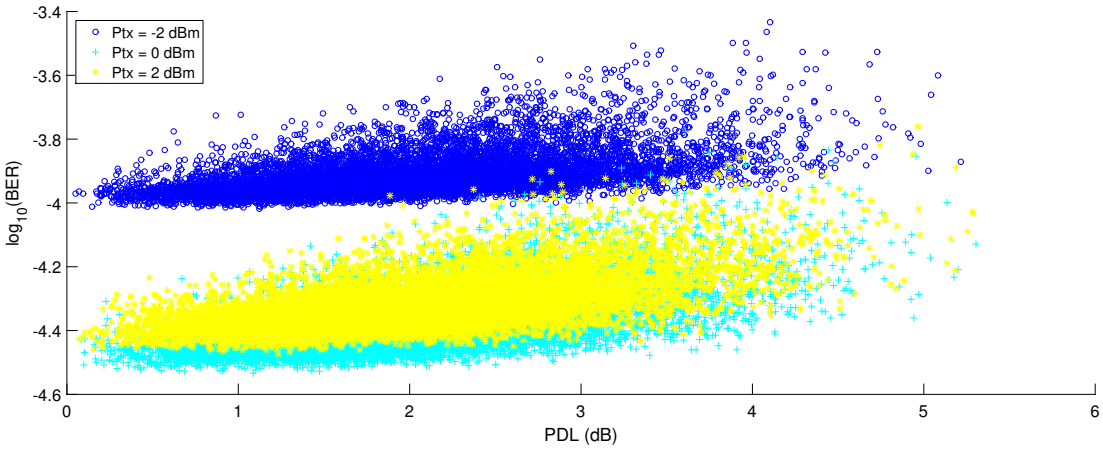

Figure 4.15: BER performance for -2, 0, 2 dBm launch power

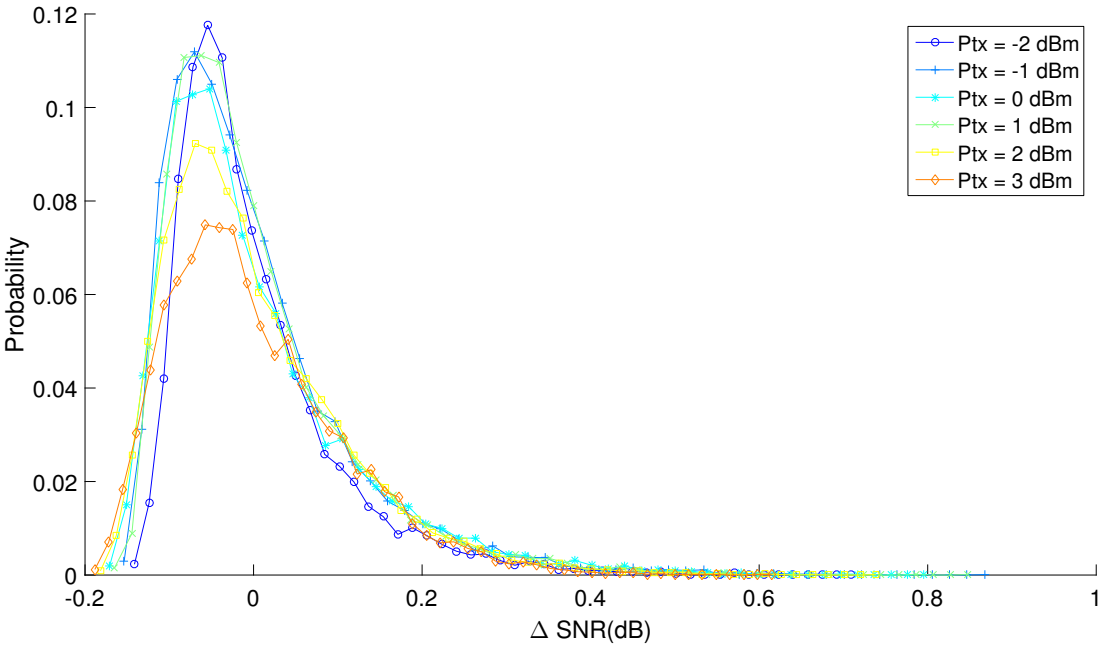

Figure 4.16: Probability distribution of the SNR spread for each launch power with respect to the mean SNR

SNR spread. The effect is less evident since PM-QPSK is more resilient to non-linear distortion since its lesser number of constellation points have more Euclidean distance between them. The distributions of the link PDL per launch power are shown in Fig 4.17. This is further reinforced in Fig. 4.18 showing the cumulative probability with respect to SNR impact which can be used to generate the PDL entry in a DCT for probabilistic design. From this it is expected that the optimum provisioning launch power with respect to link PDL will not change, as seen in Fig. 4.19.

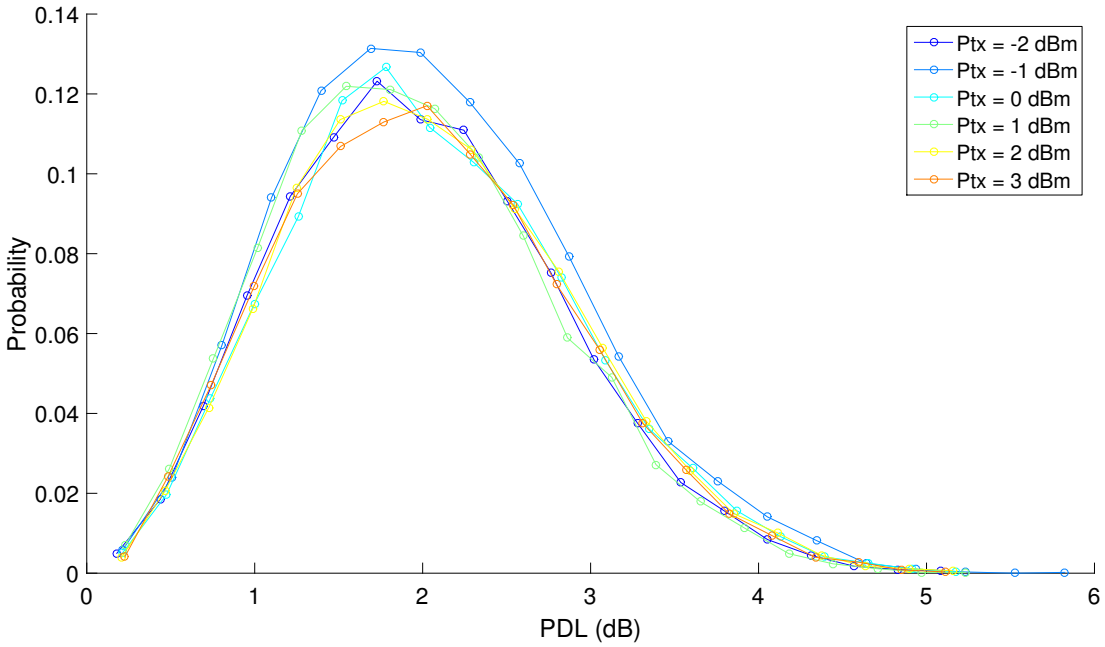

Figure 4.17: Probability distribution of the link PDL instances per launch power

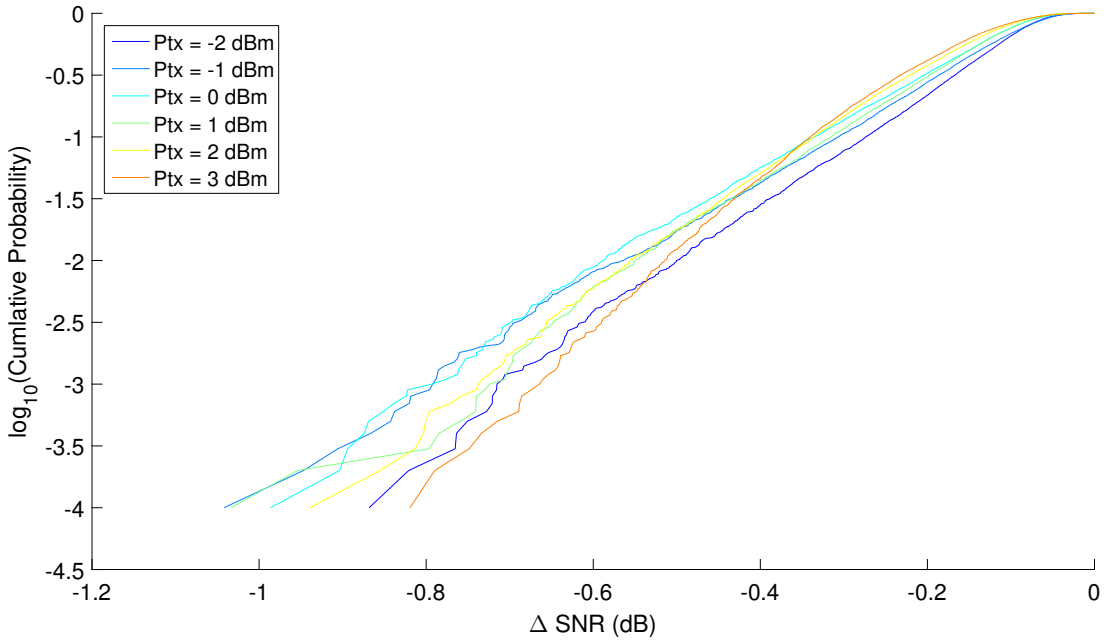

Figure 4.18: Cumulative probability for a SNR penalty with respect to the no link PDL for each PM-QPSK launch power

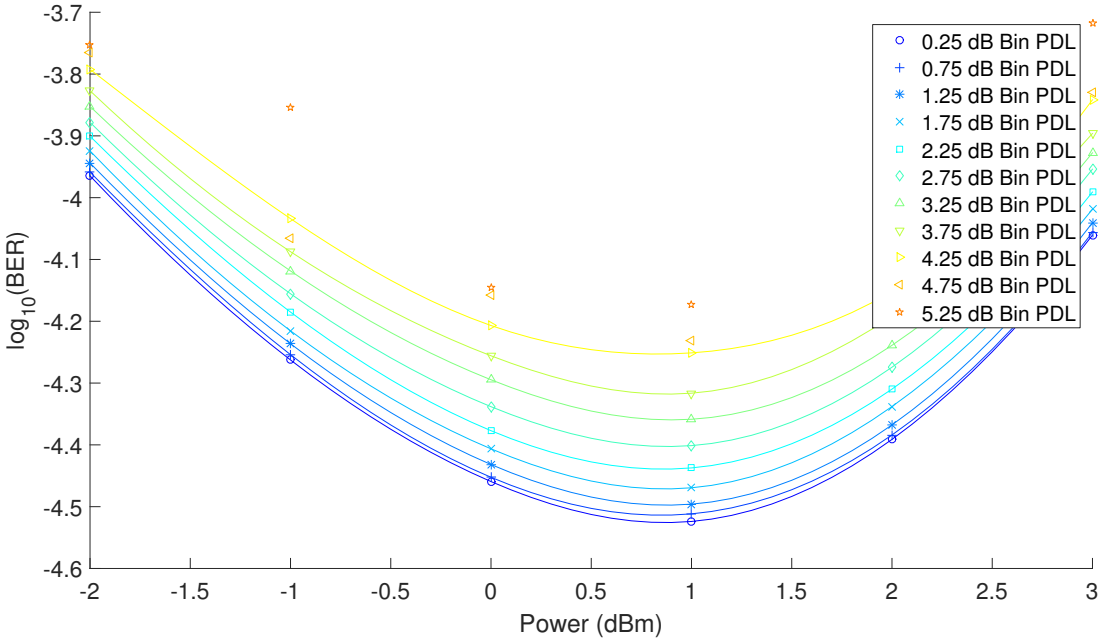

Figure 4.19: Averaged BER performance per 0.5 dB bin of PDL

4.5.3 Simulated Impact of PDL on Link Performance

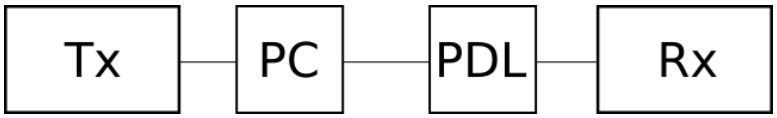

Figure 4.20: Simulation setup for lumped PDL

The exact implementation of receiver DSP used in the line card is proprietary and therefore not discussed in this chapter. The impact of the PDL is however far less than what is expected from standard coherent receiver DSP [10] as shown in [65] [67]. The implementation of DSP investigated in [66] is instead used to perform a simulation with the setup in Fig. 4.20.

A $2^{15}-1$ PRBS sequence is used to modulate PM-QPSK and PM-16QAM, the modulated signal is then passed through a polarization rotator to achieve an incident angle of $\theta = 0^{\circ}$ or $\theta = 45^{\circ}$ to establish the worst and best cases for each value of simulated PDL. The value of the PDL element is increased from 0 to 6 dB in steps of 0.2 dB. The signal is then detected by a 1 tap maximum likelihood (ML) receiver to be decoded [66]. The results in terms of the change in SNR (converted from BER) are shown in Fig. 4.21 and Fig. 4.22. It can be seen that for a PM-QPSK system, the simulated results agree well with experimental measurements. However for the PM-16QAM simulation, the experimental results are shown to perform slightly better. The received signal in a distributed PDL system has a combination of N polarization coloured noises which themselves experience PDL and attenuation during link propagation. This effect was investigated in [70] where the lumped PDL model was shown to impair system performance more than a distributed PDL model due to overestimation of the variation in SNR.

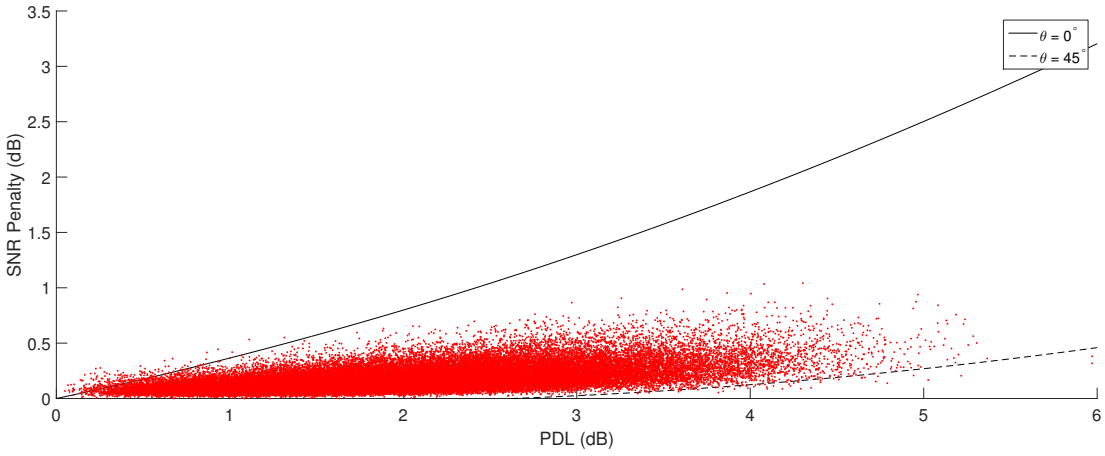

Figure 4.21: Impact of PDL on PM-QPSK performance

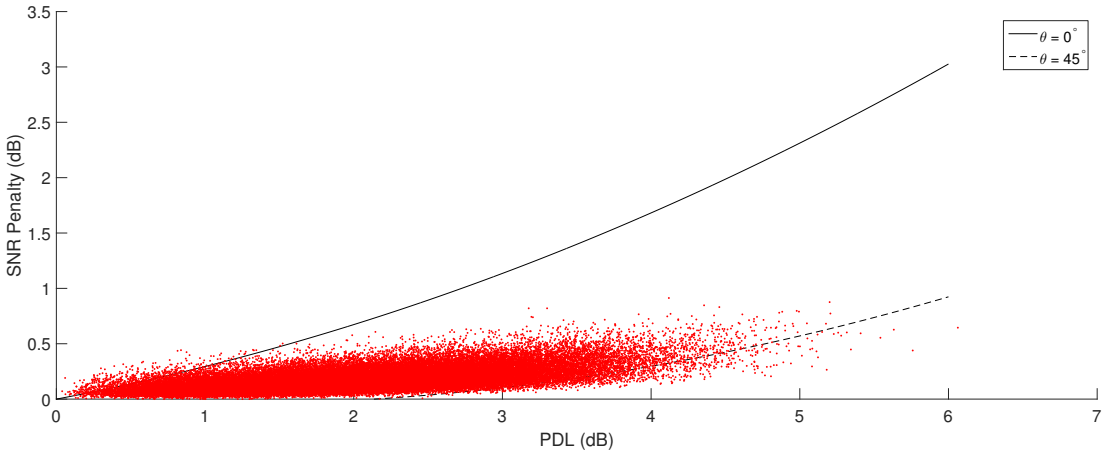

Figure 4.22: Impact of PDL on PM-16QAM performance

4.5.4 Summary

In this section, the impact of distributed PDL was examined for current generation commercially available coherent line cards operating at 35 Gbaud modulating PM-QPSK and PM-16QAM. It is expected that next generation optical systems will incorporate more optical routing elements i.e. ROADMs to provide functionality to implement SDNs. These components will have an inherent PDL and pose an interesting design challenge for next generation coherent optical fibre systems.

The experiment distributed 8 PDL elements throughout a fibre link consisting of 8 spans of 80 km SMF. Each PDL element had its own polarization controller after it, except for the last element. Initially a polarization synthesizer was used to sweep the initial transmitter polarization state across the Poincaré's sphere while the PCs were randomly set to generate 60 instances of link PDL per optical launch power. This had less than a 0.18 dB effect on the link performance. The polarization synthesizer was instead used to stabilize the transmitter SOP and the instances of link PDL increased to 120,000 due to the minimal impact of the transmitter SOP. These instances were divided between the two modulation formats and 6 optical launch powers. Monte Carlo simulations to calculate the link PDL PDFs showed a disparity between the simulated distribution and the measured PDL distribution, this is believed to be due to polarization dependent gain in the optical amplifiers. The experimental PDL value extracted from the stokes vectors measured by the polarimeter were verified by a separate measurement obtained from the line card.

It was found that there was a minimal dependence of PDL impact on the optical launch power indicating that the PDL-NL interaction is slight but present. This was reflected in a negligible change in the optimum optical launch power. The impact of up to a link PDL of 6 dB was found to be less than 0.9 dB for PM-16QAM and less than 1.05 dB for PM-QPSK.

Simulations were performed using published receiver DSP using a lumped PDL model to explain the excellent performance of the line card with respect to PDL. The simulated results for the PM-QPSK system was found to agree well with the experimental measurements however the PM-16QAM experimental system was found to be slightly better than expected. This is believed to be due to the overestimation of link impairment by the lumped PDL model compared to the experimental distributed PDL instance. Unfortunately an investigation of the distributed model would require an extensive Monte Carlo simulation involving a similar order of instances of simulated link PDL in addition to ML receiver DSP.

5 Performance Estimation

5.1 Abstract

The predicted functionality of the next generation of optical systems incorporating advanced provisioning algorithms, it is desirable to have the ability to determine the performance of the channel to be deployed. Of particular interest is the upgrade of an existing channel to a higher cardinality modulation format. The easiest solution would be to take the channel out of service, deploy the channel with new parameters and then measure and tune the channel. This would of course require down time. This chapter proposes an algorithm taking advantage of the incoherent approximation for the accumulation of non-linear effects to predict the performance margin for a PM-16QAM signal using the metrics from a currently operational PM-QPSK signal. Without this approximation, the maximum error magnitude increased from 0.8 dB to 3.5 dB. A further refinement decreased the estimation error to less than 0.5 dB in a 88 channel DWDM system transmitting at 35 Gbaud.

5.2 Introduction

Traditionally optical network have been of a static nature with link reconfigurations largely determined by equipment failure, upgrade paths or end of life situations. The next generation of optical networks is likely to incorporate elements such as EON [26], a flexible spectrum grid based on the latest ITU-T recommendation [6] and flexible modems [16]. Optimization of networks based on using such modems and flex-grid has been shown to gain up to a 5 fold increase in capacity [71] and research is on-going on the benefits of implementing link appropriate modulation formats to increase capacity on existing networks [72]. The operator may however decide to operate at a lower cardinality modulation format than the modem is capable for energy efficiency or additional performance margin. In a situation requiring a higher data rate or there is a need to reclaim a transmitter by aggregating lower bit rate channels into one high bit rate channel, it is desirable to be able to estimate the performance of the new modulation format without disturbing current operation. In this chapter the performance margin is estimated in OSNR for a 35 Gbaud PM-16QAM signal from the OSNR margin of a PM-QPSK signal in a C-band WDM configuration using a modem capable of switching the two formats for 100 Gbit/s and 200 Gbit/s net data rate operation transmitting over a distance of up to 800 km.

5.3 Theory

For a simple optical system transmitting directly from the transmitter to the receiver with no other components in between impairing the system's performance, the performance can be directly measured by counting the number of errored bits to get the corresponding BER. This measurement does not however encompass the range of the transceiver performance. To investigate the range of performance in this B2B configuration, optical noise loading is usually performed.

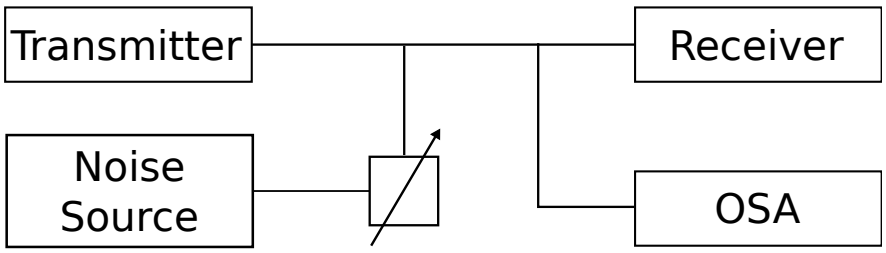

Figure 5.1: Simple noise loading experiment

The noise power being coupled in with the signal is then gradually increased and the BER is measured at each incremental value. An OSA is used to measure the OSNR over 12.5 GHz of bandwidth.

This characterisation of the transceiver is the foundation of optical network design since the best possible performance occurs in a B2B configuration. In the optical telecommunications industry, the amount of margin available to a system is measured by the two figures of merit, the ROSNR to achieve a certain BER and the OSNR at the receiver as measured by an OSA. The RxOSNR degrades with transmission distance due to the additional amount of optical amplifiers required to re-amplify the optical signal to a power level that can be detected by the receiver as per [43]

$$OSNR_{dB} = 58 + P_{out} - L_{span} - NF - 10log_{10}(N_{span}) \tag{5.1}$$

where P_{out} is the power coming out of the transmitter, L_{span} is loss of a fibre span in dB, NF is the noise figure of the optical amplifier and N_{span} is the number of fibre spans. This equation assumes that all fibre spans are of equal length which is not the case in deployed optical transmission systems which have geographical constraints.

Therefore it should be possible to estimate the system margin in OSNR at a certain transmission distance in a linear system using

$$Margin_{OSNR_{dB}} = OSNR_{span} - ROSNR_{B2B} \tag{5.2}$$

From this, it should be evident that it is possible to calculate the margin for one modulation format from the known margin of a different format, for example PM-16QAM margin estimation from PM-QPSK using

$$Margin_{PM-16QAM} = Margin_{PM-QPSK} - (ROSNR^{B2B}_{PM-16QAM} - ROSNR^{B2B}_{PM-QPSK}) \tag{5.3}$$

In practice, the optical fibre is a non-linear transmission medium through which propagation experiences the non-linear Kerr effect which places a limit on the capacity of the optical fibre [73]. This Kerr non-linearity may be modelled as an additive noise term with a variance proportional to the signal power cubed [59]. This non-linear noise term appears as a penalty to the ROSNR of the optical signal. The signal therefore has an effective signal to noise ratio (SNR_{eff}):

$$SNR_{eff} = \frac{P_{sig}}{P_{ase} + P_{nl}} \tag{5.4}$$

Due to its dependence on the power of the optical signal, if the optical amplifier for a fibre span exactly compensates for the loss of the span, the non-linear noise power will then be the same per span of the same type. It has been shown that the accumulation of the non-linear noise can be approximated as incoherent and therefore additive [59] as shown in Fig. 5.2. This means that for the example system in Fig. 5.2, using Eqn. 5.2

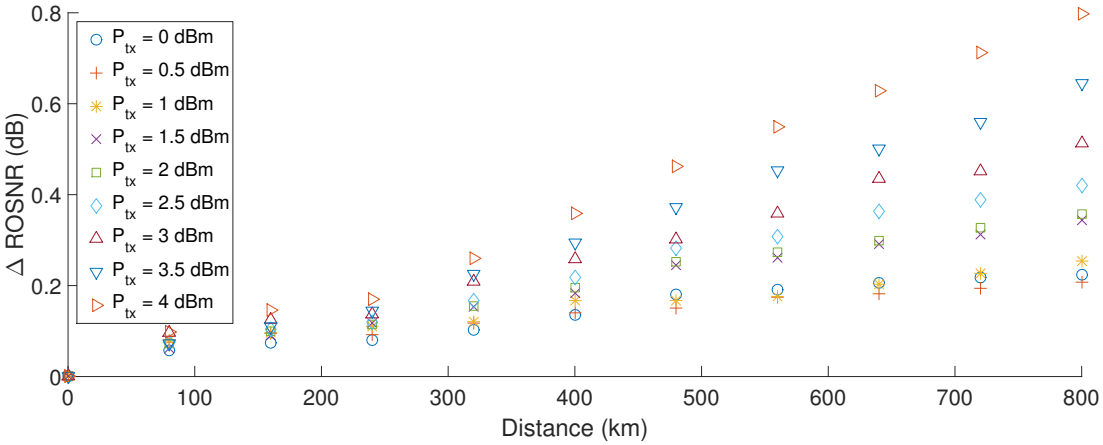

Figure 5.2: Increase in ROSNR for a 35 Gbaud PM-QPSK signal over 80 km spans of SMF with linear fit

may be up to 0.8 dB in error. This in turn means that Eqn. 5.3 may have an even greater error due to the decreased euclidean distance between constellation points belonging to PM-16QAM. To rectify this, we add in a non-linear penalty term based on incoherent linear accumulation into Eqn. 5.3 with respect to the modulation formats used, and number of spans.

$$Margin_{PM-16QAM} = Margin_{PM-QPSK} - (ROSNR^{B2B}_{PM-16QAM} - ROSNR^{B2B}_{PM-QPSK} + N_{span} \times (NLPenalty_{PM-QPSK} - NLPenalty_{PM-16QAM}) \tag{5.5}$$

where $Margin_{PM-16QAM}$ is the estimated PM-16QAM margin, $Margin_{PM-QPSK}$ is the measured PM-QPSK margin, ($ROSNR^{B2B}_{PM-16QAM}$ is the ROSNR for PM-16QAM in a B2B system, $ROSNR^{B2B}_{PM-QPSK}$ is the ROSNR for B2B PM-QPSK performance, N_{span} is the number of fibre spans. $NLPenalty_{PM-QPSK}$ and $NLPenalty_{PM-16QAM}$ are the non-linear penalties to the ROSNR per fibre span for PM-QPSK and PM-16QAM respectively.

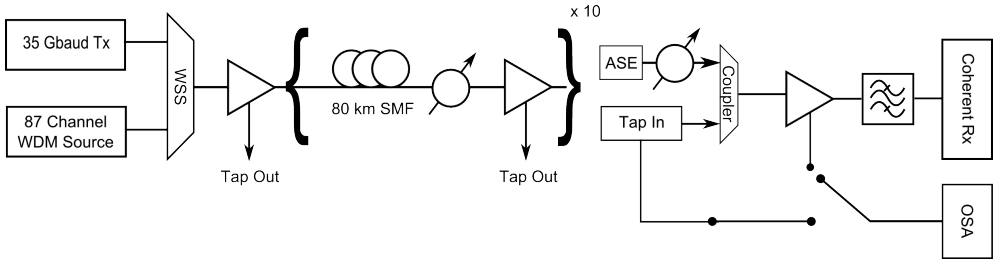

(a) Experimental setup using commercial 35 Gbaud flexible PM-QPSK/16QAM transceivers

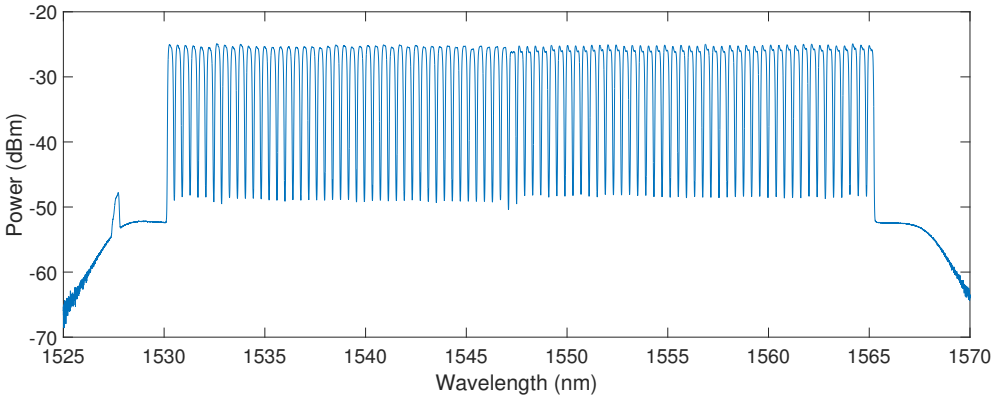

(b) OSA trace of the 88 equalized channels over the C-band

Figure 5.3

5.4 Experimental Setup

Figure 5.3a shows the experimental setup used to investigate the methodology detailed above. A commercially available 35 Gbaud real-time flexible bit rate modem [14] is used to generate a PM-QPSK or PM-16QAM test signal at 1547.316 nm. 87 ECLs with 20 kHz linewidth are spaced on the ITU-T 50 GHz frequency grid, these ECLs are then bulk modulated by a modified version of the commercial transceiver, also at 35 Gbaud. Each channel is de-multiplexed using an AWG and then optically de-correlated before being recombined using another AWG. The de-correlated DWDM channels are combined with the test channel using a WSS which also equalizes the per channel power at the launch point into the fibre link. Root raised cosine pulse shaping with a roll-off $\alpha = 0.14$ [14] of is applied to every channel. The amplifiers used are EDFAs with a nominal noise figure of 6.5, each EDFA is set into constant gain mode to compensate exactly for the loss of the preceding fibre span. The launch power into the fibre is controlled by adjusting the gain of the first EDFA after the WSS. The combined DWDM signals are transmitted over up to 800 km of standard SMF separated into 10 spans of 80 km. The test signal is tapped out using the monitor port on every EDFA, it is then noise loaded using a broadband noise source and then passes through a 50 GHz bandpass filter. The noise power is adjusted using a VOA for a desired OSNR after which the BER performance is measured using another real-time transceiver. The ROSNR for a 3.4% BER [14] is then acquired. The received OSNR is measured by the OSA straight

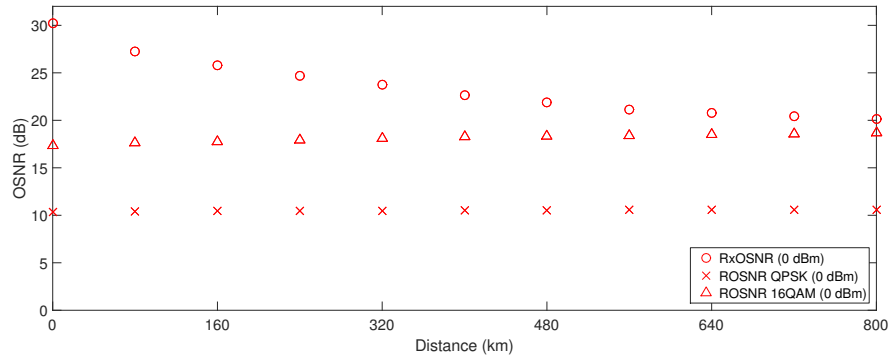

(a)

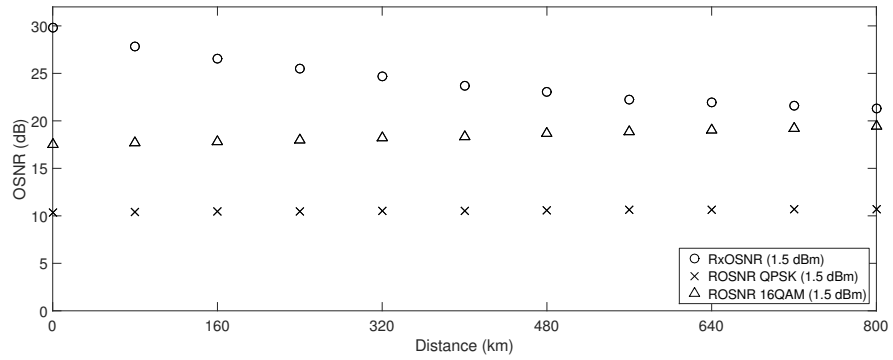

(b)

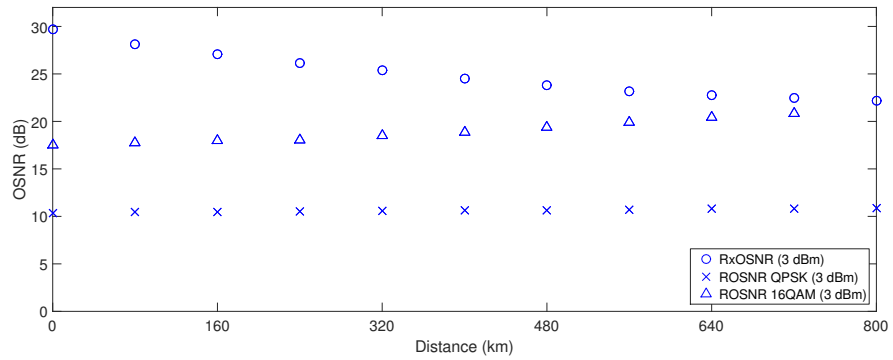

(c)

Figure 5.4: ROSNR evolution for PM-QPSK and PM-16QAM over 10 $\times$ 80 km SMF

from the tap out.

5.5 Results

We first examine the progression of ROSNR with the number of propagated spans to see if the incoherent linear accumulation assumption of non-linear noise remains valid. Figure 5.4 shows the ROSNR for PM-QPSK and PM-16QAM and also the received OSNR with respect to transmission distance at Fig. 5.4a 0 dBm, Fig. 5.4b 1.5 dBm and Fig. 5.4c 3 dBm optical launch power per channel, the 0 km points are the tap out from the first EDFA used to control the launch power into the fibre. It can be seen that

the ROSNRs for each modulation format increase linearly with distance in the figures, however the 3 dBm set for PM-16QAM begins to exhibit some break down in this and the accumulation becomes quadratic rather than linear due to the increase vulnerability of PM-16QAM to non-linear distortion compared to PM-QPSK since its constellation points are spaced tighter. We first use a linear accumulation assumption.

The experimental setup is used to sweep the per channel optical launch power from 0 to 4 dBm in 0.5 dB steps. The RxOSNR is measured using an OSA operating at 0.03 nm resolution and then noise loading is performed to acquire the ROSNR for 3.4% BER. Due to the inherent difficulty of measuring a small variation in OSNR, due to experimental variability. The non-linear penalty per span is calculated difference the measured ROSNR at the output of the seventh span and the B2B ROSNR divided by 7, Figure 5.5a and 5.5b. It should be noted that in Fig. 5.5b, the 3.5 and 4 dBm points do not fit the linear accumulation assumption.

These fits are used to predict the OSNR margin for the PM-16QAM signal over the range of 9 optical launch powers. Figure 5.5 shows the predicted margin using the linear accumulation assumption throughout with the non-linear modification and also without (naive). Overall Eqn. 5.5 works very well apart from the aforementioned 3.5 dBm and 4 dBm launch power cases, in which case the equation over-estimates the available margin. This performance can be improved by using three points to fit a quadratic and then changing Eqn. 5.5 to

$$\begin{aligned} Margin_{PM-16QAM} = Margin_{PM-QPSK} - (ROSNR^{B2B}_{PM-16QAM} - \\ ROSNR^{B2B}_{PM-QPSK} + (NLPenalty^{Nspan}_{PM-QPSK} - NLPenalty^{Nspan}_{PM-16QAM}) \end{aligned} \tag{5.6}$$

where $(NLPenalty^{Nspan}_{PM-QPSK}$ and $NLPenalty^{Nspan}_{PM-16QAM}$ are the respective accumulated non-linear penalties after N number of spans in the transmission system.

This quadratic assumption at higher powers corrects the error in the prediction incurred, Fig. 5.7a as can be seen by the change in the probability distribution using the revised assumption in Figure 5.7b.

5.6 Summary

A method to estimate the performance margin of a PM-16QAM signal based on the performance of a PM-QPSK signal was proposed and investigated using a 35 Gbaud WDM system transmitting over up to 10 spans of 80 km SMF. The transceivers are commercially available products capable of modulating PM-QPSK and PM-16QAM. The algorithm accounts for the non-linear effect of fibre propagation on the optical signal, based on the incoherently accumulated non-linearity per fibre span. The margin in OSNR for both formats was measured at the output of each span and compared

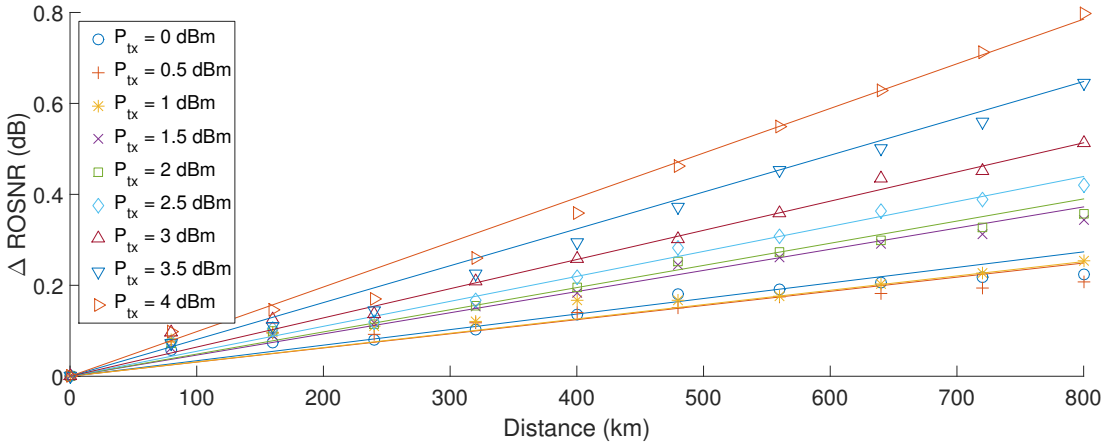

(a) ROSNR Fit for PM-QPSK

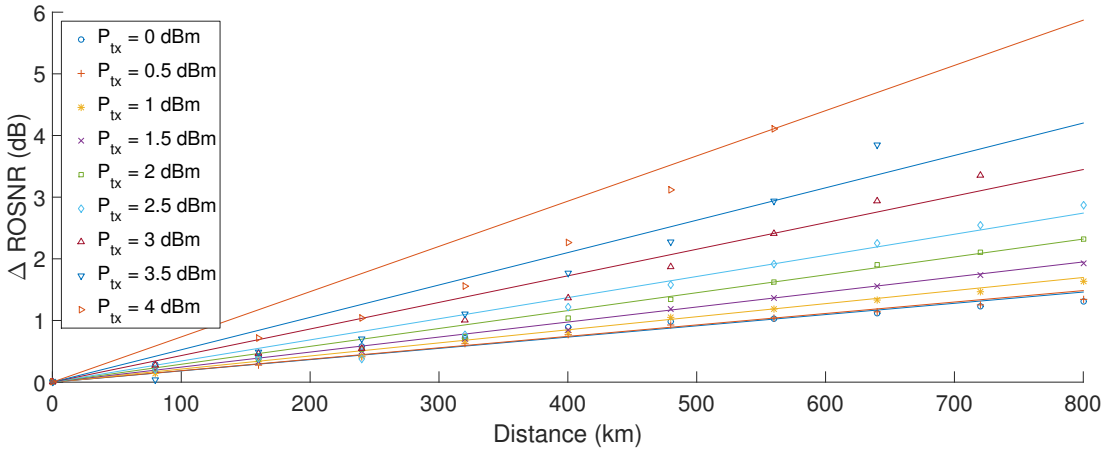

(b) ROSNR Fit for PM-16QAM

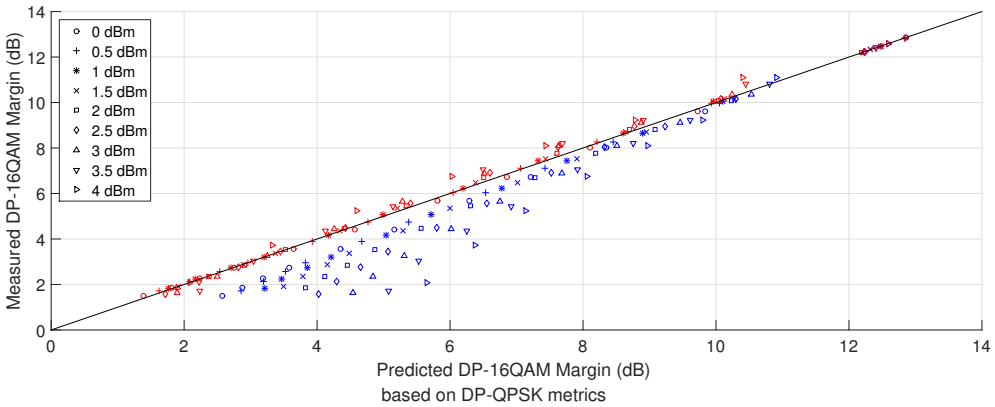

Figure 5.5: Predicted Margin using naive prediction (blue) and linear accumulation assumption (red)

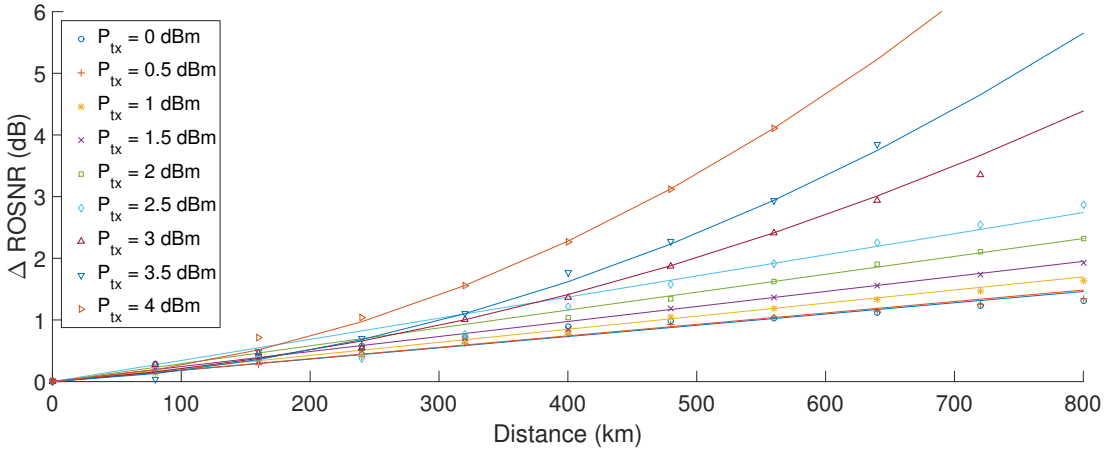

Figure 5.6: PM-16QAM OSNR progression with a quadratic fit at high powers

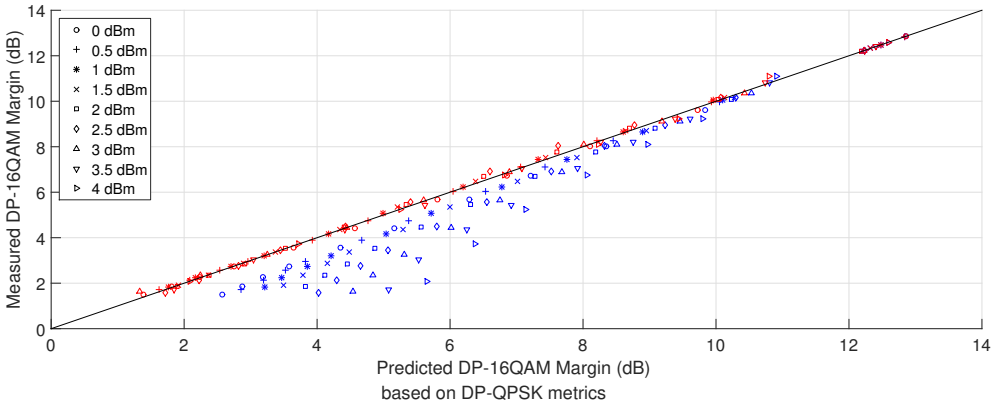

(a) Predicted Margin using naive prediction (blue) and quadratic accumulation assumption (red)

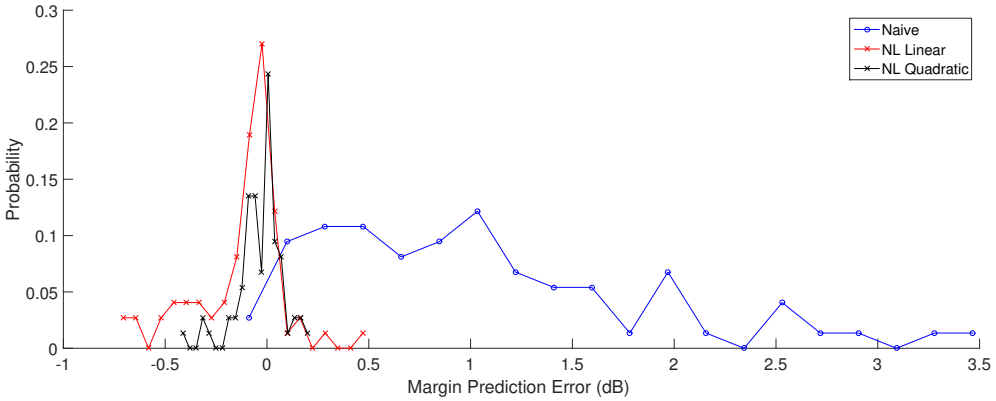

(b) Probability distribution of error in predicted margin

Figure 5.7

to the predicted PM-16QAM margin based on the measured PM-QPSK metrics then compared to the experimental. At higher powers it was found that the non-linearity did not accumulate linearly in dB, this was compensated for by taking a quadratic assumption for accumulation. The maximum error incurred by this method was 0.4 dB.

6 Future Work

6.1 Abstract

In this chapter, I describe proposed future research topics for the design of next generation optical systems. First we discuss the use of further investigations of probabilistic design methodology for coherent optical systems. We then discuss the application of the probabilistic design methodology for optical networks design. Lastly I propose a combination of chapter 3 and 4 for further examination. Finally we discuss this research project's conclusion as a whole.

6.1.1 Further investigation of Probabilistic Design

This work has performed a great deal of investigation into using probabilistic design methodology in optical fibre transmission systems. However due to the time limited nature of the work, fixed value perturbations were used in the investigations to simulate the extreme values of a Gaussian distribution. Therefore the CDFs shown in chapter 3 are a representative of that particular experimental setup. The 3 parameter model that was shown to be capable of performance prediction is a promising start for a Monte Carlo simulation of such a link. Ideally links incorporating longer link lengths, as well as a full Gaussian distribution would be used. There is however some risk since the model was validated for one particular system, albeit using two different modulation formats. It would be desirable to perform experimental validation of such an extended

setup. This would require a significant investment of laboratory or processing time.

Probabilistic Design in Optical Networks

Chapter 1 provided some background on the research that has been conducted to achieve increased capacity in optical networks. Probabilistic design was shown in chapter 3 to provide a benefit in link outage probability at a lower optical launch power. This should be advantageous in a network environment by lowering the failure of a high cardinality modulation channel to an acceptable level in addition to decreasing XPM effects as a result of the lowered optical power. A comparison of a deterministically designed network with one using probabilistic design would be extremely interesting.

6.1.2 Probabilistic Design and PDL

Though the PDL and non-linear effect interaction was shown to be minimal in chapter 4, the question arises on what impact there would be on a system when the intra-link optical power profile approaches the extreme value worst case in addition to having link PDL. This may be very impractical to perform even experimentally using real time equipment. Restricting the experiment to the parameters used in this work, there would be on the order $1024 \times 10000 \times 6$ cases. A limited test case using high values of perturbation and PDL elements to validate a modification of the three parameter model may prove to be more practical.

6.2 Conclusions

In this thesis, we examined the coherent receiver after implementation of extra functionality to create a software defined transceiver. In particular it was used as a sensing device to establish parameters for link design and provisioning. Initially the SDT was used to perform very fast wideband spectral sensing. This accomplished with the aide of DSP to form a complete estimation of the sensed bandwidth by subdividing it into detected spectral slices which were then digitally stitched together. A MTM was used to generate the spectral slices to compensate for a small number of measured samples. This was demonstrated in an estimation of the optical C-band, which used 39 tapers. This method was incorporated into a provisioning algorithm as the first step in sensing spectral occupancy. A very low power probe was used to detect of a particular channel had been dropped prior to reception indicating occupancy. The combination of the two methods established spectral occupancy of the desired wavelength. The probe's performance was then measured and using pre-calibrated LUTs, the neighbouring channel powers were estimated to determine an optimum provisioning point.

We then investigated the probabilistic design methodology by introducing uncertainty to the optical link power profile by perturbing the optical power into each span. It was shown that it could provide a significant improvement in outage probability, particularly where a high cardinality modulation format is operating close the its FEC threshold. Indeed, we showed situations where the traditional design method would have ruled out implementation of such a modulation format. The provisioning for probabilistic design was also shown to be at a lower power than traditional, due to the non-linearity of the transmission medium which should prove to be advantageous by allowing more channels for the same total power in an optical fibre. A three parameter model was proposed to fit to the perturbed system based on an understanding of the GN model. This was validated on a single channel 11.5 Gbaud PM-QPSK system and then extended to a 35 Gbaud DWDM PM-QPSK and PM-16QAM where it predicted the performance of a perturbed system excellently up the FEC threshold used by the transceivers. The DWDM PM-16QAM in particular exemplified the advantage of probabilistic design since the equivalent deterministic design was non-operable. This leads us to believe that the probabilistic design method is superior to traditional design.

The impact of multiple PDL elements in a optical system is then quantified for currently commercially available systems to provide insight into the deployment of next generation systems. This is of importance since it is predicted that due to the inclusion of more ROADMs to provide flexibility to optical networks, there will be an increase in link PDL. There has been to date no experimental investigation of DWDM high baud links with respect to link PDL which could lead to sub par design. Indeed, the experimental results showed that there was less than 1 dB penalty at 6 dB of link PDL, which is roughly the same or less than expected using a lumped PDL model with advanced DSP. Caution should be taken with these results as commercial product was used with proprietary DSP and such results may not be applicable to all transceivers.

Finally, a algorithm for on the fly estimation of PM-16QAM performance margin from PM-QPSK metrics was investigated and proved to have a decrease from 3.5 estimation error to 0.5 dB by using an adaptation based on the incoherent accumulation of non-linear impairments approximation from the GN model. It was also shown that this accumulation is not quite linear at high optical powers. This algorithm was envisaged to be used for modulation format switching without taking transceivers out of service.

It is clear that the increased functionality of the SDT based on the coherent receiver provides a multitude of functionality and unprecedented flexibility with respect to optical systems design. This flexibility also makes design of the next generation of systems quite a challenge since network dynamics will increase. The traditional response has been to design more margin to account for such an effect but the amount of margin is decreasing due to the increase in transmission systems baud as well as

modulation format cardinality. Probabilistic design was investigated to leverage the non-linearity of the transmission medium to provide an alternative provisioning while also minimising over-engineering. The drawback of probabilistic design is the large body of data required to generate the DCT for a system, however advanced DSP can mitigate this such as shown for PDL in chapter 4 allowing for a simplified version of probabilistic design to be used in conjunction with provisioning a small amount of margin. Future systems will likely incorporate such design concepts as demand for bandwidth increases.

Appendix

Deriviation of proof for link polarization dependent loss extraction from degree of polarization by Michael Reimer of Ciena Corporation, 3500 Carling Avenue,Ottawa ON, K2H 8E9, Canada. Let

$$H = exp(\frac{\alpha}{2}\hat{r}.\hat{\sigma}) = \cosh\frac{\alpha}{2}\mathbb{I} + \sinh\frac{\alpha}{2}(\hat{r}.\hat{\sigma}) \tag{6.1}$$

where $\alpha = PDL_{dB} \times \frac{ln(10)}{20}$ and $\hat{r}$ is the minimum loss axis on the Poincaré's sphere.

$$|s> = QPSK\ (or\ any\ coherent\ modulation) \tag{6.2}$$

$$P_0 =< s|s> \tag{6.3}$$

$$|r> = H|s> = signal\ after\ PDL \tag{6.4}$$

$$\begin{aligned} P &=< r|r> = received\ signal\ power \\ &=< s|H^H H|s> \\ &=< s|H^2|s> \\ &=< s|\cosh\alpha\mathbb{I} + \sinh\alpha\hat{r}.\hat{\sigma}|s> \\ &= \cosh\alpha P_0 + \sinh\alpha < s|\hat{r}.\hat{\sigma}|s> \\ &= \cosh\alpha P_0 + P_0\sinh\alpha\hat{r}.\hat{s} \end{aligned} \tag{6.5}$$

$$\tag{6.6}$$

where $\hat{s}$ = Poincaré's vector of data symbols

$$\therefore\ EP = \cosh\alpha P_0 + P_0\sinh\alpha\hat{r}.E\hat{s} \tag{6.7}$$

$\hat{r}.E\hat{s} = 0$ since modulated data is symmetrical around the Poincaré's sphere

$$\therefore\ EP = time\ averaged\ received\ power \tag{6.8}$$
$$= P_0 \cosh\alpha \tag{6.9}$$

The received Stokes vector is

$$|r> = H|s> \Rightarrow \vec{r} = <r|\vec{\sigma}|r> = <s|H^H\vec{\sigma}H|s> \tag{6.10}$$
$$= <s|H\vec{\sigma}H|s> \tag{6.11}$$

$$\begin{aligned}\therefore \vec{r} &= <s|(\cosh\frac{\alpha}{2}\mathbb{I} + \sinh\frac{\alpha}{2}\hat{r}.\vec{sigma})\vec{\sigma}(\cosh\frac{\alpha}{2}\mathbb{I} + \sinh\frac{\alpha}{2}\hat{r}.\vec{\sigma})|s> \\ &= <s|(\cosh\frac{\alpha}{2}\hat{\sigma} + \sinh\frac{\alpha}{2}(\vec{r}.\vec{sigma})\vec{\sigma})(\cosh\frac{\alpha}{2}\mathbb{I} + \sinh\frac{\alpha}{2}\hat{r}.\vec{\sigma})|s> \\ &= <s|(\cosh^2\frac{\alpha}{2}\vec{\sigma} + \cosh\frac{\alpha}{2}\sinh\frac{\alpha}{2}.\vec{\sigma}(\hat{r}.\vec{\sigma}) + \cosh\frac{\alpha}{2}\sinh\frac{\alpha}{2}(\hat{r}.\vec{\sigma})\vec{\sigma} + \sinh^2\frac{\alpha}{2}(\hat{r}.\vec{\sigma})\vec{\sigma}(\vec{r}.\vec{\sigma}))|s>\end{aligned} \tag{6.12}$$

$$\begin{aligned}\therefore \vec{r} = \cosh^2\frac{\alpha}{2} <s|\vec{\sigma}|s> &+ \cosh\frac{\alpha}{2}\sinh\frac{\alpha}{2} <s|\vec{\sigma}(\hat{r}.\vec{\sigma})|s> \\ &+ \cosh\frac{\alpha}{2}\sinh\frac{\alpha}{2} <s|(\hat{r}.\vec{\sigma})\vec{\sigma}|s> \\ &+ \sinh^2\frac{\alpha}{2} <s|(\hat{r}.\vec{\sigma})\vec{\sigma}(\hat{r}.\vec{\sigma})|s>\end{aligned} \tag{6.13}$$

Applying matrix identities

$$\vec{\sigma}(\hat{r}.\vec{\sigma}) = \hat{r}\mathbb{I} + i\hat{r}\times\vec{\sigma} \tag{6.14}$$
$$(\hat{r}.\vec{\sigma})\vec{\sigma} = \hat{r}\mathbb{I} - i\hat{r}\times\vec{\sigma} \tag{6.15}$$
$$(\hat{r}.\vec{\sigma})\vec{\sigma}(\hat{r}\vec{\sigma}) = \hat{r}(\hat{r}.\vec{\sigma}) - \vec{\sigma} \tag{6.16}$$

$$\begin{aligned}\therefore \vec{r} = \cosh^2\frac{\alpha}{2}\vec{s} &+ \cosh\frac{\alpha}{2}\sinh\frac{\alpha}{2} <s|\hat{r}\mathbb{I} + i\hat{r}\times\vec{\sigma}|s> \\ &+ \cosh\frac{\alpha}{2}\sinh\frac{\alpha}{2} <s|\hat{r}\mathbb{I} - i\hat{r}\times\vec{\sigma}|s> \\ &+ \sinh^2\frac{\alpha}{2} <s|2\hat{r}(\hat{r}.\vec{\sigma}) - \vec{\sigma}|s>\end{aligned} \tag{6.17}$$

$$
\begin{aligned}
= \cosh^2\frac{\alpha}{2}\vec{s} &+ \cosh\frac{\alpha}{2}\sinh\frac{\alpha}{2} < s|s > + \cosh\frac{\alpha}{2}\sinh\frac{\alpha}{2} i < s|\hat{r}\times\vec{\sigma}|s > \\
&+ \cosh\frac{\alpha}{2}\sinh\frac{\alpha}{2}\hat{r} < s|s > - \cosh\frac{\alpha}{2}\sinh\frac{\alpha}{2} i < s|\hat{r}\times\vec{\sigma}|s > \\
&+ \sinh^2\frac{\alpha}{2} 2\hat{r} < s|\hat{r}.\vec{\sigma}|s > \\
&- \sinh^2\frac{\alpha}{2} < s|\vec{\sigma}|s >
\end{aligned} \tag{6.18}
$$

$$
\begin{aligned}
&= (\cosh^2\frac{\alpha}{2} - \sin^2\frac{\alpha}{2})\vec{s} + 2P_0\cosh\frac{\alpha}{2}\sinh\frac{\alpha}{2}\hat{r} + 2\sinh^2\frac{\alpha}{2}(\hat{r}.\hat{s})\hat{r} \\
&= \cosh\alpha\vec{s} + P_0\sinh\alpha\vec{r} + 2\sinh^2\frac{\alpha}{2}(\hat{r}.\hat{s})\hat{r}
\end{aligned} \tag{6.19}
$$

The measured Stokes vector varies at the transmitted symbol rate

$$
\vec{r} = \cosh\alpha\vec{s} + P_0\sinh\alpha\hat{r} + 2\sinh\frac{\alpha}{2}(\hat{r}.\hat{s})\hat{r} \tag{6.20}
$$

$$
\vec{r}_{pol} = E\vec{r} = Time\ average\ of\ received\ Stokesvector \tag{6.21}
$$

Note $E\vec{s} = 0$ due to data modulation symmetry.

$$
\therefore \vec{r}_{pol} = P_0\sinh\alpha\hat{r} \tag{6.22}
$$

$$
\begin{aligned}
Degree\ of\ Polarization &= \frac{|\vec{r}_{pol}|}{P} \\
&= \frac{P_0\sinh\alpha}{P_0\cosh\alpha} \\
&= \tanh\alpha
\end{aligned} \tag{6.23}
$$

$$
\therefore DOP = tanh(PDL_{dB}\times\frac{ln10}{20}) \tag{6.24}
$$

References

[1] Cisco. Cisco Visual Networking Index: Forecast and Methodology, 2014-2019 White Paper. Technical report, Cisco, 2016. 16, 20

[2] D Lavery and S J Savory. Digital Coherent Technology for Long-Reach Optical Access. In *Optical Fiber Communication Conference*, volume 2, pages 2–4, 2014. 17

[3] Daniel Cardenas, Domanic Lavery, Philip Watts, and Seb J Savory. Reducing the Power Consumption of the CMA Equalizer Update for a Digital Coherent Receiver. In *Optical Fiber Communication Conference*, page Th4D.5, 2014. 17

[4] Richard S. Vodhanel, Aly F. Elrefaie, M.Z. Iqbal, R.E. Wagner, James L. Gimlett, and Shinji Tsuji. Performance of Directly Modulated DFB Lasers in 10-Gb/s ASK, FSK, and DPSK Lightwave Systems. *Journal of Lightwave Technologyger*, 8(9):1379–1386, September 1990. 17

[5] K. Kikuchi, T. Okoshi, and J. Kitano. Measurement of bit-error rate of heterodyne-type optical communication system - a simulation experiment. *Quantum Electronics, IEEE Journal of*, 17(12):2266–2267, December 1981. 17

[6] International Telecommunication Union. Spectral grids for WDM applications: DWDM frequency grid. *ITU-T Recommendation G.694.1*, 2012. 17, 20, 21, 90

[7] Govind P. Agrawal. *Fiber-Optic Communication Systems*. Wiley inter-Science, 2002. 17, 51

[8] D. Lavery, C. Behrens, S. Makovejs, D.S. Millar, R.I. Killey, S.J. Savory, and P. Bayvel. Long-haul transmission of ps-qpsk at 100 gb/s using digital back-propagation. *Photonics Technology Letters, IEEE*, 24(3):176–178, Feb 2012. 19

[9] Michael A Reimer, Shahab Oveis Gharan, Andrew Shiner, Akbar Ghasemi, and Maurice O'Sullivan. Performance optimized modulation formats in 4 and 8 dimensions. In *Signal Processing in Photonic Communications*, pages SpT3D–6. Optical Society of America, 2015. 19

[10] Seb J Savory. Digital filters for coherent optical receivers. *Opt. Express*, 16(2):804–817, 2008. 19, 27, 73, 74, 86

[11] Ezra Ip, Alan Pak Tao Lau, Daniel J F Barros, and Joseph M Kahn. Coherent detection in optical fiber systems. *Optics express*, 16(2):753–791, 2008. 19

[12] Qunbi Zhuge, Michael Reimer, Andrzej Borowiec, Maurice O'Sullivan, and David V Plant. Aggressive Quantization on Perturbation Coefficients for Nonlinear Pre-Distortion. *Optical Fiber Communication Conference*, page Th4D.7, 2014. 19

[13] Domanic Lavery, David Ives, Gabriele Liga, Alex Alvarado, Seb J. Savory, and Polina Bayvel. The Benefit of Split Nonlinearity Compensation for Optical Fiber Communications. *arXiv*, pages 1–4, 2015. 19

[14] Kim Roberts, Sik Heng Foo, Michael Moyer, Michael Hubbard, Andrew Sinclair, Jamie Gaudette, and Charles Laperle. High Capacity Transport at 100G and Beyond. *Journal of Lightwave Technology*, 33(3):563–578, 2015. 20, 21, 34, 61, 74, 93

[15] Masahiko Jinno, Takuya Ohara, Yoshiaki Sone, Akira Hirano, Osamu Ishida, and Masahito Tomizawa. Elastic and adaptive optical networks: possible adoption scenarios and future standardization aspects. *IEEE Communications Magazine*, 49(10):164–172, 2011. 20

[16] J K Fischer, S Alreesh, R Elschner, F Frey, M Nölle, and C Schubert. Bandwidth-Variable Transceivers Based on 4D Modulation Formats for Future Flexible Networks. In *Eur. Conf. Exhib. Opt. Commun.*, pages 1–3, 2013. 21, 90

[17] DJ Ives, Polina Bayvel, and SJ Savory. Adapting Transmitter Power and Modulation Format to Improve Optical Network Performance Utilizing the Gaussian Noise Model of Nonlinear Impairments. *J. Light. Technol.*, 32(21):3485–3494, 2014. 21

[18] Open Networking Foundation. Software-defined networking:the new norm for networks. *ONF White Paper*, 2012. 22

[19] Masato Yoshida, Toshihiko Hirooka, Keisuke Kasai, and Masataka Nakazawa. Adaptive 4˜64 QAM real-time coherent optical transmission over 320 km with FPGA-based transmitter and receiver. *Opt. Express*, 22(13):16520–7, June 2014. 22

[20] Thomas Szyrkowiec, Achim Autenrieth, Paul Gunning, Paul Wright, Andrew Lord, Jörg-Peter Elbers, and Alan Lumb. First field demonstration of cloud datacenter workflow automation employing dynamic optical transport network resources under OpenStack and OpenFlow orchestration. *Opt. Express*, 22(3):2595, January 2014. 22

[21] E. Mannie. Generalized multi-protocol label switching (gmpls) architecture, Oct 2004. 24

[22] Y. Yoshida et al. First international sdn-based network orchestration of variable-capacity ops over programmable flexi-grid eon. *Optical Fiber Conference*, 2014. 24

[23] Open Networking Foundation, *https://www.opennetworking.org*. 24

[24] Open Daylight, *https://www.opendaylight.org/odlbe*. 24

[25] S. Das et al. Why openflow/sdn can succeed where gmpls failed. *Eur. Conf. Exhib. Opt. Commun.*, 2012. 24

[26] Ori Gerstel. Elastic Optical Networking : A New Dawn for the Optical Layer ? *IEEE Comms. Mag.*, pages 12–20, 2012. 26, 90

[27] O. E. DeLange. Optical heterodyne detection. *IEEE Spectrum*, 5(10):77–85, 1968. 26

[28] T Okoshi. Feasibility studies of fdm optical communication systems using optical heterodyne or homodyne schemes'. *Record of Technical Group OQE78-139, IECE Japan*, 1979. 26

[29] T Okoshi and K Kikuchi. Frequency stabilisation of semiconductor lasers for heterodyne-type optical communication systems. *Electron. Lett.*, 16(5):179–181, 1980. 26

[30] F Favre and D Le Guen. High frequency stability of laser diode for heterodyne communication systems. *Electron. Lett.*, 16(18):709–710, 1980. 26

[31] Y Yamamoto. Receiver performance evaluation of various digital optical modulation-demodulation systems in the 0.5-10 μm wavelength region. *Quantum Electron. IEEE J.*, 16(1):1251–1259, 1980. 26

[32] Ezra Ip and Joseph M Kahn. Compensation of dispersion and nonlinear impairments using digital backpropagation. *Lightwave Technology, Journal of*, 26(20):3416–3425, 2008. 27

[33] D Millar, D Lavery, and R Maher. A baud-rate sampled coherent transceiver with digital pulse shaping and interpolation. *Optical Fiber Conference*, 2013. 27

[34] Finisar. Waveanalyzer 1500s high-resolution optical spectrum analyzer. https://www.finisar.com/optical-instrumentation/waveanalyzer-1500s-high-resolution-optical-spectrum-analyzer Accessed: 30-11-2015. 28

[35] A J Ward, D J Robbins, G Busico, E Barton, L Ponnampalam, J P Duck, N D Whitbread, P J Williams, D C J Reid, a C Carter, and M J Wale. Widely tunable DS-DBR laser with monolithically integrated SOA: Design and performance. *IEEE J. Sel. Top. Quantum Electron.*, 11(1):149–156, 2005. 28

[36] DJ Thomson. Spectrum estimation and harmonic analysis. *Proc. IEEE*, 70:1055–1096, 1982. 28, 30, 34

[37] D Slepian. Prolate spheroidal wave functions, Fourier analysis, and uncertainty. V-The discrete case. *T Tech. J.*, 1978. 29

[38] Rui Wu, VR Supradeepa, and CM Long. Generation of very flat optical frequency combs from continuous-wave lasers using cascaded intensity and phase modulators driven by tailored radio frequency. *Opt. Lett.*, 35(19):3234–3236, 2010. 30

[39] Robert Maher and Benn Thomsen. Dynamic linewidth measurement technique using digital intradyne coherent receivers. *Opt. Express*, 19(26):B313–22, December 2011. 31

[40] Hou-Man Chin, Kai Shi, Robert Maher, Milen Paskov, Benn Thomsen, and Seb Savory. Fast Optical Spectrum Estimation Using a Digital Coherent Receiver. In *Eur. Conf. Exhib. Opt. Commun.*, 2013. 35, 39

[41] Robert Borkowski, Darko Zibar, Antonio Caballero, Valeria Arlunno, and Idelfonso Tafur Monroy. Stokes Space-Based Optical Modulation Format Recognition for Digital Coherent Receivers. *IEEE Photonics Technol. Lett.*, 25(21):2129–2132, November 2013. 35

[42] Han Sun, Kuang-Tsan Wu, and Kim Roberts. Real-time measurements of a 40 Gb/s coherent system. *Opt. Express*, 16(2):873–9, January 2008. 36, 45

[43] Ivan Kaminow Tingye Li, editor. *Optical Fiber Telecommunications IV-B Systems and Impairments*. Elsevier Science, 2002. 47, 91

[44] John Proakis and Masoud Salehi. *Digital Communications, 5th Edition*. McGraw-Hill Education, 2007. 47

[45] Rogers H. Stolen. Nonlinearity in Fiber Transmission. *Proceedings of the IEEE*, 68(10):1232–1236, 1980. 49

[46] Jacklyn D Reis and António L Teixeira. Unveiling nonlinear effects in dense coherent optical WDM systems with Volterra series. *Opt. Express*, 18(8):8660–70, April 2010. 49

[47] ITU. ITU-T Series G Supplement 39. *ITU-T Recommendation G.694.1*, 2012. 49

[48] Emmanuel B. Desurvire, Clinton R. Giles, Jay R. Simpson, and John L. Zyskind. Erbium-doped fiber amplifier, 1991. 50

[49] M. W. Long and J. D. Narciso. Probabilistic Design Methodology for Composite Aircraft Structures. Technical Report June, National Aeronautics and Space Administration, 1999. 50, 70

[50] Karen S. Bernstein. Structural design requirements and factors of safety for spaceflight hardware for human spaceflight. Technical Report October, National Aeronautics and Space Administration, 2011. 50, 70

[51] Robin K. McGuire. Deterministic vs. probabilistic earthquake hazards and risks. *Soil Dynamics and Earthquake Engineering*, 21(5):377–384, 2001. 50, 70

[52] Norman Rasmussen. Reactor Safety Study. *October*, Second Pri(An Assessment of Accident Risks in U.S. Commercial Nuclear Power Plants):228, 1975. 50, 70

[53] Joseph H Yuen. *Deep space telecommunication systems engineering*. Jet Propulsion Laboratory, 1983. 50, 51, 70

[54] Richard L Horttor. Telecommunications Link Design. In *DESCANSO Seminar Talk Telecomm Link Design*, 2004. 50, 51, 52, 70

[55] Hou-Man Chin, Benn C. Thomsen, and Seb J. Savory. The effect of intra-link power perturbations on channel performance. In *European Conference and Exhibition on Optical Communications*, 2015. 51

[56] P.J. Lin. Reducing optical power variation in amplified optical network. In *Communication Technology Proceedings, 2003. ICCT 2003. International Conference on*, volume 1, pages 42–47 vol.1, April 2003. 51

[57] M. Yu, C. Kan, M. Lewis, and A. Sizmann. Statistics of polarization-dependent loss, insertion loss, and signal power in optical communication systems. *IEEE Photonics Technology Letters*, 14(12):1695–1697, 2002. 52

[58] J.A. Nagel. Statistical analysis of single-mode fiber field splice losses. *Optical Fiber Communication Conference/National Fiber Optic Engineers Conference*, 2(4):3–5, 2009. 52

[59] Pierluigi Poggiolini. The GN Model of Non-Linear Propagation in Uncompensated Coherent Optical Systems. *J. Light. Technol.*, 30(24):3857–3879, 2012. 59, 91

[60] CD Poole and RE Wagner. Phenomenological approach to polarisation dispersion in long single-mode fibres. *Electron. Lett.*, 22(19):19–20, 1986. 73

[61] G.J. Foschini and C.D. Poole. Statistical theory of polarization dispersion in single mode fibers. *J. Light. Technol.*, 9(11):1439–1456, 1991. 73

[62] Steven Gringeri, Bert Basch, Vishnu Shukla, Roman Egorov, and Tiejun J Xia. Flexible architectures for optical transport nodes and networks. *IEEE Communications Magazine*, 48(7):40–50, 2010. 73

[63] Sorin Tibuleac. ROADM Network Design Issues. *Optical Fiber Communication Conference and National Fiber Optic Engineers Conference*, page NMD1, 2009. 73

[64] Ping Lu, Liang Chen, Xiaoyi Bao, Ping Lu, Liang Chen, and Xiaoyi Bao. Statistical distribution of polarization-dependent loss in the presence of polarization-mode dispersion in single-mode fibers. *Photonics Technology Letters, IEEE*, 13(5):451 –453, 2001. 73, 79

[65] T. Duthel, C.R.S. Fludger, J. Geyer, and C. Schulien. Impact of Polarisation Dependent Loss on Coherent POLMUX-NRZ-DQPSK. In *OFC/NFOEC 2008 - 2008 Conference on Optical Fiber Communication/National Fiber Optic Engineers Conference*, pages 1–3, 2008. 74, 86

[66] Maxim Kuschnerov and Mohamed Chouayakh. On the Performance of Coherent Systems in the Presence of Polarization-Dependent Loss for Linear and Maximum Likelihood Receivers. *Photonics technology letters*, 22(12):920–922, 2010. 74, 86

[67] Olga Vassilieva, Inwoong Kim, and Takao Naito. Systematic investigation of interplay between nonlinear and polarization dependent loss effects in coherent polarization multiplexed systems. In *European Conference on Optical Communication, ECOC*, volume 1-2, pages 4–6, 2010. 74, 86

[68] C.R. Menyuk, D. Wang, and A.N. Pilipetskii. Repolarization of polarization-scrambled optical signals due to polarization dependent loss. *IEEE Photonics Technology Letters*, 9(9):1247–1249, 1997. 76

[69] Antonio Mecozzi and Mark Shtaif. The statistics of polarization-dependent loss in optical communication systems. *IEEE Photonics Technology Letters*, 14(3):313–315, 2002. 79

[70] Chongjin Xie. Polarization-Dependent Loss Induced Penalties in PDM-QPSK Coherent Optical Communication Systems. In *Optical Fiber Communication Conference*, page OWE6, 2010. 86

[71] Seb J Savory. Congestion Aware Routing in Nonlinear Elastic Optical Networks. *Photonics Technol. Lett. IEEE*, 26(10):1057–1060, 2014. 90

[72] Alex Alvarado, David J Ives, Seb Savory, and Polina Bayvel. On the Impact of Optimal Modulation and FEC Overhead on Future Optical Networks. *arXiv*, pages 1–12, 2015. 90

[73] P. P. Mitra and J. B. Stark. Nonlinear limits to the information capacity of optical fibre communications. *Nature*, 411(6841):1027–1030, 2001. 91